

Electrosynthesis and Mechanism of Copper(I) Nitrile Complexes

Dissertation

zur Erlangung des akademischen Grades
doctor rerum naturalium (Dr. rer. nat.)

vorgelegt der

Mathematisch-Naturwissenschaftlich-Technischen Fakultät
(mathematisch-naturwissenschaftlicher Bereich)
der Martin-Luther-Universität Halle-Wittenberg

von Herrn M.Sc. Marcellin M. Fotsing Kamte
geb. am 14. März 1972 in Bafoussam (Kamerun)

Gutachter:

1. Prof. Dr. Wieland Schäfer
2. Prof. Dr. Dr.h.c. Karl-Heinz Thiele
3. Prof. Dr. Lothar Dunsch

Halle (Saale), 01 November 2004

urn:nbn:de:gbv:3-000007437

[<http://nbn-resolving.de/urn/resolver.pl?urn=nbn%3Ade%3Agbv%3A3-000007437>]

To my son
FOTSING KAMGANG, Chris

Contents	Pages
1. Introduction	1
2. Electrosynthesis of metal complexes with acidic C–H compounds	
2.1. General concepts	6
2.2. Electroreduction of organic substrates	8
2.3. Organonitriles	9
3. Results and discussions	
3.1. Electrochemical behavior of different electrolytic systems at a copper electrode	11
3.1.1. Experimental results	11
3.1.1.1. Acetonitrile / Bu ₄ NBF ₄	11
3.1.1.2. Potentiodynamic measurements	15
3.1.1.3. Qualitative measurements at Cu-Pt DSE	15
3.1.1.4. Acetonitrile / LiClO ₄ , Et ₄ NClO ₄	17
3.1.1.5. Tetrahydrofuran / Bu ₄ NPF ₆	18
3.1.2. Discussion	18
3.2. Electrochemical behavior of nitriles used as starting material	21
3.2.1. 1,1,3,3-tetracyanopropane (TCP)	21
3.2.1.1. Influence of the concentration of TCP on the voltammogram	24
3.2.1.2. Effect of the temperature on the cyclic voltammogram	24
3.2.1.3. Controlled potential electrolysis of a solution of TCP	26
3.2.1.4. Behavior of TCP in the presence of different donors	27
3.2.2. Malononitrile	30
3.2.3. Phenylacetonitrile	32
3.2.3.1. Tetrahydrofuran / Bu ₄ NPF ₆	32
3.2.3.2. Acetonitrile / Bu ₄ NBF ₄	33
3.2.4. Discussion on the reduction of starting materials	34
3.3. Electrosynthesis of copper(I) complexes with nitriles possessing α- hydrogen	36
3.3.1. 1,1,3,3-tetracyanopropane as starting material	36
3.3.1.1. Electrosynthesis of [Cu(μ-C(CN) ₃)(PPh ₃) ₂] ₂ (1)	36
3.3.1.2. Structure of {cis-[Cu ₂ (μ-CN)(Phen) ₂ (PPh ₃) ₂]} ₂ [C(CN) ₃][BF ₄]·2CH ₃ CN (2)	41

3.3.1.3. Molecular Structure of $[\text{Cu}_2(\mu\text{-CN})(\text{PPh}_3)_6][\text{BF}_4]$ (3)	45
3.3.1.4. Synthesis of $[\text{Cu}_2(\text{CN})(\text{bipy})_2(\text{PPh}_3)_2][\text{BF}_4]\cdot\text{THF}$ (4)	47
3.3.1.5. Discussion	
3.3.2. Malononitrile as starting material	49
3.3.2.1. Electrosynthesis of $\{[\text{Cu}(\text{CN})(\text{PPh}_3)_2]\cdot\text{CH}_3\text{CN}\}_n$ (5)	52
3.3.2.2. Synthesis of $[\text{Cu}(\text{CN})(\text{bipy})(\text{PPh}_3)]$ (6)	52
3.3.2.3. Synthesis of $[\text{Cu}(\text{CN})(\text{phen})(\text{PPh}_3)]$ (7)	54
3.3.2.4. Discussion	56
3.3.3. Phenylacetonitrile as starting material	57
3.3.3.1. Electrosynthesis of $[\text{Cu}(\text{BPVA})(\text{PPh}_3)_2]$ (8)	59
3.3.3.2. Structure of $[\text{Cu}(\text{BPVA})(\text{Phen})(\text{PPh}_3)]$ (9)	59
3.3.3.3. Structure of $[\text{Cu}_9(\text{CN})_9(\text{PPh}_3)_8]_n$ (10)	62
3.3.3.4. Synthesis of $[\text{Cu}_3(\mu\text{-CN})_2(\text{phen})_3(\text{PPh}_3)_2][\text{BF}_4]$ (11)	64
3.3.3.4. Synthesis of $[\text{Cu}(\text{CN})(\text{phen})(\text{PPh}_3)]_2\cdot\text{H}_2\text{O}$ (12)	65
<i>Thermal analysis of 12</i>	67
<i>Electrochemical behavior of 12</i>	70
3.3.3.5. Discussion	71
3.3.4. Discussion on the coordination mode of electrogenerated cyanide	71
3.4. Electrosynthesis of copper(I) complexes with non-nitrile ligands	72
3.4.1. Electrosynthesis of $[\text{Cu}(\text{Flu})(\text{PPh}_3)_2]\cdot 2\text{CH}_3\text{CN}$ (13)	74
3.4.2. Electrosynthesis of $[\text{Cu}(\text{CPh}_3)(\text{PPh}_3)]\cdot 2\text{CH}_3\text{CN}$ (14)	74
3.4.3. Electrosynthesis of $[(\text{CuCl})_2(\mu\text{-dppe})(\eta^2\text{-dppe})_2]\cdot\text{CH}_3\text{CN}$ (15)	76
and $[(\text{CuCl})_2(\mu\text{-dppe})(\eta^2\text{-dppe})_2]\cdot(\text{CH}_3)_2\text{SO}$ (16)	77
4. Introduction to micro- and nanostructuring of metal surfaces	
4.1. Surfactant templating	81
4.2. The principle of templated electrodeposition	83
4.3. Schematic representation of the working station	84
4.4. Potentiostatic deposition of the platinum film from the liquid crystalline plating mixture	85
4.5. Galvanostatic deposition of the platinum film from the plating mixture	87
4.6. Conclusion	89

5. Experimental part	
5.1. Reagents	90
5.2. Instrumentation	90
5.3. Electrosynthesis	93
5.3.1. Electrosynthesis with nitriles as starting materials	93
1,1,3,3-Tetracyanopropane as starting material	
5.3.1.1. Electrosynthesis of $[\text{Cu}(\mu\text{-C}(\text{CN})_3)(\text{PPh}_3)_2]_2$ (1)	93
5.3.1.2. Preparation of $\text{cis-}[\text{Cu}_2(\mu\text{-CN})(\text{PPh}_3)_2(\text{Phen})_2]_2[\text{C}(\text{CN})_3][\text{BF}_4] \cdot 2\text{CH}_3\text{CN}$ (2)	95
5.3.1.3. Preparation of $[\text{Cu}_2(\mu\text{-CN})(\text{PPh}_3)_6][\text{BF}_4]$ (3)	95
5.3.1.4. Synthesis of $\text{trans-}[\text{Cu}_2(\mu\text{-CN})(\text{PPh}_3)_2(\text{bipy})_2][\text{BF}_4] \cdot \text{THF}$ (4)	95
Malononitrile as starting material	
5.3.1.5. Electrosynthesis of $[\text{Cu}(\text{CN})(\text{PPh}_3)_2] \cdot \text{CH}_3\text{CN}$ (5)	96
5.3.1.6. Preparation of $[\text{Cu}(\text{CN})(\text{bipy})(\text{PPh}_3)]$ (6)	97
5.3.1.7. Preparation of $[\text{Cu}(\text{CN})(\text{phen})(\text{PPh}_3)]$ (7)	97
Phenylacetonitrile as starting material	
5.3.1.8. Electrosynthesis of $\{[\text{C}_4\text{H}_9)_4\text{N}][\text{Cu}(\text{BPVA})(\text{PPh}_3)_2][\text{BF}_4]\}$ (8)	97
5.3.1.9. Preparation of $[\text{Cu}(\text{PAN})_2(\text{Phen})(\text{PPh}_3)]$ (9)	98
5.3.1.10. Preparation of $[\text{Cu}_9(\text{CN})_9(\text{PPh}_3)_8]_n$ (10)	98
5.3.1.11. Preparation of $[\text{Cu}_3(\text{CN})_2(\text{phen})_3(\text{PPh}_3)_2][\text{BF}_4]$ (11)	99
5.3.1.12. Preparation of $[\text{Cu}(\text{CN})(\text{phen})(\text{PPh}_3)]_2 \cdot \text{H}_2\text{O}$ (12)	99
5.3.2. Electrosynthesis with non nitrile ligands	99
5.3.2.1. Electrosynthesis of $[\text{Cu}(\text{Flu})(\text{PPh}_3)_2] \cdot 2\text{CH}_3\text{CN}$ (13)	99
5.3.2.2. Electrosynthesis of $[\text{Cu}(\text{CPh}_3)(\text{PPh}_3)] \cdot 2\text{CH}_3\text{CN}$ (14)	100
5.3.2.3. Electrosynthesis $[(\text{CuCl})_2(\mu\text{-dppe})(\eta^2\text{-dppe})_2] \cdot \text{CH}_3\text{CN}$ (15)	100
5.3.2.4. Preparation of $[(\text{CuCl})_2(\mu\text{-dppe})(\eta^2\text{-dppe})_2] \cdot (\text{CH}_3)_2\text{SO}$ (16)	101
5.4. Electrodeposition from lyotropic liquid crystalline phases	102
6. Summary / Zusammenfassung	
Summary	103
Zusammenfassung	108
7. References	113

Appendix

A1. Double Segment Electrode	I
A2. Crystal data and experimental details of X-ray structure	III
A2.1. Crystallographic data for $[\text{Cu}(\mu\text{-C}(\text{CN})_3)(\text{PPh}_3)_2]_2$ (1)	III
A2.2. Crystal data for $\{\text{cis-}[\text{Cu}_2(\mu\text{-CN})(\text{PPh}_3)_2(\text{Phen})_2]_2\}[\text{C}(\text{CN})_3][\text{BF}_4]\cdot 2\text{CH}_3\text{CN}$ (2)	III
A2.3. Crystallographic data for $\text{cis-}[\text{Cu}_2(\mu\text{-CN})(\text{PPh}_3)_6][\text{BF}_4]$ (3)	IV
A2.4. Crystal data for $\text{trans-}[\text{Cu}_2(\mu\text{-CN})(\text{PPh}_3)_2(\text{bipy})_2][\text{BF}_4]\cdot \text{THF}$ (4)	IV
A2.5. Crystallographic data for $[\text{Cu}(\text{CN})(\text{bipy})(\text{PPh}_3)]$ (6)	V
A2.6. Crystallographic data for $[\text{Cu}(\text{CN})(\text{phen})(\text{PPh}_3)]$ (7)	V
A2.7. Crystallographic data for $[\text{Cu}(\text{BPVA})(\text{Phen})(\text{PPh}_3)]$ (9)	VI
A2.8. Crystallographic data for $[\text{Cu}_3(\text{CN})_2(\text{phen})_3(\text{PPh}_3)_2][\text{BF}_4]$ (11)	VI
A2.9. Crystal data of $[\text{Cu}(\text{CN})(\text{phen})(\text{PPh}_3)]_2\cdot \text{H}_2\text{O}$ (12)	VII
A2.10. Crystal data for $[(\text{CuCl})_2(\mu\text{-dppe})(\eta^2\text{-dppe})_2]\cdot \text{CH}_3\text{CN}$ (15)	VII
A2.11. Crystal data for $[(\text{CuCl})_2(\mu\text{-dppe})(\eta^2\text{-dppe})_2]\cdot (\text{CH}_3)_2\text{SO}$ (16)	VIII

Abbreviations

ω	Rotation rate (rad s^{-1})
α	Charge transfer coefficient
ν	Kinematic viscosity ($\text{cm}^2 \text{s}^{-1}$)
A	Electrode area (cm^2)
A_f	Frequency factor
AFM	Atomic force microscopy
AN	Acetonitrile
bipy	2,2'-bipyridine
BPVA	1-benzyl-2-cyano-2-phenylvinylamine
Brij [®] 76	Decaethyleneoxide mono-octadecyl ether ($\text{C}_{18}\text{EO}_{10}$)
c	Concentration of the electroactive species (mol cm^{-3})
CE	Counter electrode
CV	Cyclic voltammetry / cyclic voltammogram
DMSO	Dimethylsulfoxide
D_o	Diffusion coefficient ($\text{cm}^2 \text{s}^{-1}$)
dppe	1,2-bis(diphenylphosphino)ethane
DSC	Differential scanning calorimetry
DSE	Double Segment Electrode
DTA	Differential thermal analysis
E_A	Energy of activation
EDX	Energy dispersive X-ray
E_F	Electrochemical efficiency
EI-MS	Electron impact mass spectrometry
E_p	Peak potential
$E_{p/2}$	Half-peak potential
ESI-MS	Electrospray ionization mass spectrometry
F	Faraday constant
FAB-MS	Fast atom bombardment mass spectrometry
FLU	Fluorene
GC-MS	Gas chromatography mass spectrometry
h	hour

HCPA	Hexachloroplatinic acid
IE	Indicator electrode
IR	Infrared
j	Flux of the reactants reaching the electrode surface (moles $\text{cm}^{-2} \text{s}^{-1}$)
k	Heterogeneous rate constant for the electron transfer
k_f	Forward heterogeneous electron transfer rate constant
m	Medium (IR) / Multiplet (NMR)
m.p.	Melting point
MDN	Malononitrile
min	minute
n	Number of exchange electrons
NMR	Nuclear magnetic resonance
OCP	Open-circuit potential
PhAN	Phenylacetonitrile
phen	1,10-phenanthroline
phen·H ₂ O	1,10-phenanthroline monohydrate
POM	Polarized optical microscopy
R	Molar gas constant (8.315 J K mol ⁻¹)
RDE	Rotating disk electrode
RE	Reference electrode
s	Strong (IR) / Singlet (NMR) / second
SCE	Saturated calomel electrode
T	Temperature (K)
TCP	1,1,3,3-tetracyanopropane
TG	Thermogravimetric
THF	Tetrahydrofuran
TPM	Triphenylmethane
v	Scan rate (V s ⁻¹)
vs	Very strong
vw	Very weak
w	Weak
WE	Working electrode

1. Introduction

The chemistry of organometallic compounds represents an important part of organic and pharmaceutical synthesis [1-6]. These compounds are used as catalysts in the stereospecific polymerization of olefins, as stabilizers of polymeric materials and lubricants, antiknock compounds and as additives to motor and jet fuels, antiseptics, biocides and pigments [3,7].

However, organocopper compounds are nowadays among the most frequently used reagents in synthetic organic chemistry [1-4], and constitute a key class of organometallic reagents with numerous applications [1-4,8]. They can be used to prepare alkanes, alkenes, alkynes, aromatics and as high regio and stereoselective reagents. The majority of experimental protocols for their preparation involve the transmetalation process from organolithium or Grignard reagents [3,4].

The alkylcopper compounds are sensitive and often difficult to isolate. However, the methyl copper compound, synthesized for the first time by *Gilman et al.* [9,10], is not subjected to β -elimination and is relatively stable. Organocopper complexes become more stable by coordinating nitrogen compounds or phosphines [4].

There is a constant development of new ways to achieve efficiently organocopper compounds [1-4]. As their properties have become gradually apparent, new synthetic routes have been discovered [1,2]. In the most cases, many reaction steps have been involved before obtaining the desired products. Therefore, the synthesis of organometallic compounds by electrochemical ways represents usually a particular alternative, an efficient and simple procedure [11,12].

Since the well-known Kolbe electrolysis, considered as the first electroorganic reaction published in 1849 which led to the oxidative decarboxylation of a carboxylic acid and the generation of a radical intermediate [13], electrochemistry is extensively used as a useful synthetic tool in the field of organic and inorganic synthesis and is considered as a powerful method for making and modifying molecules.

The electrochemical synthesis based on the anodic dissolution of a metallic electrode was elaborated in 1882 by *Gerdes* [14] for the preparation of platinum(IV) hexaaminates in a solution of ammonium carbonate. Nine decades after Gerdes's pioneering experiments,

Lehmkuhl [15] and *Garnovskii* [11], reported on the electrochemical synthesis of metal complexes in a one-step reaction, the so called "direct electrosynthesis". Soon thereafter, *Tuck* [16] has demonstrated that metal salts of weak acids can be easily prepared by an electrochemical way using a sacrificial anode in non-aqueous media with simple equipments. *Sousa* [17] gave an additional impulse by using this technique for the syntheses of Schiff base complexes. Since then, the field has grown exponentially and comprehensive reviews devoted to the electrosynthesis of organometallic compounds by the dissolution of sacrificial metal anode have appeared [11,12,16-19].

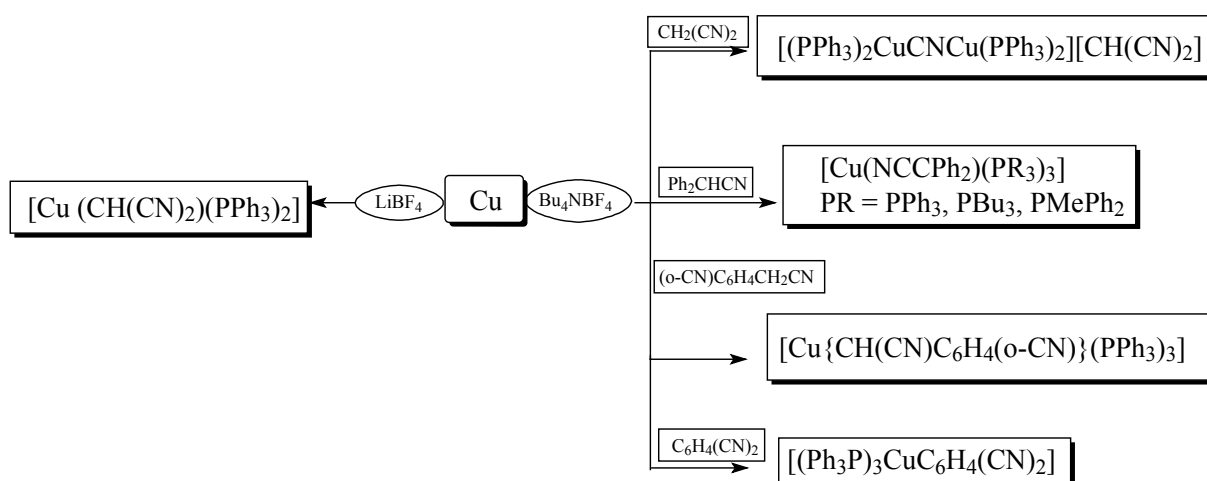
By using electrochemical route, which involves only electrons, the complications that are often observed in the process with redox reagents are avoided. Also, organic compounds with C–H acidities are usually deprotonated with alkali, alkaline-earth or aluminum and as the pK_a value increases, the deprotonation becomes more difficult whereas the cleavage of C–H bond occurs readily through electrosynthesis [20]. Among such compounds, nitriles having α -hydrogen may be regarded as prominent substrates in the electrochemical synthesis of organometallic compounds.

For the last 25 years, different kinds of ligands have been successfully used to prepare metal complexes by this method. But surprising lacunae still present concerning the use of organonitriles as starting materials. It is known that the C–H bonds in organic structure elements attached to nitrile groups show considerable carbon acidity. This plays an important role with regard to the structure of the metal complexes prepared by electrolysis. In fact, the CN-group is able to stabilize the carbanion centre so that the negative charge of the carbanion is delocalized onto the nitrogen atom. The acidities of some nitrile compounds are summarized in Table 1.

Table 1 Acidities of some nitriles in DMSO

Nitriles	pK_a	ref.	Nitriles	pK_a	ref.
CH ₃ CN	31.3	[21a]	Ph ₂ CHCN	17.5	[21c]
CH ₃ CH ₂ CN	32.5	[21b]	(C ₆ F ₅) ₂ CHCN	8.0	[21f]
PhCH ₂ CN	21.9	[21c]	(NC) ₂ CHPh	4.2	[21g]
C ₆ F ₅ CH ₂ CN	15.8	[21d]	CH(CN) ₃	-5.13	[21g]
NCCHCN	11.1	[21b]	tert-But CH(CN) ₂	13.2	[21g]
(NC) ₂ CHCH ₃	12.4	[21e]			

Recently, in our laboratory, a number of organonitrile-copper(I) and zinc(II) compounds [22] have been investigated. The experiments were devoted to the electrochemical reduction of C–H acidic nitriles (malononitrile, 1,1,3,3-tetracyanopropane and isophthalonitrile, diphenylacetonitrile and o-cyanophenylacetonitrile) concomitantly with the anodic dissolution of copper (scheme 1) or zinc in non-aqueous solvents. It was found that the structure of the metal complexes highly depends on the acidity of nitriles and three different kinds of compounds, ionic complexes, keten-imin complexes and compounds with a Cu–C– σ -bond could be achieved (scheme 1). It was also reported that the reduction of nitriles in non-aqueous solvents can occur in different ways; it takes place by either a fission of the C–H or C–CN bonds or both together[22-24].



Scheme 1

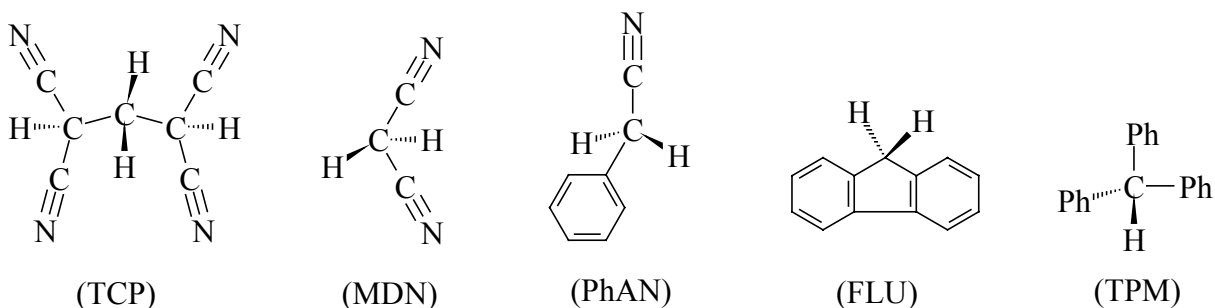
The mechanisms of the reactions occurring at the electrodes remain an important aspect. In the literature, most of them are proposed based on the electrochemical efficiency (E_F), defined as the number of moles of the metal dissolved per faraday of electricity passed through the cell [12]. However, E_F does not provide any information about the overall electrochemical reactions in the cell.

One objective of this work is to investigate the electrochemical behavior of the electrolytic solution at a copper electrode, used as working electrode, in different systems and in the presence of some nitriles having α -hydrogen. The motivation of these studies was the desire to more understand the mechanism by which α -cyanocarbanions can be achieved during electrochemical reduction of organonitriles.

Also, the electrochemical dissolution of the copper electrode is an important topic with regard to technological aspect, since it is of relevance to electrosynthesis of organocopper compounds, corrosion, etching and leaching reactions. During many decades, considerable effort has been made to understand its electrochemical behavior in different media [25-29]. By the way, various metal ions have appreciably different electrochemical behaviors in non-aqueous and in aqueous solutions; these differences is assigned in the most cases to their solvation energy which is lower in the relatively weak base than in the much stronger base water [30]. However, a specific interaction occurs between Cu(I) and acetonitrile which is a much weaker base than water [30-36]. A variety of studies on Cu(I) / acetonitrile system have been reported [30-32, 37-38].

The present part deals mainly with the electrochemical behavior of different electrolytic systems, in the negative potential range, at a copper working electrode by means of cyclic voltammetry (CV), chronopotentiometry, chronoamperometry and Double Segment Electrode (DSE) and the determination of the kinetic parameters using copper rotating disk electrode (RDE). For this purpose, acetonitrile (AN) and a non nitrile, tetrahydrofurane (THF), have been used as solvents. Electrochemical behaviors of nitriles, depicted below, have also been investigated.

Another aspect of this work is to use these nitriles to prepare electrochemically copper(I) compounds and their derivatives, in the presence of different donors, in non-aqueous media by galvanostatic dissolution of copper metal and concomitantly the reduction of nitriles at the cathode in an undivided electrochemical cell. For this proposal, 1,1,3,3-tetracyanopropane (TCP), malononitrile (MDN) and phenylacetonitrile (PhAN) have been studied. Some organic compounds with C–H acidity (non-nitriles with high pK_a value) like fluorene (FLU) and triphenylmethane (TPM) have been used as starting material. The direct electrosynthesis of organocopper(I)-chloride has also been investigated.



1,1,3,3-tetracyanopropane (TCP) has been chosen because of its charge-transfer capabilities, and as a ligand, it could behave as a π -donor as well as N-bound TCP \cdot . As alkyl substituted by more than one cyanide, it has the potential of binding more than one metal ion [39] and it exhibits different coordination modes.

Recently, the electrochemical synthesis of copper nitrile complexes by potentiostatic dissolution of copper anode and cathodic reduction of malononitrile in a one-step reaction have been reported [23]. As result, all compounds prepared are binuclear Cu(I) complexes in which the copper atoms were bridged by a cyano group. Galvanostatically, a mononuclear Cu(I) compound [Cu(NCC(H)CN)(PPh₃)] was generated by using lithium tetrafluoroborate as supporting electrolyte [22a]. As a part of a more extensive investigation of this work, it was interesting to know what happens galvanostatically in the presence of tetrabutylammonium tetrafluoroborate and also to afford a further insight into the electroreduction mechanism of malononitrile.

Copper(I)chloride with bidentate bridging diphosphine ligands exhibits tumouricidal properties [40]. Such complexes are achieved by classical route. However, the electrochemical methodology could be an efficient and a simple alternative. For this purpose, 1,2-bis(diphenylphosphino)ethane (dppe) and LiCl have been selected as starting materials.

The last part of this work is devoted to the modification of metal surfaces on micrometer and sub-micrometer scales, which is considered to be a key future technology. This has led in recent years to an interest in the generation of micro- and nanometer sized structures on surfaces. The initial goal of this part is to modify the metallic surfaces with organocopper(I) complexes through coordinative interaction. To this end, a working place for surface modification at micro and nanometer scales has been developed and will be tested. For the operating of the experimental setup, mesoporous platinum films (with a defined nanostructure) electrodeposited from lyotropic liquid crystal phases [41,42] onto a gold surface should be produced under galvanostatic control.

2. Electrosynthesis of metal complexes with acidic C–H compounds

2.1. General concepts

There are well established classical methods for the preparation of organometallic compounds [1]. Electrosynthesis presents many advantages over classical routes such as high efficiency, lower prices of metals and high reactivity of products [11,12-15,16]. In this method, complexes can be achieved either at a constant current or controlled potential.

The remarkable characteristic of the electrosynthesis is the formation of a Lewis acid at the anode and a Lewis base at the cathode. Then, the synthesis of metal complexes with organic ligand is both cathodically and anodically possible either the metal or the ligand can be subject to the primary electrochemical attack.

By applying a voltage between the electrodes, the metal is dissolved at the anode and the substrate is reduced at the cathode. The principle (Fig. 1) is standed to be an electrode process followed by a chemical reaction between both generated ions (metal ion and carbanion). During this process the electrons are transferred from the cathode to the reaction mixture and from the reaction mixture to the anode and consequently allows an electrical current to flow through the cell.

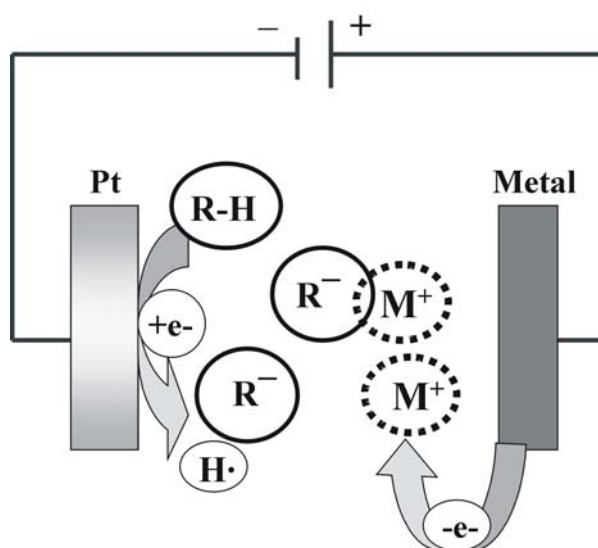
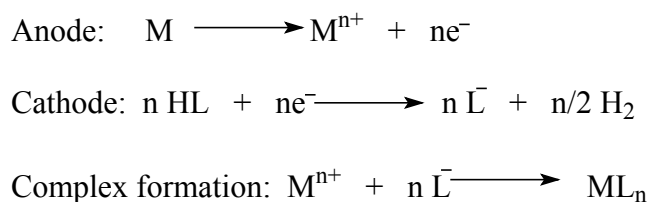


Fig. 1 The principle of the direct electrosynthesis.

The essence of the direct electrosynthesis of metal complexes with C–H acidic compounds can be resumed as follows (Scheme 2):



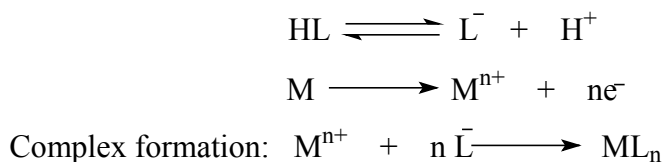
Scheme 2

In the cases of reactions dominated by the solvation conditions, the anodic reaction could be summarized as in scheme 3 [43].



Scheme 3

If ligands possess an acidic group (OH, SH, HNR, HSe) then the dissociation of the acid takes place giving L^- and the solvated proton H^+ (scheme 4) [44].

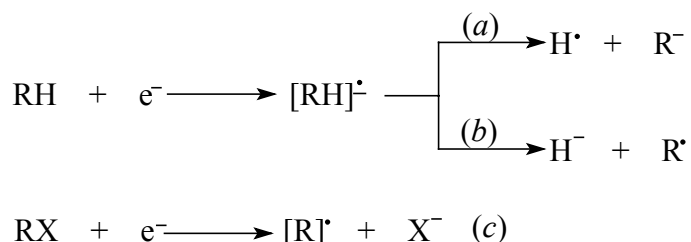


Scheme 4

This reaction can be achieved with a suitable choice of substrate, solvent and supporting electrolyte. Organic solvents and aliphatic quaternary ammonium salts, as supporting electrolyte, are frequently used. The choice of a solvent is primarily dictated by the solubility of the substrate, its redox activity and its properties such as electrochemical and chemical reactivities. A large dielectric constant promotes the dissociation of electrolytes. Due to their high resistance to oxidation in the potential range of most organic solvents, the cations of aliphatic quaternary ammonium are the most used in this method [45].

2.2. Electroreduction of organic substrates

Organic substrates, in general, demonstrating carbon acidity (scheme 6) or electron affinity (scheme 6c) are efficient to be converted into a reactive form in which it is able to react with the metal ions. The gain of an electron by a neutral molecule RH to form a radical anion is the first step of the reduction of organic molecules. Cleavage of the acidic H–C bond in radical anions can occur according two modes as illustrated in scheme 6a and 6b [46,47]. *Zhang and Bordwell* [47] reported that the choice between these two pathway is not so clear-cut. The reaction path *a* (loss of a H \cdot and formation of R $^{\ominus}$) is expected to be the favored pathway [48]. The loss of hydride in solution is generally not as favorable as hydrogen atom loss and this due to the solvation energies of H $^{\ominus}$ and R $^{\ominus}$ which are similar [49].



Scheme 6

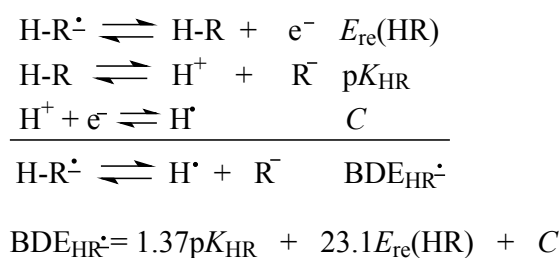
Griller et al. [49] found from the calculated thermodynamic data for toluene, fluorene and 1-methylnaphthalene, in acetonitrile, that path *b* is more endothermic than path *a* (Table 2).

Table 2 Thermodynamic data of some hydrocarbons [49].

hydrocarbon	ΔG° (kJ mol $^{-1}$)	
	$[\text{RH}]^{\ominus\cdot} \longrightarrow \text{H}\cdot + \text{R}^-$	$[\text{RH}]^{\ominus\cdot} \longrightarrow \text{H}^- + \text{R}\cdot$
toluene	31.8	136.9
fluorene	75.4	114.3
1-methylnaphthalene	108.0	195.9

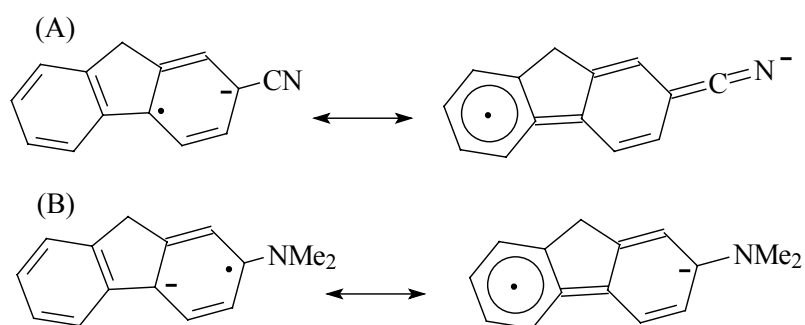
Zhang and Bordwell [50] reported that little or no quantitative information concerning the homolytic bond dissociation energies (BDE) of the H–R bonds in H–R $^{\ominus\cdot}$ -type radical anions appears to be available in the literature. Consequently, they proposed a simple method of estimating the BDE of the H–C bonds in radical anions based on the following equation

(scheme 7) where E_{re} represents the reduction potential and C a constant with a semiempirical value of $306.9 \text{ kJ mol}^{-1}$.



Scheme 7

Bordwell et al. [46,47,50] concluded that the presence of electron acceptor groups in radical anions, such as $\text{C}\equiv\text{N}$, promotes cleavage by path *a* (scheme 6) since they stabilize the product anion R^- (by stabilizing the negative charge, scheme 8A), whereas the presence of donor groups, such as Me_2N , promotes cleavage by path *b* (scheme 6), since they stabilize the product radicals (by the odd electron, scheme 8B).



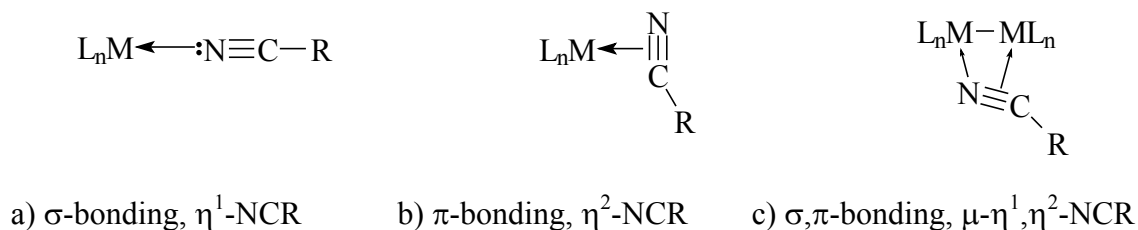
Scheme 8

A variety of substrates have been used [44] but nitriles may be regarded as prominent one in the electrosynthesis of organometallic compounds.

2.3. Organonitriles

Organonitriles present well-recognized chemical versatility, charge-transfer capabilities and have been extensively used as convenient starting materials in pharmaceutical and organic syntheses [51]. With their weak σ -donor and π -acceptor ability, nitriles can be converted into other organic ligands as a consequence of chemical processes such as insertion, coupling or cleavage. Nitriles present different interaction modes with metal centers and can be bonded in different ways (scheme 9) [20]. The more common coordination mode of nitrile occurs by σ bonding in the usual manner through the lone pair of electrons on N and shows the

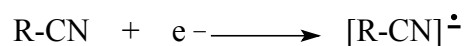
characteristic increase in the $\nu(\text{C}\equiv\text{N})$ stretching frequency of $30 - 110 \text{ cm}^{-1}$. The shift in the CN stretching frequency observed is indicative of nitrile coordination through CN triple bond [20]. The coordination mode types (b) and (c) are uncommon but are encountered in the literature [52].



Scheme 9

One of the fundamental aspects in the reactivity of nitriles is the ability to act as weak bases which are frequently used for the preparation of chemical functional groups such as amides, carboxylic acids or aldehydes [53].

The electrochemical investigations of organonitriles are of interest not only because the radical ions are used to achieve organonitrile metal complexes but also these anions, according to conditions, may undergo further chemical or electrode reactions. In acidic medium, nitriles are reduced to amines whereas in neutral or in alkaline media they undergo an electrolytic reductive cleavage of C–CN bond [54]. Their reduction process in dimethylsulfoxide (DMSO) corresponds to the loss of a hydrogen atom with the formation of the corresponding anion; however, no general conclusion concerning their behavior was reached [55,56]. *Rieger et al.* [57] reported the cathodic reactions of a series of aromatic and aliphatic nitriles in DMF solution of tetra-*n*-propylammonium perchlorate. They found that most of the nitriles studied undergo a one-electron reduction to give an anion radical in the initial step (scheme 10).



Scheme 10

Many of the radicals were stable but a few decayed quite rapidly. The stable radicals were obtained from aromatic nitriles whereas aliphatic nitriles, such as 1,1,2,3,3-pentacyanopropenide and 1,1,3,3-tetracyano-2-dimethylaminopropenide, generated unstable radical anions [57]. The reduction of the isomeric cyanopyridines, can occur in three different ways which depend highly on the pH of the solution: a one-electron process to a dimer, a splitting off of the cyanide ion and a reduction of —CN to —CH₂NH₂ [58].

3. Results and discussions

3.1. Electrochemical behavior of different electrolytic systems at the copper electrode

3.1.1. Experimental results

3.1.1.1. Acetonitrile / Bu_4NBF_4

The cyclic voltammograms (CVs) of the acetonitrile / Bu_4NBF_4 solution were recorded between 0 V and -1.80 V at the platinum working electrode and between -0.26 V and -1.80 V at the copper working electrode (Fig. 2). After many cycles, the CVs present no electron transfers in the scan region at the platinum electrode. But at the copper electrode, two well defined redox processes labeled I and II are observed at -0.346 V and -1.437 V respectively. These two processes are reductive and irreversible as evidence by the lack of the oxidation peaks during the reverse scan. As it is shown in Fig. 2, the process (II) does not appear during the first cycle of the scan but appears during the following scans and grows continuously meanwhile the redox process (I) decreases in the same way.

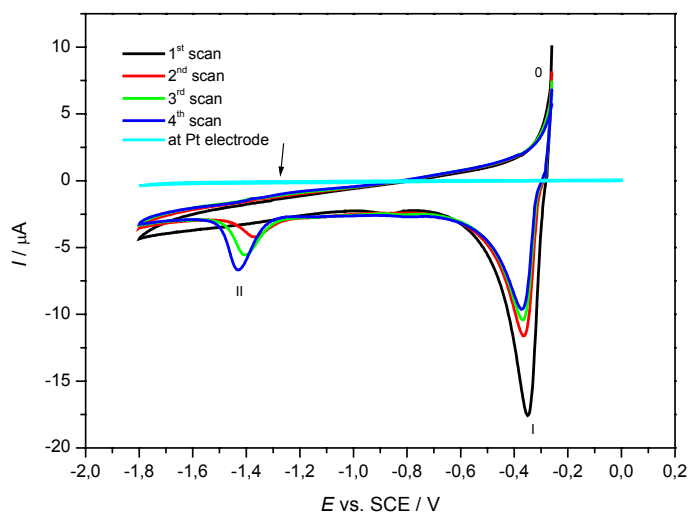


Fig. 2 CVs recorded in AN / Bu_4NBF_4 (0.1 mol dm^{-3}) at a Pt and at a Cu electrode ($v = 0.1 \text{ V s}^{-1}$).

The peak (I) obtained at the first scan was analyzed by coulometry (Q_I) and compared with the charge of peaks (I) and (II) obtained at the last scan, noted $Q_{I'}$ and Q_{II} respectively. We found that $Q_I = Q_{I'} + Q_{II}$. This result demonstrates quite conclusively that there is a

connection between both processes. When the forward scan begins from -1.8 V to -0.26 V, then the process (II) appears during the first scan and the process (I) appears too small in height.

The influence of the scan rate was examined in order to get some insight into the mechanism of the irreversible reaction at the potential of peak (II). It appears that peaks (II) grows and is shifted at more negative potential as the scan rate increases. The variation of peak current I_{pII} against the square root of the voltage scan rate on a stationary copper electrode was plotted according to the following equation at 25°C [59]:

$$I_p = 2.99 \times 10^5 \alpha^{1/2} c A D_0^{1/2} \nu^{1/2} \quad (1)$$

where c is the concentration of the electroactive species in mol cm^{-3} , ν is the scan rate in V s^{-1} , A is the electrode area in cm^2 , D_0 is the diffusion coefficient in $\text{cm}^2 \text{s}^{-1}$, n is the number of exchange electrons.

A straight line which is obtained pass closely to the origin. The slope of the $\ln I_p$ vs. $\ln \nu$ plot (Fig. 3) for process (II) is approximately 0.52 ± 0.01 . This result suggests that (II) is under diffusion control.

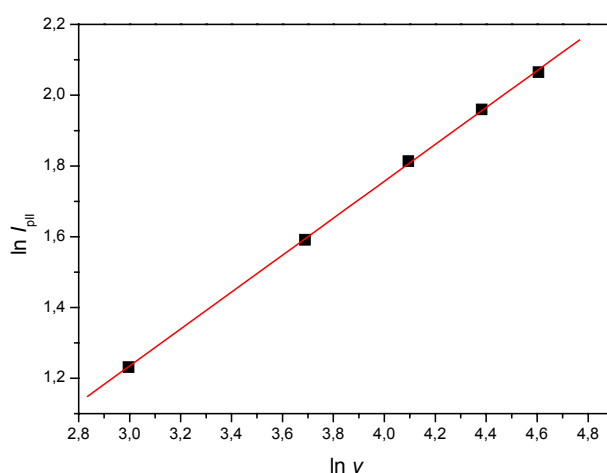


Fig. 3 Variation of the $\ln I_p$ with $\ln \nu$ (AN / Bu_4NBF_4 (0.1 mol dm^{-3}), copper electrode).

The number of electron (n) involved in the reaction can be determined according to the following equation [59,60]:

$$E_p - E_{p/2} = -47.7 / (an) \text{ mV} \quad (2)$$

where E_p stands for peak potential, $E_{p/2}$ for half-peak potential and α the charge transfer coefficient. The number of electrons involved in the process (II) was determined from equation (2); αn was comprised between 0.8 and 0.95 with an average of 0.9 and $n = 1$ could be a reasonable hypothesis according to the height of the peak.

The influence of the concentration of the Bu_4NBF_4 has also been studied from 0.04 to 0.1 mol dm^{-3} . It appears that the peak current of the process (II) grows with the concentration of BF_4^- . The order of reaction in relation to BF_4^- ion concentration is determined by plotting the logarithm of the peak current (II) versus the logarithm of the concentration of BF_4^- (Fig. 4). The order of the reaction is found to be close to one (slope = 1.15).

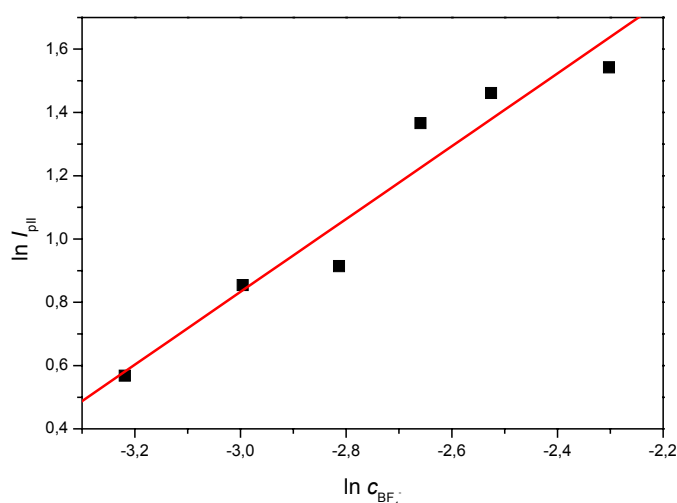


Fig. 4 Influence of the concentration of BF_4^- on $I_{p\text{II}}$ recorded in similar conditions as in Fig. 2 (AN, copper electrode, $\nu = 0.1 \text{ V s}^{-1}$).

The measurement of the steady-state currents as a function of the electrode angular velocity and electrode potential has been carried out using the rotating disk electrode (RDE). The RDE voltammograms were recorded under identical experimental conditions as in Fig. 2. The voltammograms exhibit a well-defined reduction wave in the same potential range as the previous cyclic voltammograms as shown in Fig. 5 which represents the influence of the angular velocity on the RDE voltammograms recorded in AN / Bu_4NBF_4 (0.1 mol dm^{-3}) at the copper electrode with a scan rate of 5 mV s^{-1} at different angular velocities.

The nature of the limiting diffusion current was verified using the Levich equation [60-62]:

$$I_d = 0.62nFAD_0^{2/3}\nu^{-1/6}\omega^{1/2}c \quad (3)$$

where c is the concentration of the electroactive species in mol cm^{-3} , ν is the kinematic viscosity in $\text{cm}^2 \text{s}^{-1}$, ω is the rotation rate in s^{-1} , A is the electrode electroactive area in cm^2 , D_0 is the diffusion coefficient in $\text{cm}^2 \text{s}^{-1}$, n is the number of electrons exchanged and F is the Faraday constant.

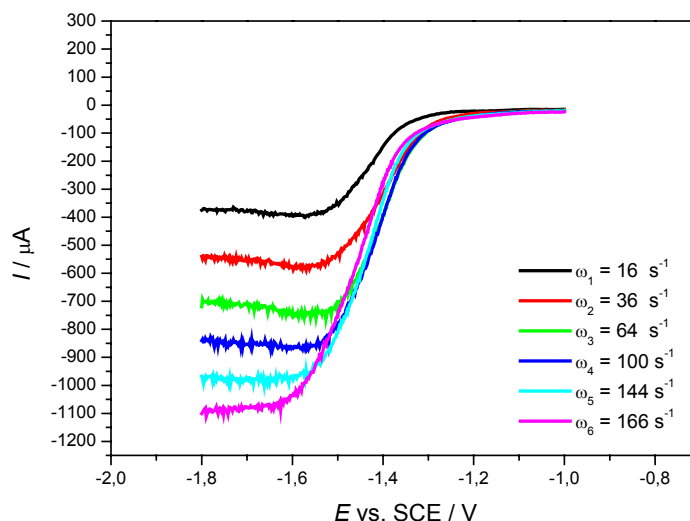


Fig. 5 Cu-RDE voltammograms recorded in AN / Bu₄NBF₄ (0.1 mol dm⁻³) with a scan rate of 5 mV s^{-1} at different angular velocities.

The disk currents at constant potentials are plotted against the square root of the angular velocities. The plots of I vs. $\omega^{1/2}$ overlap in the range from -1.60 V to -1.80 V and are linear. Fig. 6 shows a Levich plot at -1.60 V . This behavior indicates the mass transport control of the current.

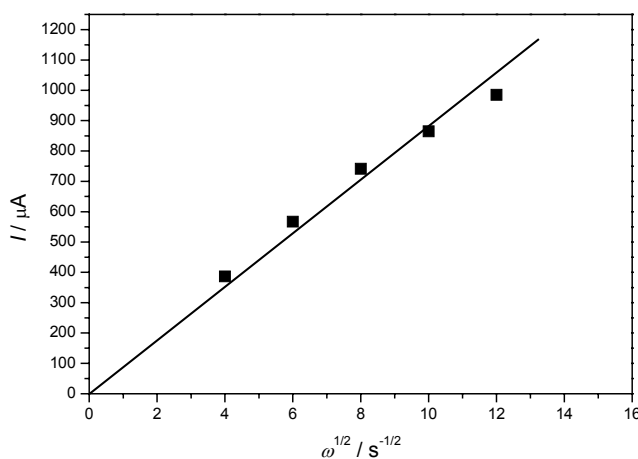


Fig. 6 Levich plot recorded in AN / Bu₄NBF₄ (0.1 mol dm⁻³) with a scan rate of 5 mV s^{-1} at different angular velocities.

3.1.1.2. Potentiodynamic measurements

Potentiodynamic measurements have been performed in order to investigate if the copper electrode, in the potentials range from -300 to -400 mV, is covered with an adsorbed layer of $[\text{Cu}(\text{BF}_4)]_{\text{ads}}$.

Potentiostatically, copper electrode is oxidized at a potential of -0.260 V in 0.1 mol dm^{-3} of Bu_4NBF_4 in acetonitrile, the current–time transient was measured for 10 s and afterwards, the open-circuit potential (OCP)–time transient is recorded (Fig. 7). The potential falls rapidly to approximately -290 mV, close to the Cu(I) reduction potential (process I, Fig. 2). This result indicates the diffusion of the generated copper(I) ions.

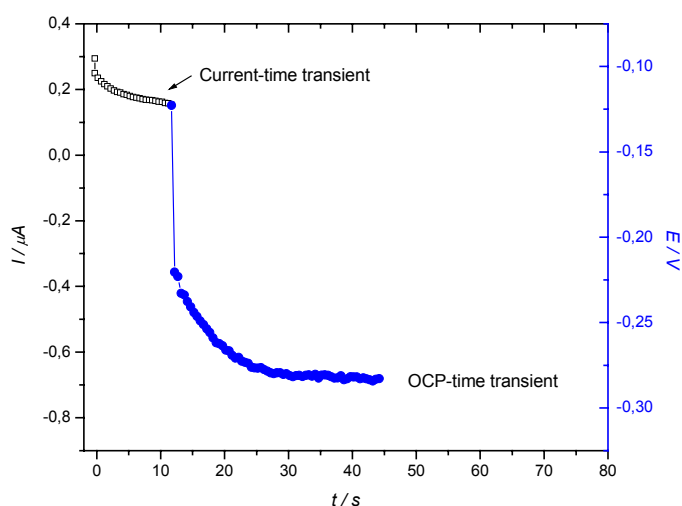


Fig. 7 Potentiostatic current-time transient (\square) and open-circuit potential-time transient (\bullet); (oxidation of the copper electrode at a potential of -260 mV in AN / Bu_4NBF_4 (0.1 mol dm^{-3})).

3.1.1.3. Qualitative measurements at Cu-Pt-DSE

To ascertain the transport of $[\text{Cu}(\text{CH}_3\text{CN})]^+$ ions from the electrode surface to the bulk solution, a Cu-Pt-Double Segment Electrode (DSE) made of a copper ring segment as working electrode (WE), a platinum ring segment as indicator electrode (IE) [63,64] has been used. This electrode is described fully in appendix A1. DSE was used only for qualitative measurements.

The copper working electrode and the platinum indicator electrode, are potentiostatically polarized at -260 mV and -400 mV, respectively. The indicator electrode is switched on

15 s (A) after the bipotentiostat and 50 s later the copper electrode is switch on (B). An anodic current is recorded and few seconds later a signal of equal intensity appears at the indicator electrode (C). When the working electrode is switch off (D), the cathodic current returns to its initial state (E) as it is shown on Fig. 8.

The working electrode is also polarized galvanostatically ($I = 0.6 \text{ mA}$) for 120 s and the indicator electrode is switch on 25 s (A1) after the beginning of the measurements. A cathodic current is recorded and by switching off the copper working electrode (B1), the signal observed at the platinum indicator electrode returns to its initial state (Fig. 9a). By polarizing continuously the WE, the IE is switched on (A2) and when it is switching off (B2), the current returns to zero (Fig. 9b). These experiments with DSE argue favorably to the mass transport of $[\text{Cu}(\text{BF}_4)]^+$ through the solution.

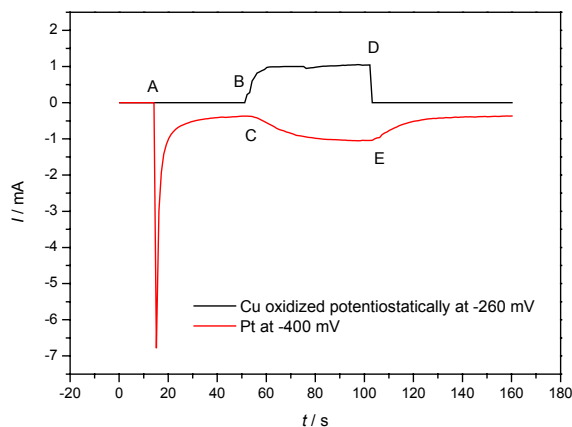


Fig. 8 Current–time curve at the DSE when the copper working electrode is polarized potentiostatically in AN / Bu_4NBF_4 (0.1 mol dm^{-3}).

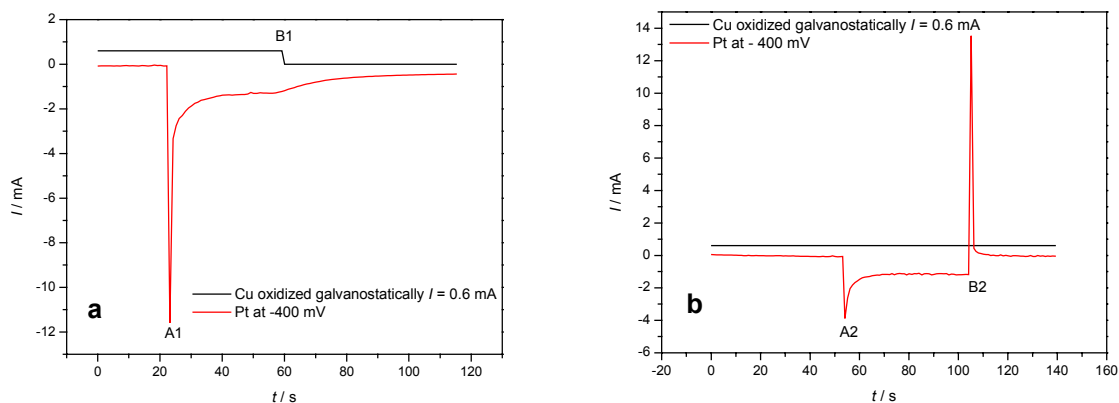


Fig. 9 Current–time curve at the DSE when the copper working electrode is polarized galvanostatically in AN / Bu_4NBF_4 (0.1 mol dm^{-3}).

3.1.1.4. Acetonitrile / LiClO_4 , Et_4NClO_4

The cyclic voltammograms are also recorded in AN / LiClO_4 (Fig.10) and AN / Et_4NClO_4 (Fig.11) at the copper electrode in order to examine the effect of the supporting electrolyte on the process (II). In both cases the process (I) appears at -0.409 V whereas the process (II) appears at more negative potential, -1.60 V at the same potential. This result indicates that the size of the cation of supporting electrolyte does not affect the reduction potential of both systems. Therefore, the process (II) is related to the reduction of the copper(I) perchlorate complex. The potential value of the peak (II) is shifted in the cathodic direction compared to Fig. 2 where it appears at -1.437 V.

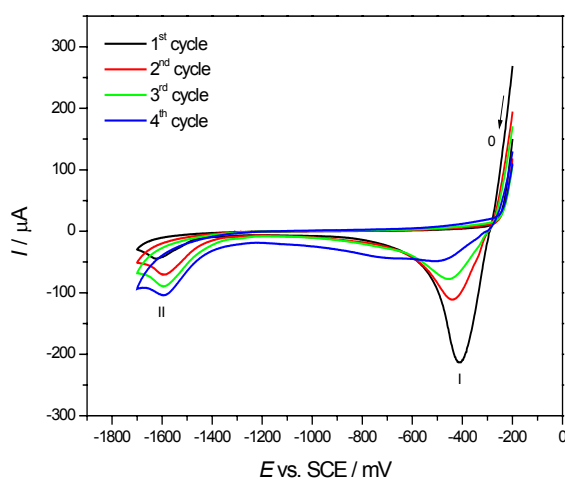


Fig. 10 CVs recorded in AN / LiClO_4 (0.1 mol dm^{-3}) at the Cu electrode ($\nu = 0.1 \text{ V s}^{-1}$).

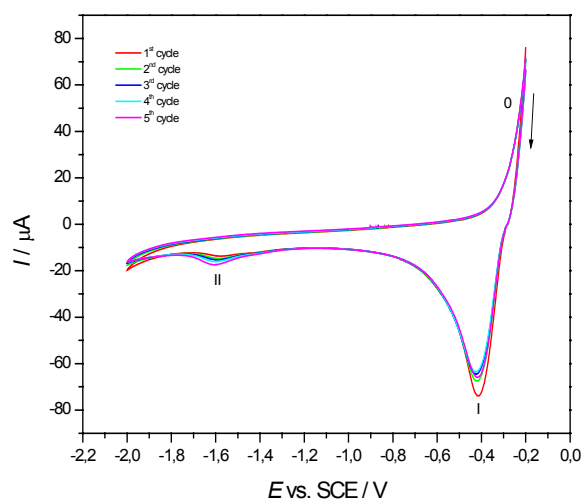


Fig. 11 CVs recorded in AN / Et_4NClO_4 (0.1 mol dm^{-3}) at the Cu electrode ($\nu = 0.1 \text{ V s}^{-1}$)

3.1.1.5. Tetrahydrofuran / Bu_4NPF_6

In an effort to enter somewhat fully into the factors governing the process (II), the solvent has been changed and the voltammograms recorded in THF / Bu_4NPF_6 .

The cyclic voltammograms recorded at a copper electrode, between +0.66 V and -2.00 V, exhibit two redox processes (as in AN / Bu_4NBF_4) as shown in Fig. 12. Both processes appear at +0.341 V and -1.712 V, respectively. Compared with AN, the process (I) appears at more positive potential whilst the process (II) appears at more negative potential in THF.

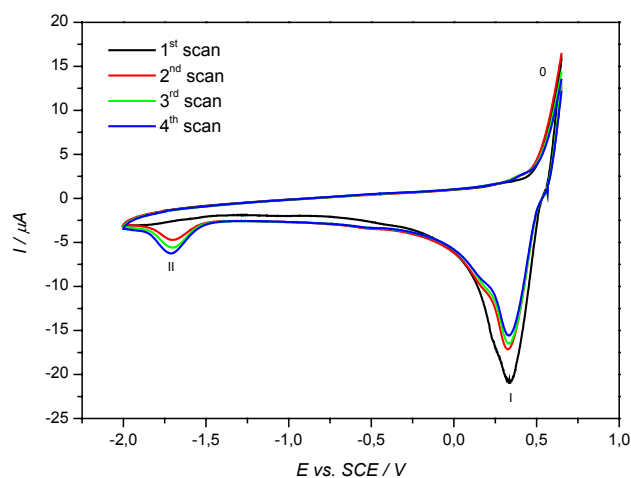


Fig. 12 CVs recorded in THF / Bu_4NPF_6 (0.1 mol dm^{-3}) at the copper electrode ($\nu = 0.1 \text{ V s}^{-1}$).

3.1.2. Discussion

The cyclic voltammograms recorded in acetonitrile / Bu_4NBF_4 have revealed two well defined irreversible cathodic peaks (labelled I and II) As evidence by the rotating disk voltammograms, the process (II) is reductive and connected with the process (I). It is well known that the Cu(I) is stabilized by acetonitrile and also organic nitriles interact strongly with cations which are capable of back donation such as Cu^+ , Ag^+ , Au^+ , which donate d electrons into π^* antibonding orbital of the nitrile group [65-69]. Due to its nucleophilicity, acetonitrile solvates strongly Cu(I) [66]. Thus, the process (0) is attributed to the anodic oxidation of copper whereas the process (I) to the reduction of the solvated $[\text{Cu}(\text{CH}_3\text{CN})_4]^+$ [66a] which was observed at -0.346 V for AN / Bu_4NBF_4 system. *Kolthoff* and *Coetzee* [70] found that the reduction Cu(I), at the dropping mercury electrode, in acetonitrile occurs at -0.36 V.

The attribution of the process (II) was more complicated. The peak current of the process (II) is found to be dependent on the concentration of the anion of the supporting electrolyte. The peak current I_{pI} decreases with an increasing of the concentration of BF_4^- whereas I_{pII} increases in the same manner and could indicate the complexation of Cu(I) by BF_4^- . The order of reaction in relation to BF_4^- concentration in AN / Bu_4NBF_4 suggests the attribution of the process (II) to the reduction of the copper(I) tetrafluoroborate complex.

Potentiodynamic measurements reveals no formation of $[\text{Cu}(\text{BF}_4)]$ -film onto the electrode surface as suggested by *Padma* [71] for $[\text{Cu}(\text{PF}_6)]$, rather the dissolution of the copper. The OCP-time investigation shows that the potential decreases exponentially as expected for the diffusion of the copper(I) complex in the electrolytic solution (Fig. 7).

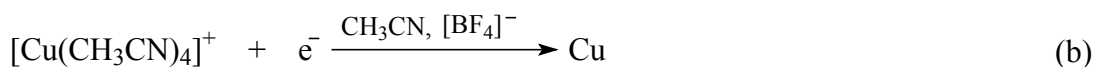
The diffusional mass transport has been ascertained by the double segment electrode. Also, the cyclic voltammograms recorded simultaneously at the copper working electrode and the platinum indicator electrode of the DSE presented similar behaviors as in Fig. 2.

The depletion of anions in the neighborhood of the electrode area, into motionless electrolyte, results in a decrease of the dissolution of copper with an increase of the number of cycles and therefore the peak height (I) decreases.

A qualitative interpretation of the cyclic voltammograms of a copper electrode in acetonitrile in the presence of Bu_4NBF_4 can be summarized by the following mechanisms (scheme 11).

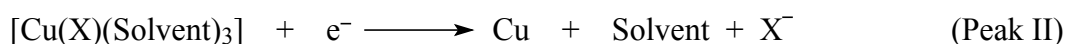
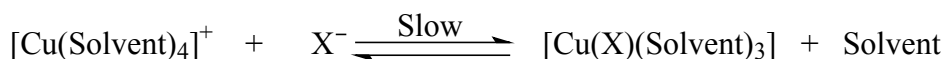
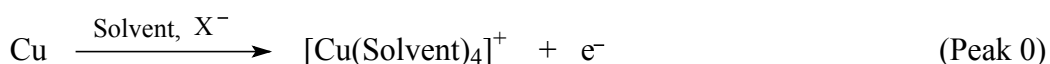
The anodic dissolution of copper occurred in the region of peak (0) at around -0.260 V (schema 11a); the Cu(I) generated is stabilized by acetonitrile by forming of $[\text{Cu}(\text{AN})_4]^+$ ions which are reduced to copper in the region of peak (I) at around -0.346 V (schema 11b). A part of $[\text{Cu}(\text{AN})_4]^+$ reacts with $[\text{BF}_4]^-$ by a slow substitution reaction (schema 11c); this reaction was suggested by studying the influence of the concentration of $[\text{BF}_4]^-$ on the process (II) which revealed an order of reaction equal to 1. Then, the copper(I) complex formed with $[\text{BF}_4]^-$ is reduced at more negative potential at around -1.437 V (schema 11d).

This mechanism (scheme 11) is corroborative with the coulometry investigations where we found a relation between the charge of processes (I) and (II), $Q_I = Q_{I'} + Q_{II}$.


Scheme 11

The cyclic voltammograms recorded in acetonitrile / LiClO_4 , Et_4NClO_4 were quite similar to those of acetonitrile / Bu_4NBF_4 system and resulted to a shift of potential of both processes towards more negative potential.

Investigations in THF, which does not contained CN group, reveal similar behavior with the process (I) appearing at more positive potential and the process (II) at more negative potential than the previous systems. The process (I) is attributed to Cu(I) and the process (II) to the reduction of complex formed between Cu(I) and the anion (X^-) of the supporting electrolyte. The mechanism is quite identical to those described in scheme 11. Thus, one can suggest the following mechanism occurring at the copper electrode (scheme 12):


Scheme 12

The solvated Cu(I) is reduced at more negative potential (-0.346 V and -0.409 V respectively) in AN / Bu_4NBF_4 and in AN / LiClO_4 , Et_4NClO_4 systems whereas the less solvated Cu(I) is reduced at more positive potential ($+0.341$ V) in THF / Bu_4NPF_6 . However, the process (II) appears at -1.437 , -1.600 and -1.712 V in AN / Bu_4NBF_4 , AN / LiClO_4 , Et_4NClO_4 and THF / Bu_4NPF_6 systems, respectively.

3.2. Electrochemical behavior of nitriles used as starting material

3.2.1. 1,1,3,3-tetracyanopropane (TCP)

The cyclic voltammogram (CV) of TCP recorded in AN / Bu₄NBF₄ at the platinum electrode shows two well-defined reduction peaks (Fig. 13) at -1.228 V (A) and at -1.453 V (B). The reduction products decompose slowly to give a kinetically linked product which is oxidized at -1.225 V (B1) and irreversibly at a much more positive potential, +0.606 V (C).

The cyclovoltammogram of the same solution at the copper electrode exhibits three redox processes (Fig. 14). They are observed during the forward scan at -0.343 V (I), -1.342 V (A) and -1.608 V(B), respectively. The process (I) is attributed to the reduction of the solvated Cu(I) obtained in the anodic region more positive than -0,200 V (0).

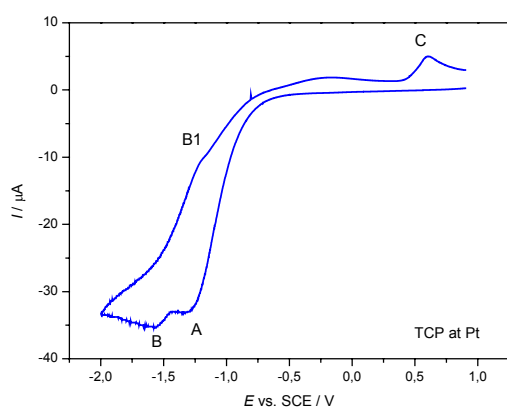


Fig. 13 CV of TCP at a platinum (AN, 0.1 M Bu₄NBF₄, 0.1 V s⁻¹).

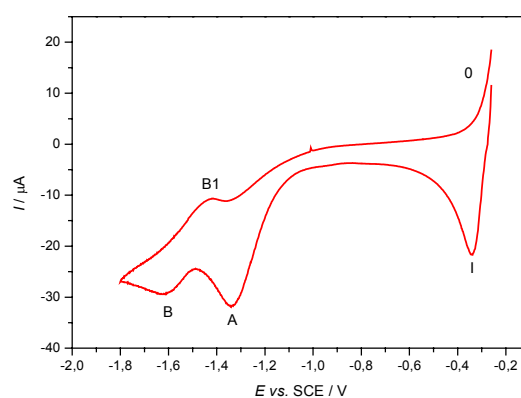


Fig. 14 CV of TCP at a copper (AN, 0.1 M Bu₄NBF₄, 0.1 V s⁻¹).

The voltammograms reveal that TCP has the characteristic features of systems that undergo two electron transfer processes at two localized redox centers and characterized by a successive two step reduction. The variation of peak currents is proportional to the square root of the potential scan rates. The peak currents increase with the scan rate (Fig. 15). The ratio of the current peak I_{pB1}/I_{pB} increases also with the scan rate and is approached to 1 at high scan rate (Fig. 16). The difference between the cathodic (B) and the anodic (B1) peak potentials (average, 0.243 V) is greater than 0.059/1 V and increases with increasing scan rate. These results show that the third system (B) is not reversible moreover it is consistent with a quasi-

reversible behavior. Both cathodic peaks were found to show a linear shift towards cathodic potentials with increasing scan rate (Fig. 17).

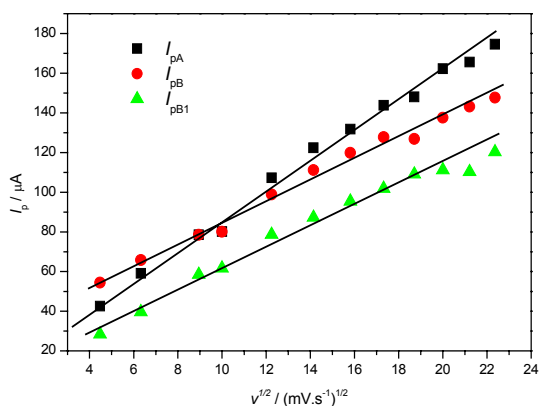


Fig. 15 Variation of peak currents with $v^{1/2}$ for TCP (AN, 0.1 M Bu_4NBF_4 , 0.1 V s^{-1}).

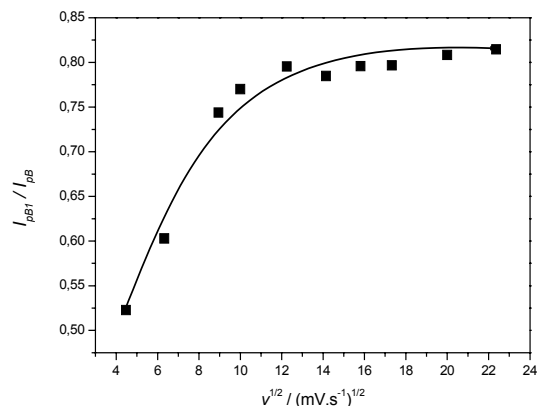


Fig. 16 Variation of I_{pB1} / I_{pB} with $v^{1/2}$ for TCP (AN, 0.1 M Bu_4NBF_4 , 0.1 V s^{-1}).

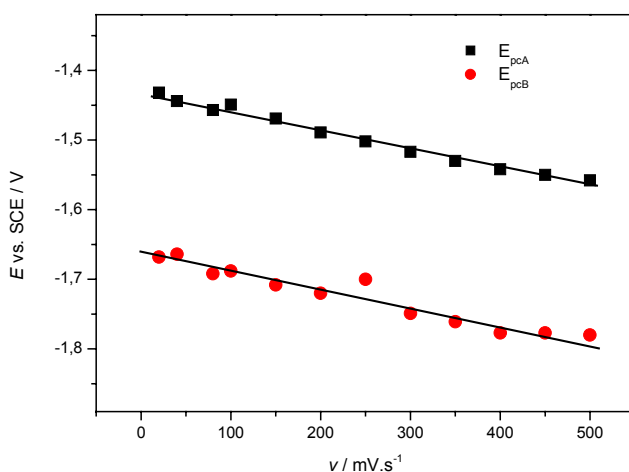


Fig. 17 Effect of the variation of the scan rate on the cathodic peak potentials (AN, TCP, 0.1 M Bu_4NBF_4 , 0.1 V s^{-1}).

The peaks (A) and (B) appear at sufficiently different potentials. The potential separation of both peaks $\Delta E = E_B - E_A$ are negative and are fairly constant with the scan rate, the average value is -230 mV. Thus, the electroactive species responsible of (A) is easier to reduce than (B) and the first charge transfer process has the properties of the irreversible EC mechanism [72]. This is confirmed by the variation of peak current function of process (A) with the scan rate (Fig. 18). Indeed, the peak current function decreases as the scan rate increases. This behavior is indicative for an EC mechanism and may be the product of the first electron transfer is being consumed by a very fast chemical reaction.

The peak current function of (B) is also plotted against the scan rates as shown in Fig. 19. The shape of $I_{pB}/v^{1/2}$ vs. v for process (B) is that predicted by *Nicholson and Shain* [73-75] for EC mechanism [76]. The peak current function decreases slightly as the scan rate increases and combining this to the behavior of the ratio I_{pB1} / I_{pB} with the scan rate (Fig. 16), we suggest that the product of the second electron transfer reaction is consumed by a very slow chemical reaction [77]. Similar behaviors were found by *Adams et al.* [78] with aromatic amines. They report that such behavior could be due to the fact that the follow-up chemical reaction is minimized at rapid scan rates.

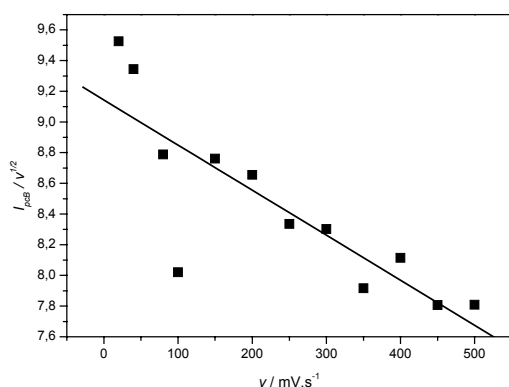


Fig. 18 Variation of the peak current function with scan rate for the process (A) (AN, TCP, 0.1 M Bu_4NBF_4 , 0.1 V s^{-1}).

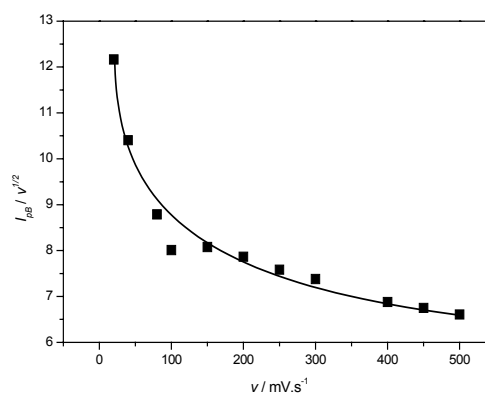


Fig. 19 Variation of the peak current function with scan rate for the process (B) (AN, TCP, 0.1 M Bu_4NBF_4 , 0.1 V s^{-1}).

In order to shed some light on the mechanism that give rise to the processes (A) and (B), we have studied the influence of the concentration of TCP on the voltammogram. This influence is reported as an important diagnostic, indicative of second-order, following chemical reaction [72].

3.2.1.1. Influence of the concentration of TCP on the voltammogram

The voltammograms obtained by varying the concentration of TCP in the solution are shown in Fig. 20. The CVs result in an increase of the peak currents related to the processes (A) and (B) and in a shift of their potentials towards more negative values. Surprising is the appearance of a fourth redox signal at -0.937 V (D) between the processes (I) and (A). This new process is chemically irreversible. It seems to be connected to the reduction of a copper(I)-nitrile complex.

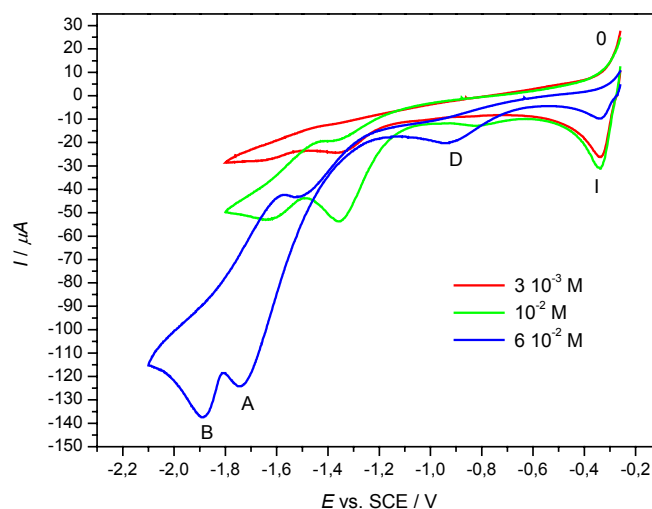
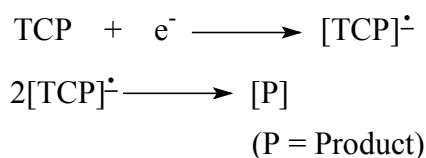


Fig. 20 Influence of the concentration of TCP on the CVs (AN, 0.1 M Bu₄NBF₄, 0.1 V s⁻¹).

The qualitative pictures obtained from the cyclic voltammograms run at different scan rates and at different concentration, with respect to potential shifts, peak current ratio and the current peak function, ascertain that the first electron transfer in the reduction of TCP occurs with an irreversible, second-order, following reaction as described by *Rossiter and Hamilton* [72].



Scheme 13

However, the overall reduction processes involve an ECEC (Electron transfer – Chemical transfer – Electron transfer – Chemical transfer) mechanism.

3.2.1.2. Effect of the temperature on the cyclic voltammogram

The electrochemical behavior of TCP process in a temperature range between 22 and –30 °C was studied in AN / Bu₄NBF₄. Fig. 21 depicts the cyclic voltammograms obtained at the copper electrode. The decrease in temperature from 22 to –30 °C results in a cathodic shift of the peak potentials with the appearance of a peak (D) in the potential range comprises between –0.60 and –0.90 V. The potential of the process (A) shifts significantly towards more

negative values whereas the processes (I) and (D) shift slightly in the same manner. The peaks (A), (B) and (I) decrease with the temperature. The peak (B) disappears at around $-17\text{ }^{\circ}\text{C}$ whereas the new peak (D) grows out at around $+0.840\text{ V}$. At this potential, no electron transfer was observed at the platinum electrode. The disappearance of the cathodic peak (B) could indicate the dissociation or the inactivity of the species from which it derives in the potential range from -1.6 to -2.0 V .

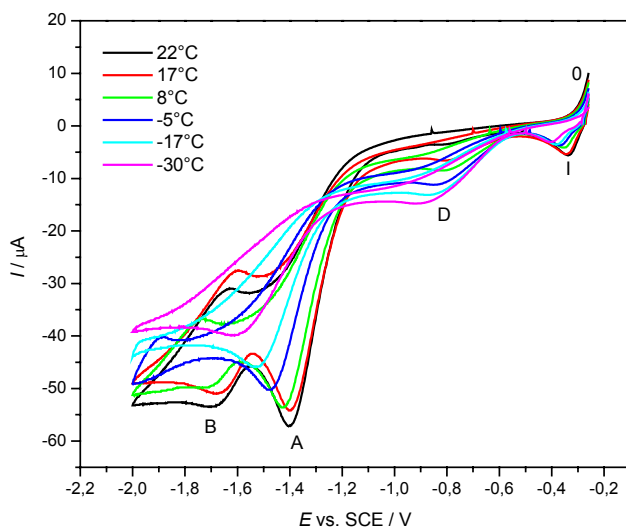


Fig. 21 Effect of the temperature on the cyclic voltammograms of TCP.

The temperature dependence of the peak currents is qualitatively indicative of the diffusion coefficient which is related to the mass transport. The magnitude of the current is given by the relation [79]:

$$I = A F j \quad (4)$$

$$\text{with } j = k c \quad (5)$$

$$\text{and } k = A_f \exp(-E_A/RT) \quad (6)$$

Where F is the Faraday constant ($96\,485\text{ C mol}^{-1}$), A is the electrode area (cm^2) and j the flux of the reactants reaching the electrode surface ($\text{moles cm}^{-2}\text{ s}^{-1}$). k is the heterogeneous rate constant for the electron transfer, c the concentration (moles cm^{-3}) of the reactants at the electrode surface, E_A the energy of activation, A_f the frequency factor, R the molar gas constant ($8.315\text{ J K mol}^{-1}$) and T the temperature (K). By combining equations 4-6:

$$I = A A_f F c \exp(-E_A/RT) \quad (7)$$

The energy of activation can be obtained by rewriting equation 7, known as Arrhenius equation, in logarithmic form as:

$$\ln I = \ln (A A_F F c) - E_A/RT \quad (8)$$

from which it follows that a plot of $\ln I$ versus $1/T$ (Fig. 22) should be a straight line having a slope of $-E_A/R$. A straight line was obtained only for process (A). The process(I) decreases exponentially whereas the process(D) increases in the same manner (Fig. 22).

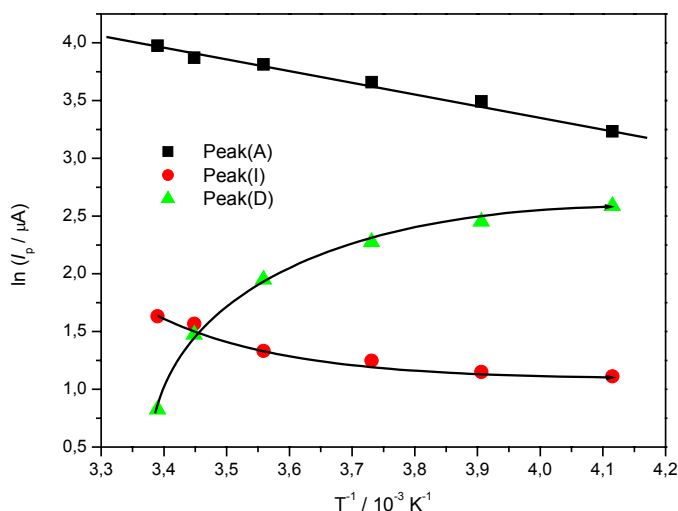


Fig. 22 Arrhenius plots the temperature dependence of the energy of activation (AN, TCP, 0.1 M Bu_4NBF_4 , 0.1 V s^{-1}).

From the straight line of the Arrhenius plot related to the process (A), the energy of activation for the process(I) is found to be 8.1 kJ mol^{-1} . Levich found for diffusion process the energy of activation of 12 kJ mol^{-1} . The energy of activation of chemical reactions is clearly larger.

In an effort to characterize the process (D) (Figs. 20 and 21), potential-controlled electrolysis has been carried out.

3.2.1.3. Controlled potential electrolysis of a solution of TCP

Potential-controlled electrolysis was carried out, in $4 \cdot 10^{-2} \text{ mol dm}^{-3}$ solution of TCP in AN / Bu_4NBF_4 (0.1 mol dm^{-3}), at -2 V . At the end of the electrolysis, the solution was examined by cyclic voltammetry. The voltammograms were recorded before and after the electrolysis at the platinum (Fig. 23) and at the copper electrode (Fig. 24).

At the platinum, the voltammogram reveals the appearance of the process (D) at the same potential (at around -0.83 V) as in Figs. 20 and 21. The processes (A) and (B) shift towards more negative potentials. An oxidative process appears around -0.028 V during the backward scan and ascribed to the oxidation of copper generated during the reduction of Cu(I)-nitrile complex (process D).

More interestingly, the cathodic peak current (D) become high and large at the copper electrode indicating that the electroactive species from which it derives has increased. The peak current (A) decreases whereas the peak current (B) increases. The processes (A) and (B) shift also cathodically in contrast with (D) which remains at the same potential (-0.797 V). Thus, the process (D), observed during the reduction of TCP, is originated from Cu(I)-nitrile complex.

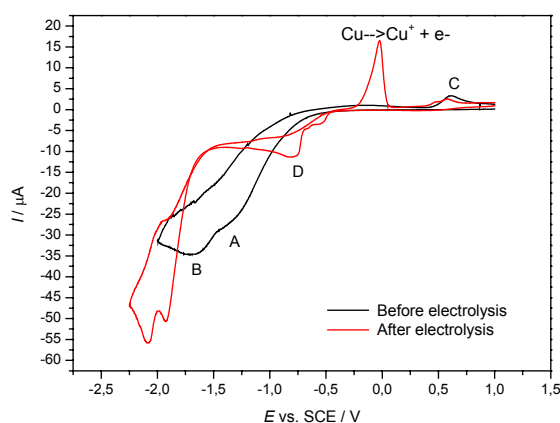


Fig. 23 CVs of TCP after electrolysis at the platinum electrode (AN, 0.1 M Bu_4NBF_4 , 0.1 V s^{-1}).

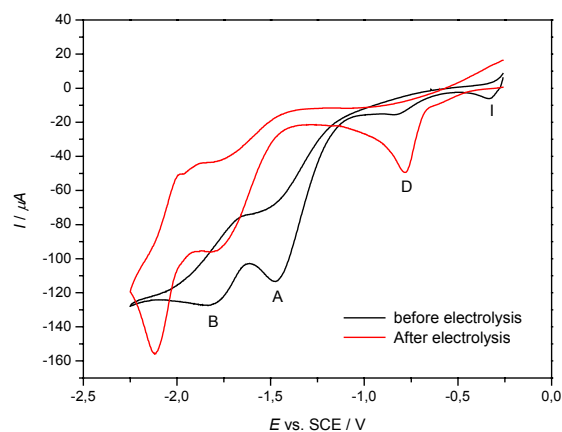


Fig. 24 CVs of TCP before and after electrolysis at the copper electrode (AN, 0.1 M Bu_4NBF_4 , 0.1 V s^{-1}).

3.2.1.4. Behavior of TCP in the presence of different donors

The cyclic voltammetry of TCP has been investigated in the presence of different donors used in this work to prepare Cu(I)-TCP derivatives. The aim of this investigation was to shed some light on the influence of each donor on the cyclic voltammograms.

Thus, cyclic voltammograms of TCP ($5.2 \cdot 10^{-3}$ M) have been investigated in the presence of different donors such as PPh_3 (10^{-2} M) and phenanthroline (phen, $4 \cdot 10^{-3}$ M). Fig. 25 shows comparative voltammograms run at 100 mV s^{-1} at the copper electrode in AN / Bu_4NBF_4

within the potential range from -0.26 V to -1.80 V. When PPh_3 is added to a solution of TCP, the voltammogram reveals four well defined cathodic peaks, namely (I), (E), (A) and (B). A new peak (E) appears at -0.704 V very close to the potential of (D). The addition of phen to the solution mixture results in an increasing of the peak current of the process (B) whereas the peak (E) remains constant within the potential range scanned. Investigation of the CV of the PPh_3 alone reveals the presence of peak (E) at the same potential (Fig. 25) and is not affected by addition of phen. The process (E) could be unambiguously assigned to the electroreduction of Cu(I)-PPh_3 complex.

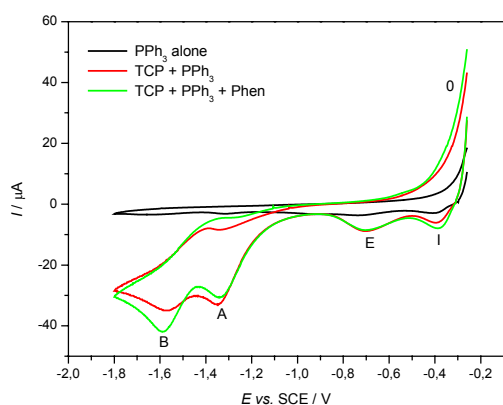


Fig. 25 CVs of TCP in the presence of PPh_3 and Phen (AN, 0.1 M Bu_4NBF_4 , 0.1 V s^{-1})

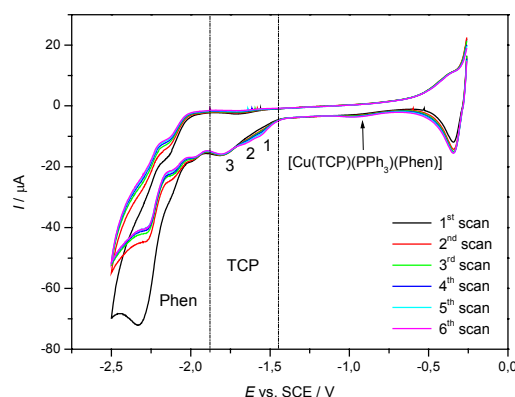


Fig. 26 CVs of TCP in the presence of PPh_3 and Phen at an extended potential range recorded as in Fig. 25.

It appears that Phen is reduced at more negative potentials as shown in Fig. 26. The voltammograms are more complicated and all mechanism of the different processes cannot be assigned presently due to the electron-donating capabilities, provided by the lone electron pair of the nitrogen, and to the conjugated π -electron system of 1,10-phenanthroline which provides a possibility of electronic charge delocalization [80]. We found that an increase of the potential range results in a negative shift of peak (E) by about 260 mV suggesting the reduction of $[\text{Cu}(\text{TCP})(\text{PPh}_3)(\text{Phen})]$ complex.

From the experimental results described above, the potential range of some components present in the electrolytic solution have been delimited (Fig. 26). Three peak currents are found, as the scan is performed, in the domain assigned to the reduction of TCP and namely (1), (2), (3). Peak (1) appears at -1550 mV near the reduction peaks of TCP and grows with the scan. *Santhanam* and *Bard* [81] reported, on the basis of cyclic voltammetry, the electroreduction of

PPh₃ in N,N-dimethylformamide (DMF) and they found a one-electron reversible reduction at around -2.715 V. They suggest, after a spectrometric examination of the solution, that this reduction process is a PPh₃-CH₃CN reaction.

In order to know more about PPh₃ / CH₃CN system, by cyclic voltammetry, we have investigated the voltammograms of a solution of PPh₃ in CH₃CN at different scans (Fig. 27). At the first scan, only two processes (I) and (E) are observed. As it is shown in Fig. 27, the process (II) does not appear during the first cycle of the scan but appears during the following scans and grows continuously meanwhile a new one (F) is formed at -0.934 V. The process (II) appears around -1.360 V in the same way as in Fig. 2 and is assigned to the reduction of [Cu(BF₄)(CH₃CN)₃]. *Wagenknecht* cited by *Dessy et al.* [82] explored the electrolytic reduction of PPh₃ at large-scale and after identification of the products he concluded that the initially formed radical anion is decomposed to phenyl radical and diphenylphosphane anion. We propose, based on our results, that process (E) deals with Cu(I)-PPh₃ complex, whereas the process (F) could be ascribed to the reduction of the free PPh₃ released from the complex.

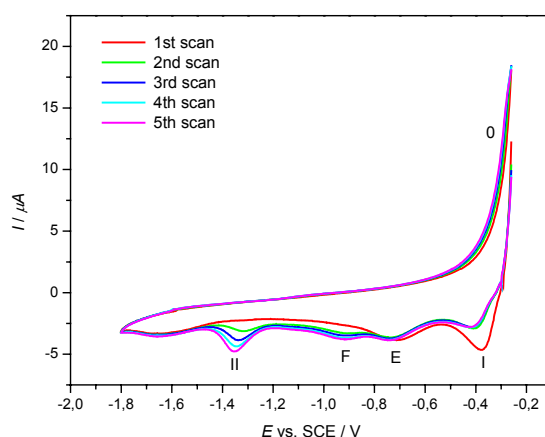


Fig 27 CV of PPh₃ (10^{-2} M) at the copper electrode (AN, 0.1 M Bu₄NBF₄, 0.1 V s⁻¹).

Several studies on the electrochemistry of PPh₃ have been published [81-83]. Many investigators have studied the behavior of PPh₃ in acetonitrile at the carbon paste electrode [84], platinum electrode [83a], hanging mercury drop electrode [81] and vitreous carbon electrode [83e]. But little is known on their behavior in the negative potential region.

The cyclic voltammetry behaviors of TCP reveal that it presents the characteristic features of systems that undergo two electron transfer processes, at two localized redox centers, characterized by a successive two steps reduction on both electrodes. Due to the minus-I

effect of the cyano groups, the acidity of the C–H bonds at the terminal carbon of the substituted propane is higher than that of the central CH₂ group. This has been proved theoretically by quantum calculation of the deprotonation energies which were found to be –219 kJ mol⁻¹ for the terminal carbon and –127 kJ mol⁻¹ for the central CH₂ [22b]. In our first analyses, it had been suggested erroneously that the hydrogen radical splitting at the terminal carbon occurs first at –1.342 V followed by the reduction of H on the central CH₂ group.

It appears that the second reduction process is more difficult than the first as ascertained by the negative value of $\Delta E = E_B - E_A = -230$ mV. Thus, the first charge-transfer process has the properties of the irreversible EC mechanism [72]. The potential of (A) and (B) shift cathodically as the scan rate increases, also similar behavior is observed when the concentration of TCP in the solution increases. The peak current of (A) and (B) increase with the scan rate and the ratio I_{pB1}/I_{pB} increases in the same manner to become independent at high scan rates.

The peak current function, $I/v^{1/2}$, of the process (A) decreases as the scan rate increases. This diagnostic criteria argue favorably for an electrochemical reaction coupled to an irreversible, second-order, following reaction. However, the peak current function of the process (B) is large at low scan rates and decreases to a constant value at higher scan rates indicating an electrochemical reaction coupled to an irreversible, first-order, following reaction [72]. Thus, the peak current function of both processes measured as a function of the scan rate argue unambiguously and favorably for ECEC mechanism.

3.2.2. Malononitrile

Electrochemical behavior of malononitrile has been examined by cyclic voltammetry in AN / Bu₄NBF₄. The CVs recorded at the platinum (Fig. 28) and at the copper electrode (Fig. 29) are presented.

At the platinum electrode, a reduction peak appears at –1.402 V (G) and the reduction product decomposes slowly to give a product which is oxidized irreversibly on reversal scan at a much more positive potential, +0.426 V (H).

At the copper electrode, CV shows three well-defined reduction peaks (Fig. 29). The first reduction peak appears at –0.334 V (I), the second one at –0.860 V (J) and the third one appears at –1.749 V (G). The processes (0) and (I) are already known (Fig. 2) whereas the

process (J) appears within the same potential range as the previous process (D) and is assigned to the reduction of Cu(I)-nitrile complex. The process (G) is unambiguously ascribed to the reduction of free malononitrile.

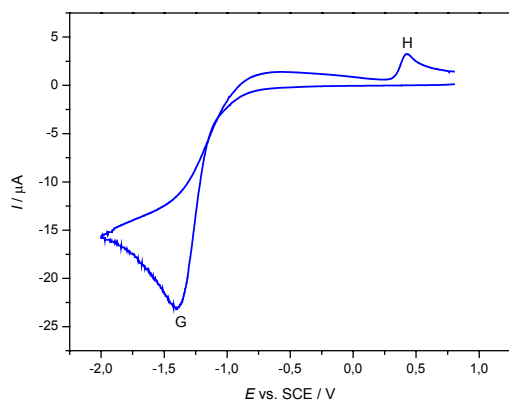


Fig. 28 CV of malononitrile ($2.54 \cdot 10^{-2}$ M) at Pt electrode (AN, 0.1 M Bu_4NBF_4 , 0.1 V s^{-1}).

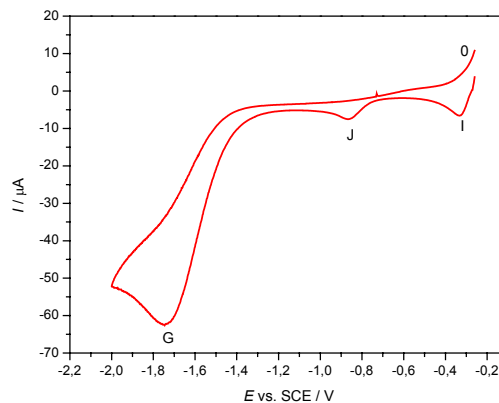


Fig. 29 CV of malononitrile ($2.54 \cdot 10^{-2}$ M) at Cu electrode (AN, 0.1 M Bu_4NBF_4 , 0.1 V s^{-1}).

The peak height of all processes varies with the square root of the scan rate (Figs. 30 and 31) indicating diffusion controlled processes. The peak current function ($I_p / \nu^{1/2}$) of the reduction process (G) decreases with an increasing of the scan rate (Figs. 32 and 33). The potential of processes (I) and (J) at the copper electrode, shift slightly whereas the peak potential of third process (G) shifts cathodically towards negative potentials as the scan rate increases. This results indicate that the reduction product is not stable within the time of the scan [81,85]. Such behaviors are indicative for an electrochemical reaction coupled to an irreversible, first-order, following reaction (EC mechanism) [72].

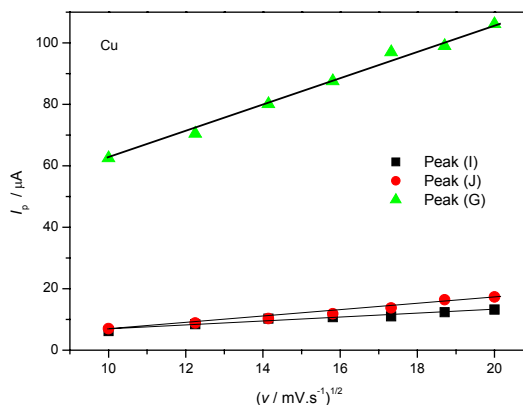
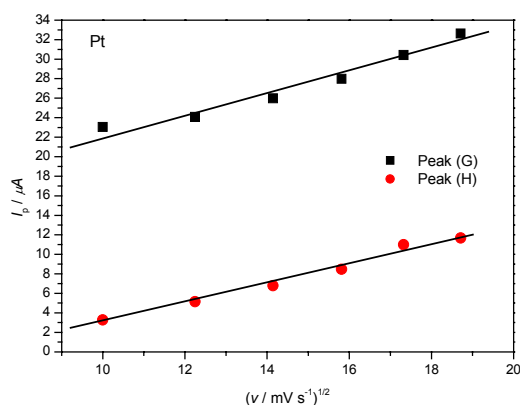


Fig. 30 Effect of the variation of the scan rate on the peak potentials at platinum electrode (AN, 0.1 M Bu₄NBF₄, 0.1 V s⁻¹).

Fig. 31 The variation of the cathodic peak potentials with scan rate at copper electrode (AN, 0.1 M Bu₄NBF₄, 0.1 V s⁻¹).

Investigation of the peak height of processes (I), (J) and (G) as function of the scan rate shows that the peak (G) grows faster than the others as shown in Figs. 30 and 31. The reduction of malononitrile is followed up by a chemical reaction which yields a species oxidizable at more positive potential (+0.426 V).

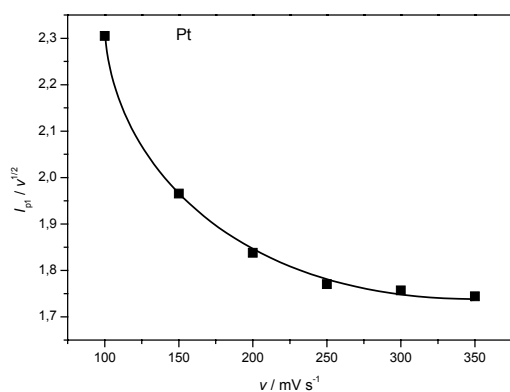


Fig. 32 The variation of the peak current function vs. scan rate at Pt electrode (AN, 0.1 M Bu₄NBF₄, 0.1 V s⁻¹).

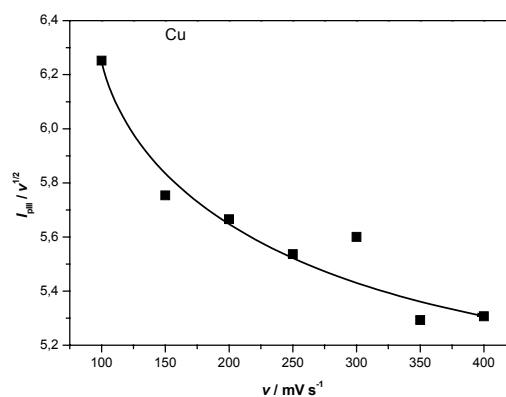


Fig. 33 The variation of the peak current function vs. scan rate at Cu electrode (AN, 0.1 M Bu₄NBF₄, 0.1 V s⁻¹).

3.2.3. Phenylacetonitrile

3.2.3.1 Tetrahydrofuran / Bu₄NPF₆

The cyclic voltammetric behavior of phenylacetonitrile (PhAN) is investigated in THF / Bu₄NPF₆ at the platinum and at the copper electrodes. At the platinum electrode one oxidation peak was found in the potential range studied and appears at -550 mV (M). However, at the copper electrode, the voltammogram shows four reduction peaks, namely (I), (K), (II) and (L) at +0.32, -1.483, -1.723 and -1.902 V respectively (Fig. 34). On reversal of scan, an oxidation peak appears at around -590 mV (M) close to the oxidation one observed at the platinum electrode.

In Fig. 35, a comparative cyclic voltammograms recorded in THF / Bu₄NPF₆ / PAN and in THF / Bu₄NPF₆ systems is presented. It shows that peak (II) appears at the same potential as in THF / Bu₄NPF₆ system which was attributed to the reduction of copper(I) complex formed with hexafluorophosphate. The process (I) shift towards less positive potential range by about 299 mV indicating the strong interaction between copper(I) and phenylacetonitrile.

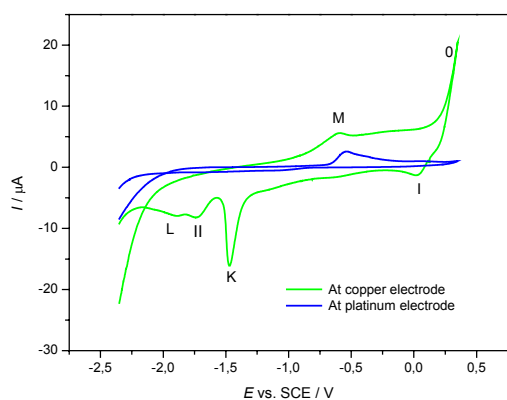


Fig. 34 CVs of PAN at the Pt and Cu electrodes (THF, 0.1 M Bu₄NPF₆, 0.1 V s⁻¹).

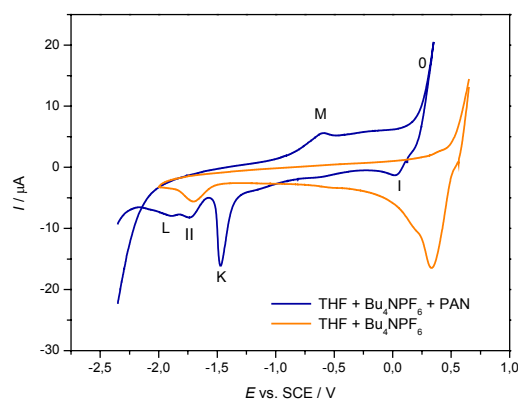


Fig. 35 Comparative CVs of PAN at the Cu electrode (THF, 0.1 M Bu₄NPF₆, 0.1 V s⁻¹).

3.2.3.2. Acetonitrile / Bu₄NBF₄

The cyclic voltammograms of PhAN are also recorded in AN / Bu₄NBF₄. At the platinum electrode, a reduction peak is observed at -1.462 V (N) during the forward scan and an oxidation peak appears at +0.242 V (P) during the reverse scan (Fig. 36). The height of the peaks increase with the scan rate indicating diffusion controlled processes. Both redox systems are attributed to the reduction and oxidation of PhAN.

At the copper electrode, the cyclic voltammogram shows three redox processes labeled (I), (Q) and (N) at around -0.371, -0.907 and -1.478 V, respectively (Fig. 37). The reduction of PhAN is similar to the reduction of malononitrile. Peaks (Q) and (N) are broad. The cathodic peak height increases also with an increase of the scan rate (Fig. 38). The peak current function decreases with an increase of the scan rate (Fig. 39) indicating that the reduction product undergoes further chemical reaction. Thus PhAN is reduced like MDN according an EC mechanism. The processes (K) in THF and (N) in AN appear at the same potential (ca. 1.480 V) at the copper electrode suggesting their attribution to the reduction of PhAN to PhAN^{•-}. In THF a cathodic peak (L) remains not assigned and could be ascribe to the

reduction of Cu(I)-PhAN complex which yields PhAN oxidizable to $\text{PhAN}^{\cdot+}$ on reversed scan at about +0.590 V (M) at a platinum and at a copper electrode.

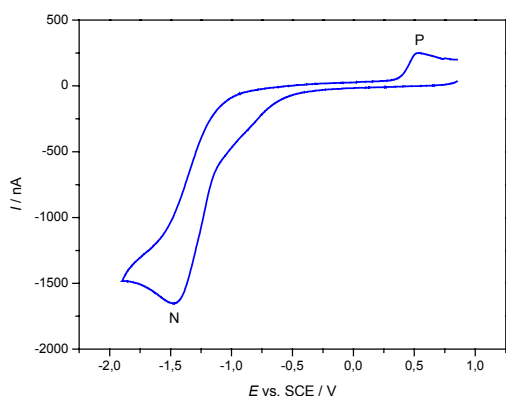


Fig. 36 CV of PAN at the platinum electrode (AN, 0.1 M Bu_4NBF_4 , 0.15 V s^{-1}).

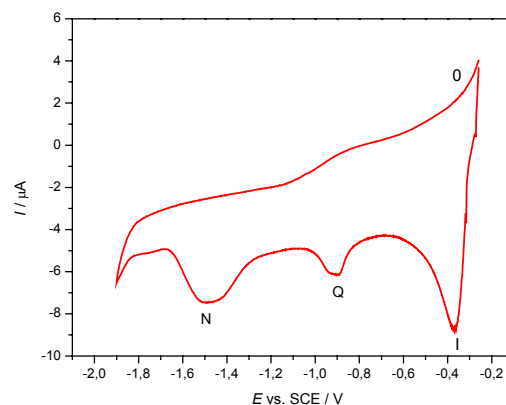


Fig. 37 CV of PAN at the copper electrode (AN, 0.1 M Bu_4NBF_4 , 0.15 V s^{-1}).

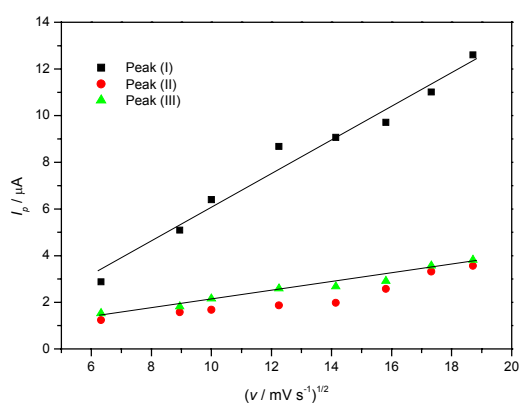


Fig. 38 The variation of the scan rate with the peak potentials at Cu electrode (AN, 0.1 M Bu_4NBF_4 , 0.1 V s^{-1}).

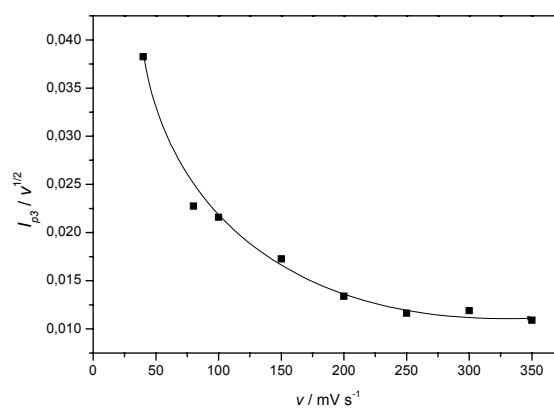


Fig. 39 The variation of the peak current function (N) vs. scan rate at Cu electrode (AN, 0.1 M Bu_4NBF_4 , 0.1 V s^{-1}).

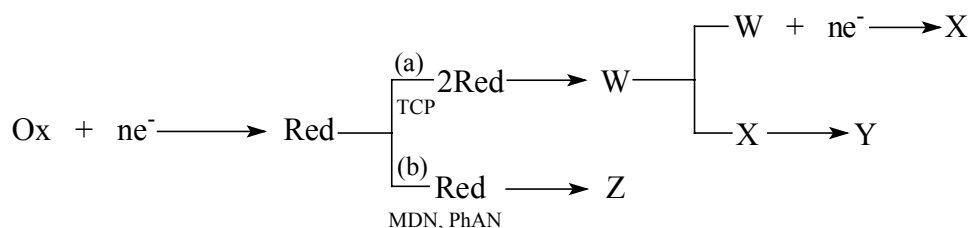
3.2.4. Discussion on the reduction of starting materials

The results of the electrochemical behavior of three kinds of nitriles with $\text{p}K_a > 10$ (1,1,3,3-tetracyanopropane, malononitrile and phenylacetonitrile) reveal that they are electrochemically reduced according to an electrochemical reaction coupling with an irreversible chemical reaction (EC mechanisms).

The interpretation of the electrochemical behavior of TCP was more complicated. The voltammograms recorded both at the platinum and at the copper electrodes reveal that TCP undergoes two electron transfer processes at two localized redox centers. The properties of cyclic voltammetric data recorded suggest that the first reduction process (A) is easier than

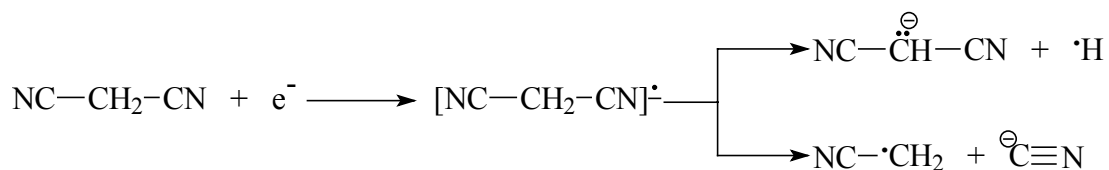
the second (B). The process (A) undergoes an electrochemical reaction coupled to an irreversible, second-order, following reaction whereas (B) undergoes an electrochemical reaction coupled to an irreversible, first-order, following reaction. The overall electrochemical mechanism is assumed to be an ECEC mechanism.

Malononitrile and Phenylacetonitrile present similar electrochemical behavior both at the platinum and at the copper electrode in AN / Bu₄NBF₄. Experimental data reveal that they are reduced according to an electrochemical reaction coupled to an irreversible, first-order, following reaction EC mechanism. The electrochemical behavior of TCP, MDN and PhAN is summarized on scheme 14.



Scheme 14

Schäfer et al. [23] reported the electrochemical syntheses of copper nitrile complexes by potentiostatic dissolution of a copper anode and cathodic reduction of malononitrile in a one-step reaction. As results, all compounds proved to be ionic binuclear Cu(I) complexes which crystallized with dicyanomethyl anion and in which the copper atoms are bridged by a cyano group. These results indicate that malononitrile undergoes an electrolytic reduction which could be summarized as in scheme 15.



Scheme 15

At the copper electrode, the cyclic voltammograms of the nitriles studied in this work present an irreversible peak between -800 mV and -1000 mV. This reduction peak is attributed unambiguously to the reduction of Cu(I)-nitrile complex. *Lebrilla et al.* [85] mentioned that *end-on* coordination of Cu(I) with nitrile should occur from simple electrostatic considerations. This could also be explained by a synergetic effect between back bonding and the normal weak acid-base interaction (between Cu(I) and nitrile) which provides a strong interaction [66b].

3.3. Electrosynthesis of copper(I) complexes with nitriles possessing α -hydrogen

3.3.1. 1,1,3,3-tetracyanopropane as starting material

The first series of experiments related to the direct electrosyntheses of organonitrilecopper(I) compounds is devoted to the preparation of TCP–Cu(I) and its derivatives. Such compounds were already achieved potentiostatically by *Günther* [22b] whom achieved cuprate complexes with the general formula $\{(C_4H_9)_4N[Cu(TCP)BF_4]\}_n$ using TCP in AN / Bu₄NBF₄ at –1.920 V. However, the structure of these compounds was not possible schematically due to the complexities of the spectra and consequently, the mechanism of the reaction was very difficult to describe fully. In an effort to elucidate the structure and the mechanism of the reaction by which TCP–Cu(I) can be prepared, the electrosynthesis has been carried out by the galvanostatic procedure using TCP as starting material in AN / Bu₄NBF₄.

3.3.1.1. Electrosynthesis of bis{ $(\mu$ -tricyanomethanido)bis(triphenylphosphane)copper(I)} [Cu(μ -C(CN)₃)(PPh₃)₂]₂ (**1**)

The complex **1** is obtained after anodic dissolution ($I = 50$ mA) of metallic copper into a solution of TCP and triphenylphosphane (PPh₃) in AN / Bu₄NBF₄ at 0 °C:



Scheme 16

As shown in the previous paragraphs, the cyclic voltammetry has revealed that TCP undergoes a successive two-step reduction. This has also been shown by performing the electrosynthesis by controlling the current externally and measuring the changes in cathodic potential (vs. SCE) with the evolution of TCP during the electrolysis (Fig. 40). The cathodic potential decreases in the beginning and is stabilized at around –1.50 V for a long time. The reduction of the proton from the strong acidic TCP gives hydrogen gas at platinum cathode. After the passage of one Faraday per mole TCP, the potential decreases during the third hour of the electrolysis to reach –2.0 V.

The electrosynthesis of copper complex **1** is stopped after the passage a charge of 966 C, which corresponds to one electron per mole, has passed through the solution. The carbanion $\text{TCP}^{\cdot-}$ generated is not stable and initiates a decomposition pathway.

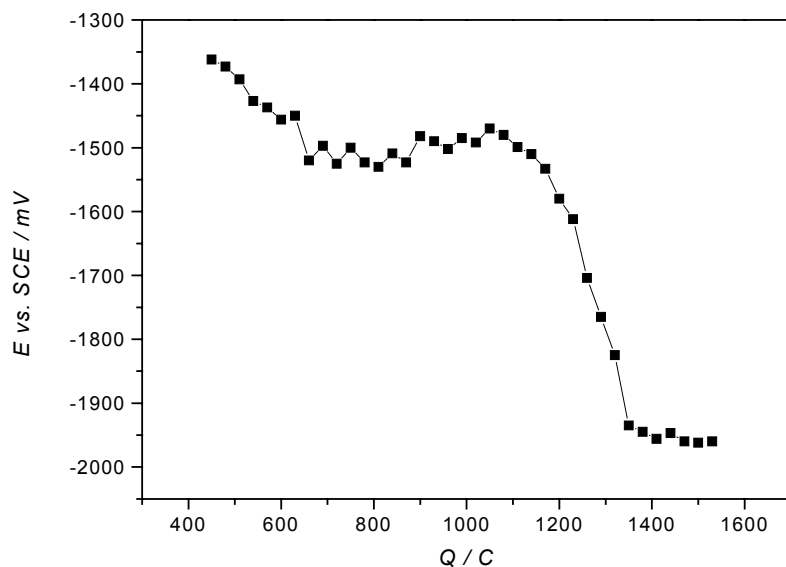


Fig. 40 Changes in the cathodic potential during the electrosynthesis ($I = 100$ mA).

After the electrolysis, two phases have been obtained, an upper acetonitrile phase and a lower oil like. The complex **1** crystallizes as colorless crystals from acetonitrile phase of the electrolytic solution at low temperature after evaporation of 50 % of the solvent. **1** has been characterized by X-ray crystal structure analysis which revealed the formation of the tricyanomethanidocopper(I) complex instead of the tetracyanopropanidocopper(I) compound.

The structure of **1** is quite identical to the compound obtained by *Bessler et al.* [86] by classical method using $\text{CuC}(\text{CN})_3$ with an excess of molten PPh_3 .

The molecular structure of **1** is depicted in Fig. 41. The bis(μ -tricyanomethanide) binuclear copper(I) comprises two copper centres bridged by a pair of ionic tricyanomethyl anions $[\text{C}(\text{CN})_3]^-$ and terminally ligated by four triphenylphosphane molecules. So the binuclear complex core structure, composed by a twelve-membered atom ring ($\text{Cu}_2\text{N}_4\text{C}_6$) which folds into a pronounced chair conformation, is formed including a crystallographic centre of inversion in the middle of that ring. Each copper atom is tetrahedrally coordinated and has a distorted tetrahedral geometry with a N_2P_2 donor set, contributed by PPh_3 and $[\text{C}(\text{CN})_3]^-$. Selected interatomic distances and angles are collected in Table 3.

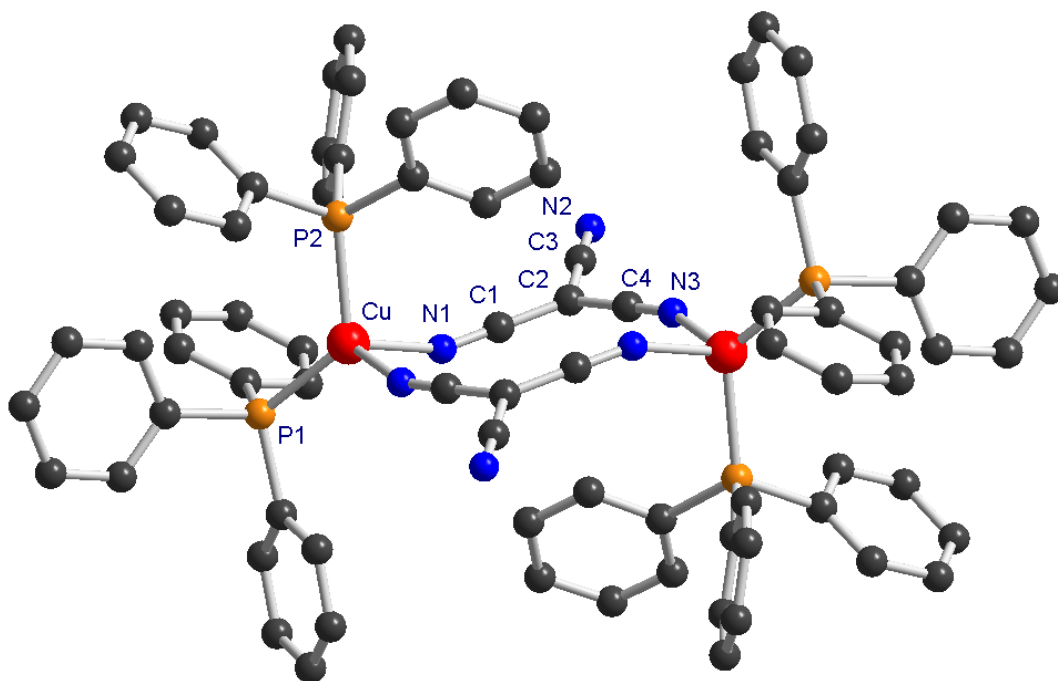


Fig. 41 Crystal structure of the electrochemical synthesized $[\text{Cu}(\mu\text{-C}(\text{CN})_3)(\text{PPh}_3)_2]_2$ (**1**) with selected atomic labelling (Hydrogen atoms are omitted for clarity).

The distortions, around the Cu(I), are due to the steric bulk of the triphenylphosphane ligands which results in large P-Cu-P angles ($124.8(3)^\circ$), intermediate angles N-Cu-P ($102.9(8)^\circ$), and small N-Cu-N angles ($96.1(9)^\circ$). The Cu-N(1) distance ($2.103(2) \text{ \AA}$) is longer than N(3)-Cu ($2.031(2) \text{ \AA}$). The longer Cu-N distance can be assigned to the deviation from the linearity of the C-N-Cu. The P(1)-Cu ($2.261(9) \text{ \AA}$) and P(2)-Cu ($2.306(10) \text{ \AA}$) distances are very close to the average value of 2.26 \AA found for similar complexes [87-89]. For comparison, in Table 4 are summarized selected bond lengths and angles of some similar Cu(I) complexes with CuN_2P_2 core. The Cu-P distances with similar values are in good agreement with the average value of $2.252(44) \text{ \AA}$ established for Cu(I)- PPh_3 complexes[89,90] and the Cu-N distances are comparable. The P-Cu-P angles are also comparable but the N-Cu-N angles are quite different and could be attributed to the angle distortions.

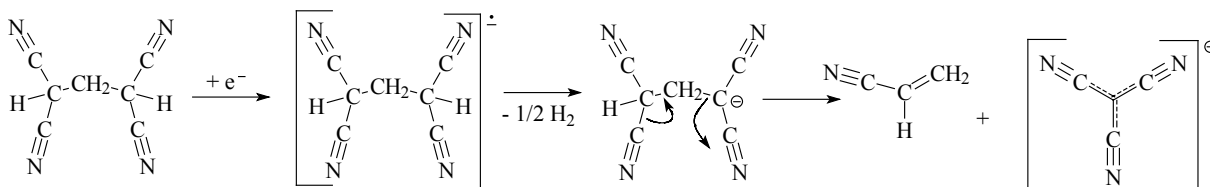
Table 3 Selected bond lengths (\AA) and angles ($^\circ$) of **1**

Bond lengths		Bond angles			
P1-Cu	2.261(9)	C1-N1-Cu	151.9(2)	N1-Cu-P1	105.0(7)
P2-Cu	2.306(10)	C4-N3-Cu	159.4(2)	N3-Cu-P2	103.7(8)
Cu-N3	2.031(2)	N3-Cu-N1	96.1(9)	N1-Cu-P2	102.9(8)
Cu-N1	2.103(2)	N3-Cu-P1	119.3(8)	P1-Cu-P2	124.8(3)

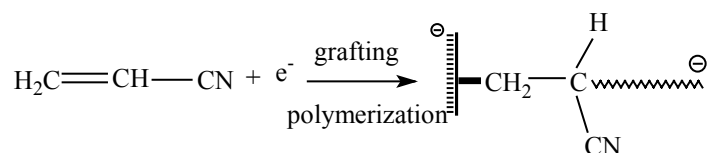
Table 4 Selected bond lengths and angles of related copper(I) complexes

Complex	Cu-P (Å)	Cu-N (Å)	P-Cu-P (°)	N-Cu-N (°)	ref.
[Cu(μ -C(CN) ₃)(PPh ₃) ₂] ₂	2.261(9)	2.103(2)	124.8(3)	96.1(9)	This work
	2.306(10)	2.031(2)			
[Cu{N(O)C(CN) ₂ }(PPh ₃) ₂] ₂	2.285(8)	2.080(3)	122.6(3)	104.9(10)	[87]
	2.294(8)	2.042(3)			
[Cu(NC(N)O ₂)(PPh ₃) ₂] ₂	2.261(1)	2.066(2)	123.5(2)	88.8(7)	[88]
	2.268(1)	2.204(2)			
[Cu(4-MeC ₆ H ₄ -NCN)(PPh ₃) ₂] ₂	2.284(1)	2.045(2)	121.7(1)	94.7(1)	[89]
	2.257(1)	2.095(2)			

X-ray crystal structure analysis reveals that 1,1,3,3-tetracyanopropane is reduced yielding the tricyanomethanide anion but a question about its mechanism arises. Then, we have suggested that 1,1,3,3-tetracyanopropane at the platinum cathode, could be reduced yielding not only the tricyanomethanide anion but also acrylonitrile as depicted in scheme 17.

**Scheme 17**

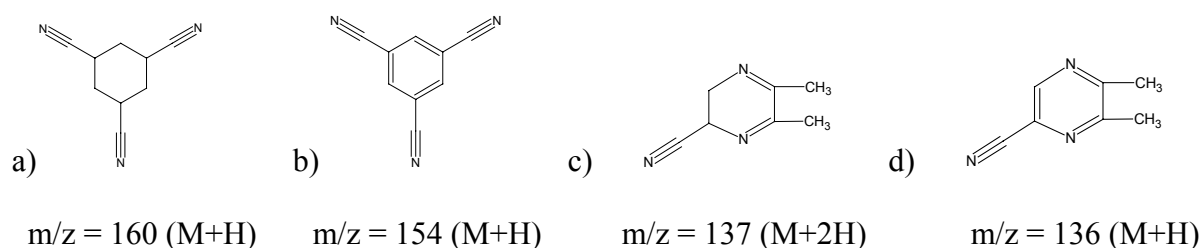
No traces of acrylonitrile were found in the solution after its analysis by NMR spectroscopy and GC-MS. The analysis of the thin film grafted on the cathode, done by IR spectroscopy and mass spectrometry, reveals rather its electropolymerization onto the cathode. The mechanism is reported by different authors [92-98]. The schematic reaction of the grafting and the polymerization of acrylonitrile at the cathode could be presented as in scheme 18:

**Scheme 18**

The IR spectrum (in KBr) of the thin film collected on the cathode exhibits a number of absorption bands, but the most characteristic ones were those at 3417, 1635, 1570 cm⁻¹ which

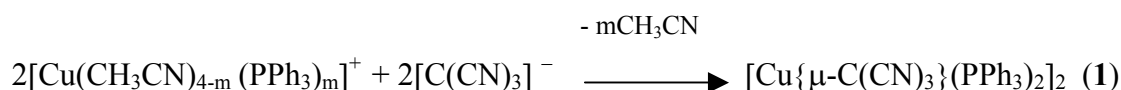
are very broad and intense bands and could indicated relatively polar bonds [91]. The band at 3417 cm^{-1} could correspond to N–H absorption. In the $1700 - 1500\text{ cm}^{-1}$ range, the absorption bands characteristic of $-\text{C}=\text{N}-$ and $-(\text{C}=\text{N})_n-$ chains appears exhibiting a very strong broad band at 1635 cm^{-1} and at 1570 cm^{-1} respectively [91]. Also $\text{C}=\text{C}$ absorbs in the range of $1660 - 1610\text{ cm}^{-1}$. A medium broad band appears at 2523 cm^{-1} and is assigned to $\equiv\text{N}\cdots\text{H}-$ chelated. A strong band assigned to the CN group is observed at 2205 cm^{-1} $\nu\text{C}\equiv\text{N}$ [91].

Fast atom bombardment (FAB) mass spectrometry shows significant mass peaks and the most important are for species of $m/z = 136.0$ (73.79%), 137.0 (63.07%), 154.0 (100%), 160.1 (65.83%), 313.1 (50.51%) and 466.1 (5.02%). The peak at $m/z = 160$ is derived from an assembly of three molecules of acrylonitrile leading to cyclohexan tri-substituted (Scheme 19a) and by the loss of 6H leads to benzene tri-substituted at $m/z = 154$ (100%) (scheme 19b) and corresponds to the base peak. Also, the peak at $m/z = 137$ could derived from an assembly of two molecules of acetonitrile and one molecule of acrylonitrile leading to dihydropyrazine (scheme 19c) and the peak $m/z = 136$ is derived from 137 by loose of one H giving pyrazine (scheme 19d). The peak at $m/z = 313$ could be derived from an assembly of $6(\text{H}_2\text{C}=\text{CH}-\text{CN})$ by loss of 5H and the peak at $m/z = 466.1$ is attributed to an assembly of $8(\text{H}_2\text{C}=\text{CH}-\text{CN})$ and one CH_3CN .



Scheme 19

The overall reaction of the synthesis derives from an ionic process leading to the formation of the complex **1** :



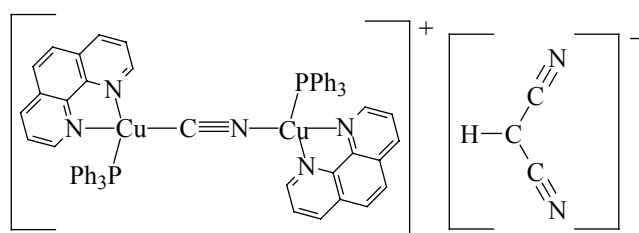
Scheme 20

3.3.1.2. Structure of bis{ cis-(μ -cyano)bis(triphenylphosphane)bis(phenanthroline)dicopper(I)}-tricyanomethanide-tetrafluoroborate-diacetonitrile
{cis-[Cu₂(μ -CN)(Phen)₂(PPh₃)₂]}₂[C(CN)₃][BF₄] \cdot 2CH₃CN (2**)**

The direct electrosynthesis of Cu(I) complex with TCP, as described above, leads to two phases. From the liquid phase, a neutral binuclear compound, **1**, has been isolated. By adding 1,10-phenanthroline (phen), with the unique ability to stabilize coordinatively unsaturated copper(I) in the solid state, to the solution containing the oil phase, a second crystalline complex has been received.

Thus, from this reaction mixture an ionic binuclear copper(I) complex in which the copper atoms are bridged by one cyano group is collected as orange crystals and characterized by X-ray crystal analysis as {cis-[Cu₂(μ -CN)(Phen)₂(PPh₃)₂]}₂[C(CN)₃][BF₄] \cdot 2CH₃CN (**2**).

The crystal structure of **2** has been investigated to uniquely determine the composition of the product of reaction described above, especially with respect to the analogous reaction of μ -cyano-tetrakis(triphenylphosphane)dicopper(I)-dicyanomethanide with phen described in [23] yielding a crystalline binuclear copper(I) [Cu₂(μ -CN)(phen)₂(PPh₃)₂][CH(CN)₂] (Scheme 21) [23].



Scheme 21

Crystals of **2** are built up by [Cu₂(μ -CN)(phen)₂(PPh₃)₂]⁺ cations of the same composition as in [23], non-coordinated [C(CN)₃]⁻ and BF₄⁻ anions, and CH₃CN solvate molecules in a ratio of 2:1:1:2. The structure of the four moieties within the crystals of **2** is shown along with selected atom numbering in Fig. 42.

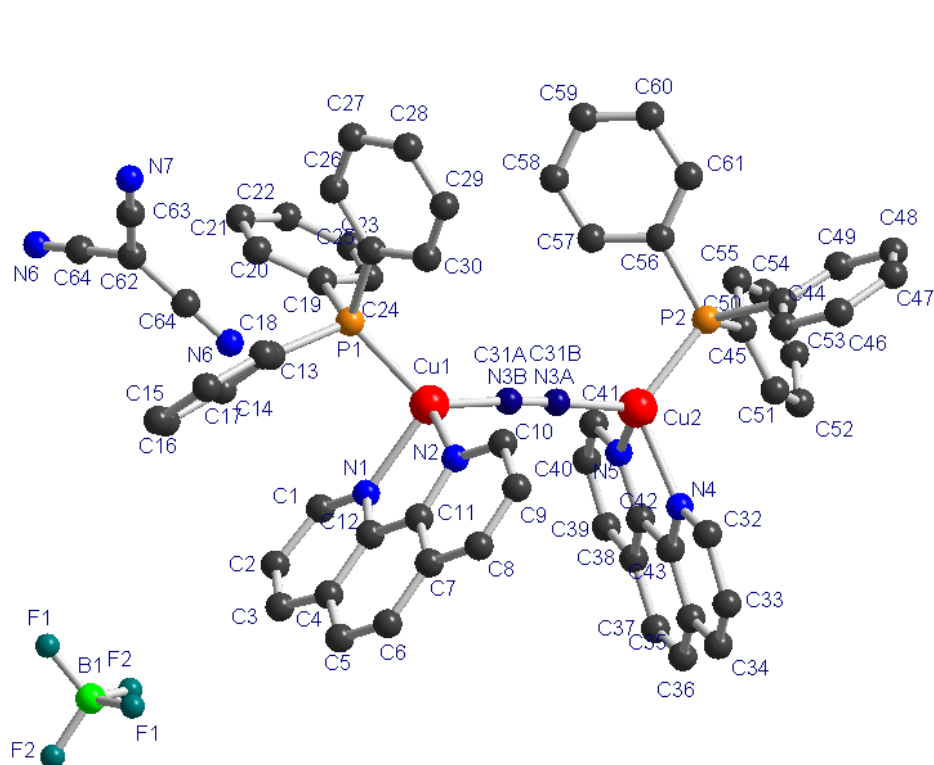


Fig. 42 Molecular structure of the four moieties in $\text{cis-}[\text{Cu}_2(\mu\text{-CN})(\text{phen})_2(\text{PPh}_3)_2]_2 \cdot [(\text{CN})_3] \cdot [\text{BF}_4] \cdot 2\text{CH}_3\text{CN}$ (**2**) with selected atom labelling (H atoms omitted for clarity).

A projection of the crystal packing is shown in Fig. 43. Selected geometrical bond parameters have been compiled in Table 5.

In contrast to the centrosymmetric structure of the Cu(I) complex cation with trans orientation of equivalent ligands at the two Cu(I) nuclei [23], the ligands in **2** are in cis configuration (cp. dihedral angles about Cu1---Cu2 in Table 5) and the complex ions have no symmetry. The current structure model (see experimental section) explains the geometry of the bridging cyano group by a disorder of C31 and N3 with probabilities of 63 and 27% for the two orientations of the cyano group (atom labels a and b, respectively, in Fig. 42). The resulting distances between Cu1 and the mean position of C31A/N3B and between Cu2 and the mean position of C31B/N3A differing by 0.037(9) Å are in a good agreement with values observed for completely ordered structures (e.g. 0.19(2) Å difference between Cu-N and Cu-C bond lengths for Cu(μ -cyano)2,9-dimethyl-1,10-phenanthroline [99]) and in disordered structures with site occupancy fixed to 0.5 for both orientations due to symmetrical reasons (e.g. Cu-C/N distances 1.945(2) Å in [23]). The Cu1-C31A/N3B- C31B/N3A and Cu2-C31B/N3A-C31A/N3B bond angles in Table 5 indicate an approximate linearity of the bridging group with the same slightly widened C31-N3 bond length as in [23] (1.159(4) Å).

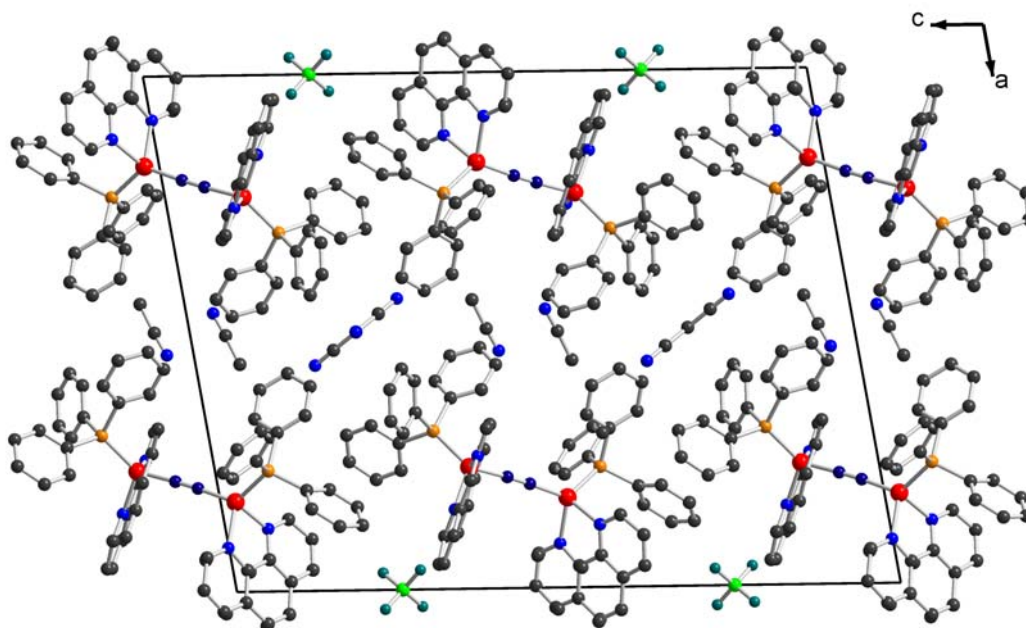


Fig. 42 Projection of the crystal packing of **2** in [010] direction (H atoms omitted for clarity)

The tetrahedral coordination of the two Cu(I) atoms is somewhat more distorted as in the trans-isomer in [23], the bond angles in Table 5 varied between the smallest ones imposed by the chelating phenanthroline ligands and the values for P-Cu-C31/N3. The latter are significantly larger compared with those of $120.67(8)^\circ$ in [23], probably due to the cis-position of the bulky triphenylphosphane ligands. The Cu-P and Cu-N(phen) distances (mean values $2.235(13)$ and $2.114(9)$ Å, respectively) agree well with expected values in the range of their experimental uncertainties, especially with the corresponding lengths in a (Cu-P $2.2319(6)$ and mean Cu-N(phen) $2.095(35)$ Å) [87-90,99,100].

The phenyl rings of the phosphane ligands are planar within experimental error with a maximum deviation of an atom from the mean plane of $0.019(5)$ Å (C44). Their orientation with respect to one another is nearly the same in case of P2(PPh₃) in **2** and P1(PPh₃) in [23], a propeller-like arrangement with a rough threefold symmetry viewed along the Cu-P bond (torsion angles Cu2-P2-C44-C45 $-23.4(7)$, Cu2-P2-C51-C52 $-52.6(6)$, Cu1-P2-C56-C57 $-29.5(7)$ in **2** and Cu1-P1-C13-C14 $-33.2(2)$, Cu1-P1-C19-C20 $-29.3(2)$, Cu1-P1-C25-C30 $-54.5(2)^\circ$ in [23], but P1(PPh₃) in **2** differs much more from this model (torsion angles Cu1-P1-C13-C14 $-80.9(5)$, Cu1-P1-C19-C20 $-29.9(6)$, Cu1-P1-C25-C30 $-14.8(6)^\circ$). As in [23], the phenanthroline ligands show stronger deviations from planarity (maximum distance 0.0731 Å for C1), with torsion angles N1-C12-C11-N2 = $5.0(11)$ and N4-C43-C42-N5 = $-4.8(8)^\circ$ ($4.0(3)^\circ$ in a) for the slight twist about the bonds C11-C12 and C42-C43.

Table 5 Selected bond lengths (Å), angles and dihedral angles (°) of (2)

Cu(I) complex ion:			
Cu1-P1	2.244(2)	Cu2-P2	2.226(2)
Cu1-N1	2.121(6)	Cu2-N4	2.100(5)
Cu1-N2	2.116(7)	Cu2-N5	2.117(6)
Cu1-C31A/N3B	1.920(6)	Cu2-C31B/N3A	1.957(6)
C31A/B-N3A/B	1.158(8)		
P1-Cu1-N1	101.7(2)	P2-Cu2-N4	120.0(2)
P1-Cu1-N2	114.9(2)	P2-Cu2-N5	103.6(2)
P1-Cu1-C31A/N3B	126.2(2)	P2-Cu2-C31B/N3A	123.9(2)
N1-Cu1-N2	79.0(2)	N4-Cu2-N5	79.1(2)
N1-Cu1-C31A/N3B	115.9(2)	N4-Cu2-C31B/N3A	106.8(2)
N2-Cu1-C31A/N3B	109.3(2)	N5-Cu2-C31B/N3A	114.7(2)
Cu1-C31A/N3B-N3A/C31B	176.8(5)	Cu2-C31B/N3A-C31A/N3B	177.6(6)
P1-Cu1---Cu2-N4	-176.6(2)	N1-Cu1---Cu2-P2	166.9(2)
N1-Cu1---Cu2-N5	36.9(2)	N2-Cu1---Cu2-N4	38.0(2)
P1-Cu1---Cu2-P2	37.6(1)		
Tricyanomethanide			
C62-C63	1.39(2)	C62-C64	1.40(1)
C63-N7	1.14(2)	C64-N6	1.16(1)
C62-C63-N7	180	C62-C64-N6	180(1)
C63-C62-C64	119.4(6)	C64-C62-C64'	121(1)
Tetrafluoroborate			
B1-F1	1.33(1)	B1-F2	1.36(1)
Acetonitrile			
C11-C21	1.44(2)	C11-N11	1.13(1)
C21-C11-N11	176(1)		

Both counter ions, the tricyanomethanide and the tetrafluoroborate anions, possess crystallographically induced C2 symmetry because of their special positions at twofold axes in the unit cell. Their geometrical bond parameters (Table 5) show no deviations from expected values within experimental error and need no further discussion, the same holds for the solvate acetonitrile molecule.

The complex cations are packed in layers parallel (010) in a way leading to a concentration of the phenanthroline ligands about $x = 0$ and a concentration of the P(Ph₃) ligands about $x = 0.5$. The tetrafluoroborate ions are buried in this sea of phenanthroline moieties, whereas the tricyanomethanide ions and the solvate molecules are arranged in a narrow layer about $x = 0.5$ covered by the phenyl rings. Two short intermolecular non-H --- H contact distances between the phenanthroline ligand at Cu2 and a neighbouring tetrafluoroborate ion (geometrical parameters C32-H32 0.93 (fixed), H32---F1 2.38, C32---F1 3.160(9) Å, C32-H32---F1 142°, symmetry relation for F1 $x, 1-y, -0.5+z$) and a solvate molecule (C41-H41 0.93 (fixed), H41---N11 2.58, C41---N11 3.34(1) Å, C41-H41---N11 139°, symmetry relation for N11 $(x, 1-y, -0.5+z)$) cannot be uniquely verified as weak hydrogen bonds, since the H-atoms have been geometrically positioned neglecting the influence of possible H-bond acceptors. There are no unusually short intermolecular contact distances between non-H atoms in the crystal packing.

3.3.1.3. Molecular Structure of $\{(\mu\text{-cyano})\text{hexakis}(\text{triphenylphosphane})\text{dicopper(I)}\}\text{-tetrafluoroborate } [\text{Cu}_2(\mu\text{-CN})(\text{PPh}_3)_6][\text{BF}_4] \text{ (3)}$

In order to shed some light on the structure of oil phase, it has been dissolved readily in THF. Few months later single colorless crystals suitable for X-ray analysis were collected and characterized as $[\text{Cu}_2(\mu\text{-CN})(\text{PPh}_3)_6][\text{BF}_4] \text{ (3)}$.

Crystals of **3** are built up by $[\text{Cu}_2(\mu\text{-CN})(\text{PPh}_3)_6]^+$ cation and $[\text{BF}_4]^-$ anion. The structure of **3** is depicted with selected atom numbering in Fig. 43. Selected bond lengths and angles are given in Table 6. The Cu(I) complex is ionic and binuclear with a distorted tetrahedral coordination environment of the two Cu(I) atoms. BF_4^- is uncoordinated and centrosymmetric. The cation $[\text{Cu}_2(\mu\text{-CN})(\text{PPh}_3)_6]^+$ is also centrosymmetric and has the same composition as in $[\text{Cu}_2(\mu\text{-CN})(\text{PPh}_3)_6][\text{TCNE}]$ where TCNE = tetracyanoethylene, reported by *Olmstead et al.* [101]. The structural differences between both complexes are established (Table 7). The Cu-C-N bond angle (178.49(20)°) in Table 6 indicates an approximate linearity of the bridging group with the same slightly widened C-N bond length 1.150(4) as in **2**

(1.159(4) Å). The centre of symmetry at the CN group requires that the bridging –CN– be disordered with –NC– [23,101]. Inspection of the crystal packing reveals that BF_4^- buried in the sea of phenyl rings (Fig. 44).

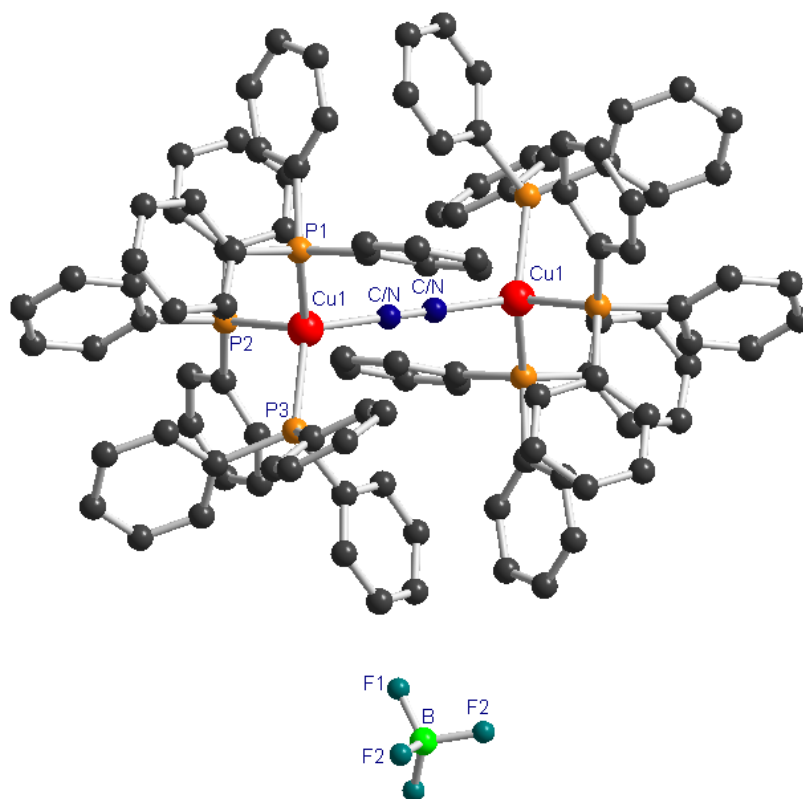


Fig. 43 Molecular structure of $[\text{Cu}_2(\mu\text{-CN})(\text{PPh}_3)_6][\text{BF}_4]$ (**3**) with selected atomic labelling (Hydrogen atoms are omitted for clarity)

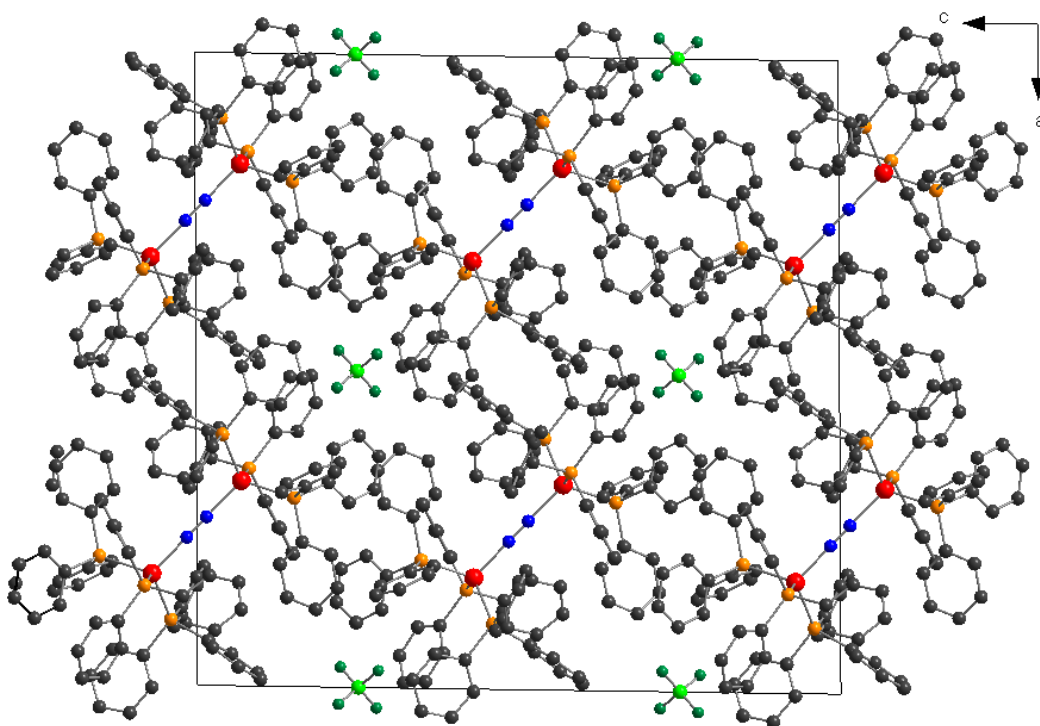


Fig. 44 Projection of the crystal packing of **3** in [010] direction (H atoms omitted for clarity)

Table 6 Selected bond lengths (Å) and angles (°) of **3**.

Bond	Lengths (Å)		Angles (°)
Cu-P1	2.410(18)	N-Cu-P1	108.67(7)
Cu-P2	2.378(2)	N-Cu-P2	105.74(8)
Cu-P3	2.391(18)	N-Cu-P3	113.14(6)
Cu-N	2.039(31)	P1-Cu-P2	114.01(4)
N-C	1.150(4)	P2-Cu-P3	108.67(7)
B-F1	1.309(15)	P3-Cu-P1	109.15(3)
B-F2	1.290(16)	C-N-Cu	178.49(20)

Table 7 Important structural features of $[\text{Cu}_2(\mu\text{-CN})(\text{PPh}_3)_6][\text{BF}_4]$ and $[\text{Cu}_2(\mu\text{-CN})(\text{PPh}_3)_6][\text{TCNE}]$.

Parameters	$[\text{Cu}_2(\mu\text{-CN})(\text{PPh}_3)_6][\text{BF}_4]$	$[\text{Cu}_2(\mu\text{-CN})(\text{PPh}_3)_6][\text{TCNE}]$ [101]
Crystal system	monoclinic	triclinic
Cell dimension		
a	25.666(5)	12.979(4)
b	13.481(3)	14.420(4)
c	26.107(5)	14.553(5)
α		106.35(2)
β	91.06(3)	116.19(2)
γ		90.62(2)
V (Å ³)	9031.56(300)	2316.3(10)
Space groupe	C 2/c 1 (no. 15)	P $\bar{1}$
Z	4	1

3.3.1.4. Synthesis of {trans-(μ -cyano)bis(bipyridine)bis(triphenylphosphane)di-copper(I)}-tetrafluoroborate-tetrahydrofuran $[\text{Cu}_2(\text{CN})(\text{bipy})_2(\text{PPh}_3)_2][\text{BF}_4]\cdot\text{THF}$ (**4**)

The Complex **4** is prepared by a reaction between **3** and 2,2'-bipyridine (bipy). **4** is received as green-yellowish crystals and identified by single-crystal X-ray structure determination, IR spectroscopy, EDX and elementary analyses.

Crystals are built up by $[\text{Cu}_2(\text{CN})(\text{bipy})_2(\text{PPh}_3)_2]^+$ cation, non-coordinated fluoroborate anion and THF solvate molecule in a ratio of 1:1:1. The structure of **4** is shown along with selected atom numbering in Fig. 45. It presents an hexacoordinated compound which is characterized

as $[\text{BF}_4^-]$ with a strong broad band at 1093 cm^{-1} (1084 cm^{-1} in **2**) on the IR spectrum. Also EDX reveals the percentage weight to be $48.35 \pm 1.02\%$ for fluorine and $24.18 \pm 1.16\%$ for copper.

The selected bond lengths and angles are given in Table 8. The Cu(I) complex cation is centrosymmetric with trans orientation of the ligands at the two Cu(I) nuclei. The coordination geometries about the copper atoms are consistent with a distorted tetrahedral environment. This deviation arises from the geometrical constraints around copper atoms imposed by the N3-Cu-N2 angle of $78.65(14)^\circ$. The Cu-P and Cu-N(bipy) distances of $2.225(12)$ and $2.101(3)\text{ \AA}$ (mean value) are in good agreement with expected values [100]. The lengthening of the coordinated C1-N1 bond ($1.155(9)\text{ \AA}$) was explained by *Bruce et al.* [102] by the presence of the electron-donating groups which increases electron density at the metal centre so that the CN is stabilized by back-bonding from the metal to the CN π^* orbitals. The projection of the crystal packing is presented in Fig. 46.

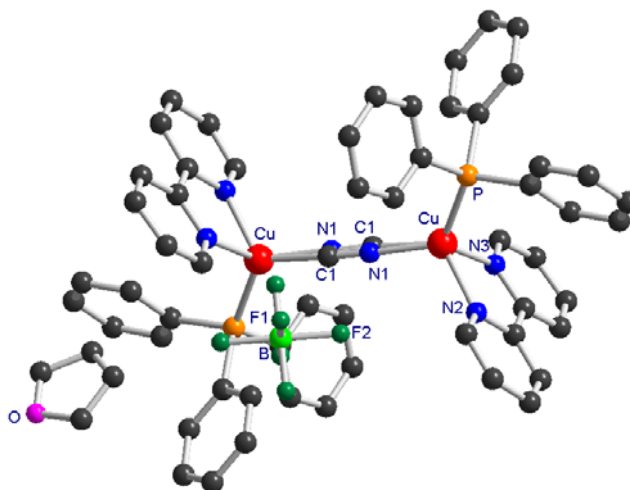


Fig. 45 Molecular structure of $[\text{Cu}_2(\mu\text{-CN})(\text{bipy})_2(\text{PPh}_3)_2][\text{BF}_4]\cdot\text{THF}$ (**4**)

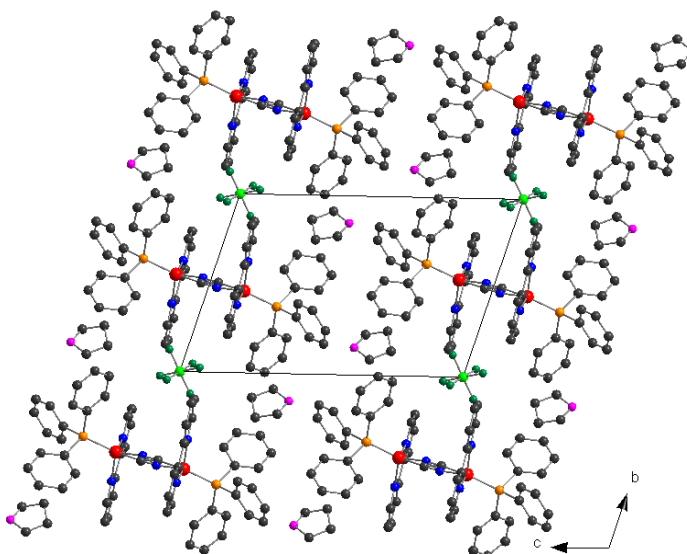


Fig. 46 Projection of the crystal packing of **4** in $[100]$ direction (H atoms omitted for clarity).

Table 8 Selected bond lengths (Å), angles and dihedral angles (°) of (4)

Cu(I) complex ion:			
Cu-P	2.225(12)	N1-Cu-P	122.4(4)
Cu-N1	2.105(3)	N3-Cu-P	115.2(10)
Cu-N2	2.105(3)	N2-Cu-P	108.52(9)
Cu-N3	2.097(3)	N1-C1-Cu	177.8(11)
N1-C1	1.155(9)	N3-Cu-N2	78.65(14)
C1-Cu	1.96(2)	N1-Cu-N2	113.9(4)
N1-Cu-N3	110.0(4)		

3.3.1.5. Discussion

The electrosynthesis of Cu(I)–TCP complex by anodic dissolution of a copper metal and cathodic reduction of 1,1,3,3-tetracyanopropane in AN / Bu₄NBF₄, PPh₃ has revealed to be a new and an efficient way to generate the tricyanomethanyl anion. Indeed, the electrogenerated tetracyanopropyl radical anion is not stable, as evidenced by cyclic voltammetry, and undergoes a cleavage leading to tricyanomethanyl and CN[−] anions and acrylonitrile which is electropolymerized at the cathode. Further reactions in the presence of different donors such as 1,10-phenanthroline and 2,2′-bipyridine reveal ionic Cu(I) complexes, bridging by the cyanide, in which the donors are in cis (Fig. 42) and trans (Fig. 45) orientations.

The cyclic voltammetry studies of a solution of TCP in AN / Bu₄NBF₄ both at a platinum and at a copper electrodes have predicted the decomposition of TCP but the mechanism was not up to now established. It appears at the platinum electrode that the reduction products decompose slowly to give a kinetically linked product which is oxidized irreversibly at a much more positive potential. Qualitative analyses reveal that the first reduction process (A) is easier than the second (B) and the properties of cyclic voltammetric data recorded suggest that the first electron transfer (process (A)) is coupled to an irreversible, second-order, following reaction whereas the second electron transfer (process (B)) is coupled to an irreversible, first-order, following reaction. The overall electrochemical mechanism is assumed to be ECEC mechanism.

In order to characterize all the product of the decomposition, electrolysis of a solution of TCP in CD₃CN has been carried out in a small volume cell (picture presented in experimental part). After the electrolysis at platinum working and counter electrodes, the ¹H NMR

spectrum shows a weak singlet at 4.61 ppm (Fig. 47) which could be ascribed to malononitrile, $\text{CH}_2(\text{CN})_2$. The proton of this compound appears in the literature as singlet at 4.44 ppm in $\text{DMSO-}d_6$ [39]. Also, MDN is used as starting material in the synthesis of TCP [39].

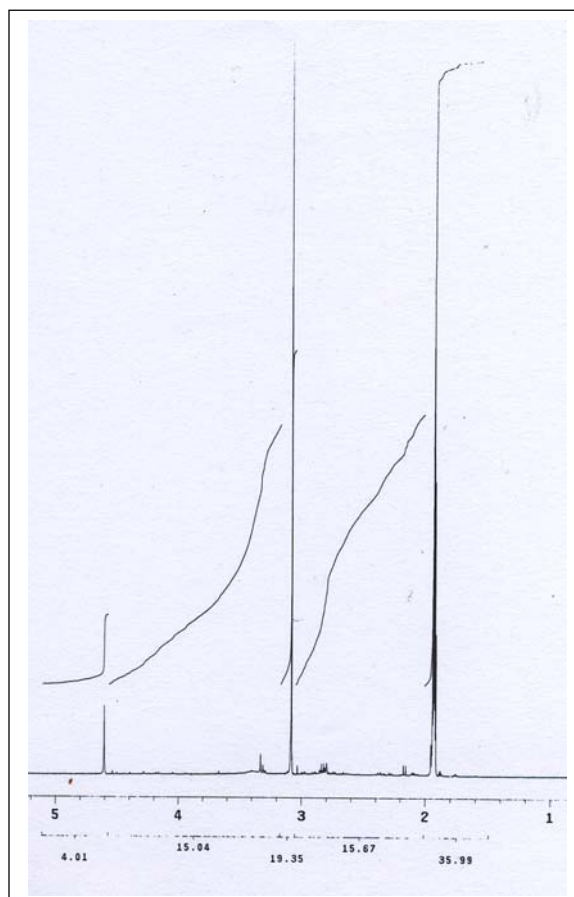


Fig. 47 NMR spectrum of an electrolytic solution of TCP at Pt working and Pt counter electrodes.

As shown with the study of the electrochemical behavior of TCP, the cyclic voltammogram of a solution of TCP after the electrolysis at a copper working electrode and a platinum counter electrode (Fig. 24), reveals a steep decrease of the peak height (A) with an increase of (B). This finding indicates that a species from which the process (B) derived has increased during the electrolysis. Therefore, it has been decided to study the influence of malononitrile on the voltammogram of 1,1,3,3-tetracyanopropane

The addition of malononitrile to the solution of TCP results in the loss of the quasi-reversibility of the second process (B) with a significant increase of the peak current as it is shown on Fig.48. This could indicate that the process (B) is connected with the reduction of malononitrile. The loss of the quasi-reversibility could indicate that a chemical reaction occurs between malononitrile and the oxidized species responsible for the peak (B1).

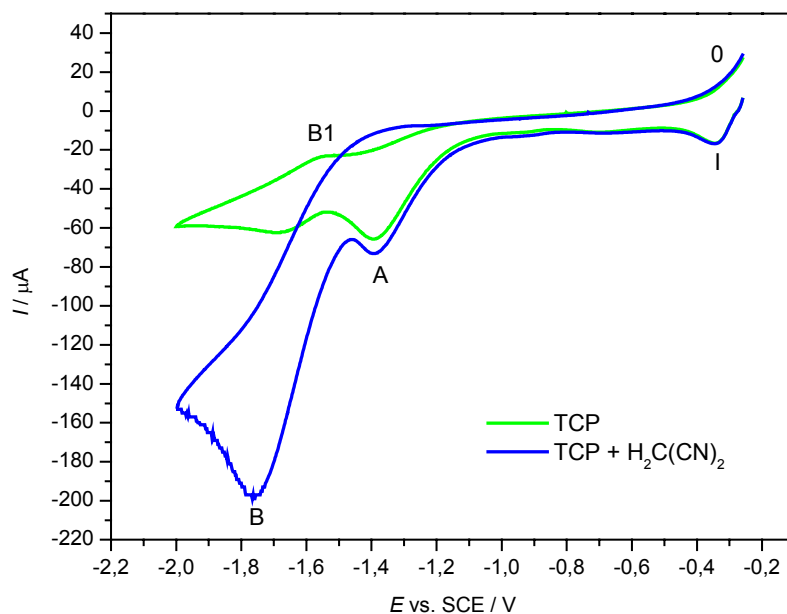
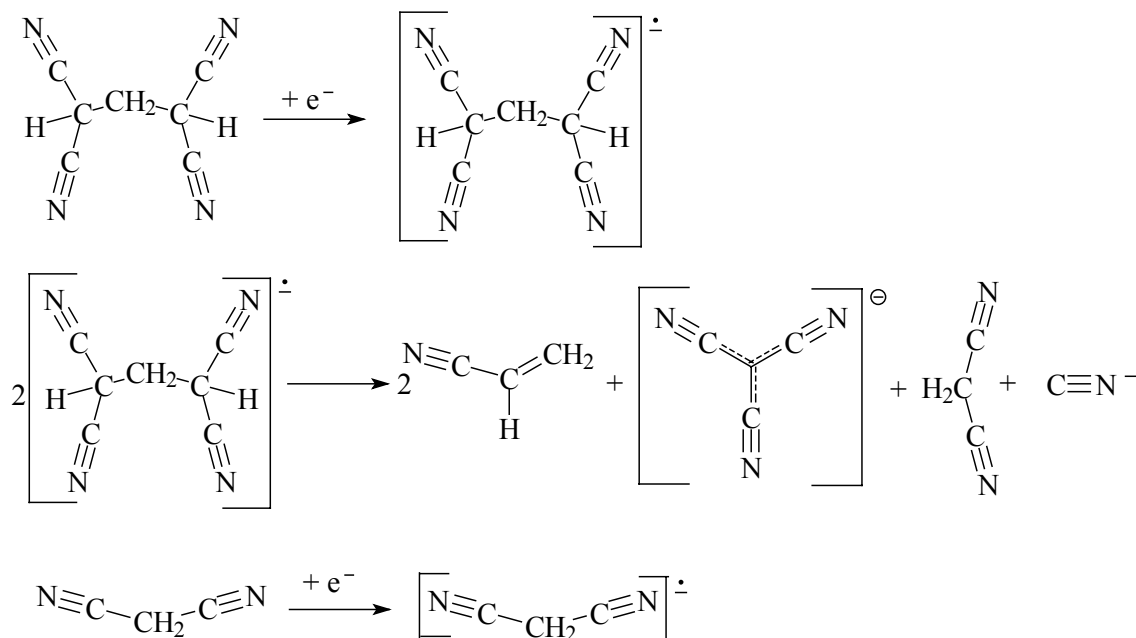


Fig. 48 Effect of MDN on the CV of TCP at the Cu electrode (AN, 0.1 M Bu₄NBF₄, 0.1 V s⁻¹).

In the light of these results, the following mechanism can be proposed as a probable reduction pathway of TCP during the direct electrosynthesis of TCP-Cu(I) compound (scheme 22).



Scheme 22 A possible reduction pathway of TCP.

Electrosynthesis of TCP-Cu(I) complex has been carried out at different temperatures (0, -35 °C and at room temperature). The X-ray crystal structure analysis revealed the reaction product to be the complex **1**. All compounds (**1**, **2**, **3** and **4**) are stable on exposure to the air.

3.3.2. Malononitrile as starting material

The synthesis of MDN-Cu(I) compound has held the attention in a second attempt of electroynthesis. Depending on experimental conditions, malononitrile (MDN) can be used to achieve electrochemically different compounds [22,23]. By potentiostatic dissolution of Cu anode, in AN / Bu₄NBF₄, PPh₃ at room temperature, ionic binuclear Cu(I) compounds, [(PPh₃)₂Cu(μ-CN)Cu(PPh₃)₂][HC(CN)₂] and its derivative depicted in scheme 21, have been received [23]. Galvanostatically, mononuclear Cu(I) compounds [Cu(NCC(H)CN)(PPh₃)] and its derivative have been prepared in AN / LiBF₄, PPh₃ at 0 °C [22a]. As an extension of these studies, the influence of the size of the cation of the supporting electrolyte has been investigated. Thus, the galvanostatical electroynthesis of MDN-Cu(I) has been attempted in AN / Bu₄NBF₄, PPh₃. Reactions between the product and different donors are also investigated.

3.3.2.1. Electroynthesis of {[Cu(CN)(PPh₃)₂]·CH₃CN}_n (**5**)

Complex **5** has been achieved by galvanostatic dissolution of copper metal (*I* = 50 mA) and cathodic reduction of malononitrile at 0 °C. The electrochemical cell for this system is presented as follows: Pt₍₋₎ / CH₃CN + CH₂(CN)₂ + PPh₃ + [(C₄H₉)₄N][BF₄] / Cu₍₊₎. The electrochemical efficiency is found to be close to 1 mol F⁻¹.

The compound **5** is received as a white precipitate stable on exposure to the air and soluble in DMSO. The electrochemical behavior of malononitrile reported previously, reveals that the electron transfer is followed by an irreversible chemical reaction. It appears that an electrochemical reductive cleavage of malononitrile takes place at the cathode yielding CN⁻. The overall reaction mechanism in the cell is assumed to be:



Scheme 23

The polymeric structure {[Cu(CN)(PPh₃)₂]·CH₃CN}_n has been characterized by ESI-MS, EDX and C, H, N elemental analyses, ¹H-, ³¹P-NMR and IR spectroscopies.

The IR spectrum (in KBr) exhibits several bands which may be taken as diagnostic for the presence of cyanide and triphenylphosphane ligands. The bands characteristic to ν_{CN} are observed at 2187 and 2104 cm^{-1} . *Zhao et al* [103] found a strong peak, ν_{CN} , at 2106 cm^{-1} for hexanuclear $[\text{Cu}(\text{CN})(\text{PPh}_3)_2]_6$ complex obtained by chemical way. *Singh and Dikshit* [104] prepared $[\text{Cu}(\text{CN})(\text{PPh}_3)_2]$ by a chemical reaction between CuCN and PPh_3 in benzene in a ratio 1:4 and found a red shift of *ca* 51 cm^{-1} (ν_{CN} band at 2121 cm^{-1}) indicating that the CN group is terminally coordinated.

The ^{31}P NMR spectrum shows two singlets at 24.72 and -2.83 ppm. The later is assigned to free PPh_3 .

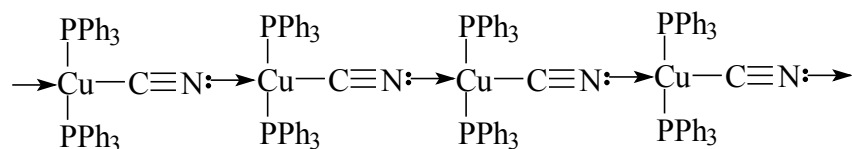
In the ^1H NMR spectrum, the aromatic protons appears between 7.2 and 7.8 ppm.

The positive-ion electrospray mass spectrum in THF / CH_3CN (Table 9) shows a number of peaks and the most abundant ion, $[\text{Cu}(\text{PPh}_3)_2]^+$, appears at m/z 587.111.

Table 9 ESI-MS of **5**

m/z	Assignment	m/z	Assignment
197.55	$[\text{Cu}(\text{CN})(\text{PPh}_2)]^+$	849.55	$[\text{Cu}(\text{PPh}_3)_3]^+$
587.55	$[\text{Cu}(\text{PPh}_3)_2]^+$	875.55	$[\text{Cu}(\text{CN})(\text{PPh}_3)_3]^+$
613.55	$[\text{Cu}(\text{CN})(\text{PPh}_3)_2]^+$		

The possible polymeric structure the (Cyano-C)bis(triphenylphosphane)copper(I) complex can be assumed to be as follows (Scheme 24):



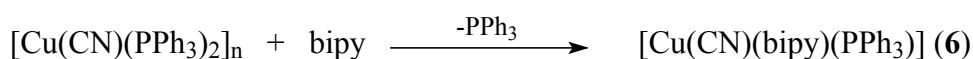
Scheme 24

A chemical reaction, between 2,2'-bipyridine (bipy) and **5** on the one hand, and between 1,10-phenanthroline (phen) and **5** on the other hand, has also been carried out not only to stabilize the product of the reaction in the solid state but also to prepare mixed ligand Cu(I) compounds [103-107]. It is reported that such compounds have found prominent uses in supramolecular chemistry as useful building blocks [110].

3.3.2.2. Synthesis of (Cyano-C)(2,2'-bipyridine-N,N')(triphenylphosphane)copper(I)

[Cu(CN)(bipy)(PPh₃)] (6)

The (Cyano-C)(2,2'-bipyridine-N,N')(triphenylphosphane)copper(I) has been prepared in AN by a reaction of {[Cu(CN)(PPh₃)₂]·CH₃CN}_n with 2,2'-bipyridine, in a ratio 1:2, which leads to a substituted neutral mononuclear copper(I) complex received as yellowish crystals (Scheme 25):



Scheme 25

The product of the reaction mixture has been characterized by IR spectroscopy and X-ray crystal structure determination.

The IR spectrum of [Cu(CN)(bipy)(PPh₃)] shows a strong peak at 2173 cm⁻¹ that can be assigned to C≡N valence vibration for copper bound to cyanide ion. The νC≡N band, in solid cuprous cyanide, occurs at 2172 cm⁻¹. *Singh and Dikshit* [104] synthesized [Cu(CN)(bipy)(PPh₃)] by classical routes and found a small red shift of νC≡N (*ca* Δ = 13 cm⁻¹). A single crystal X-ray was performed to determine the composition of the product of reaction in scheme 25.

The structure of **6** consists of a monomeric [Cu(CN)(bipy)(PPh₃)] unit as shown in Fig. 49. Selected geometrical bond parameters have been reported in Table 10. The copper atom is coordinated by the carbon atom of the cyano group, by the phosphorous atom of the PPh₃ and chelated by two nitrogen atoms of the 2,2'-bipyridine ligand. The distorted tetrahedral coordination environment about the copper is consistent with oxidation state of +1. The deviation arises from the geometrical constraints imposed by the bond angle N2-Cu-N3 of 78.59(7)° which differs significantly from the ideal value of 109.5°. The N2-Cu-P and N3-Cu-P angles of 112.29(5)° and 105.43(6)° compared to 114.93(8)° and 112.89(8)° for the C1-Cu-N3 and C1-Cu-N2 and 123.66(6)° for C1-Cu-P angles reflect the steric bulk of PPh₃ and bipy ligands compare to the cyano group. This group is almost linear (Cu-C1-N1 174.81(2)°).

The Cu-P distance with similar value is in good agreement with the average value of 2.25(4) Å (Table 10) establish for Cu(I)-PPh₃ complexes [22,23, 87,88,108,109]. The value of the

N1-C1 bond length of 1.142(3) Å is closely compared with that expected for a CN triple bond. Also the Cu-C1 bond distance of 1.936(2) Å is in good agreement with literature [100].

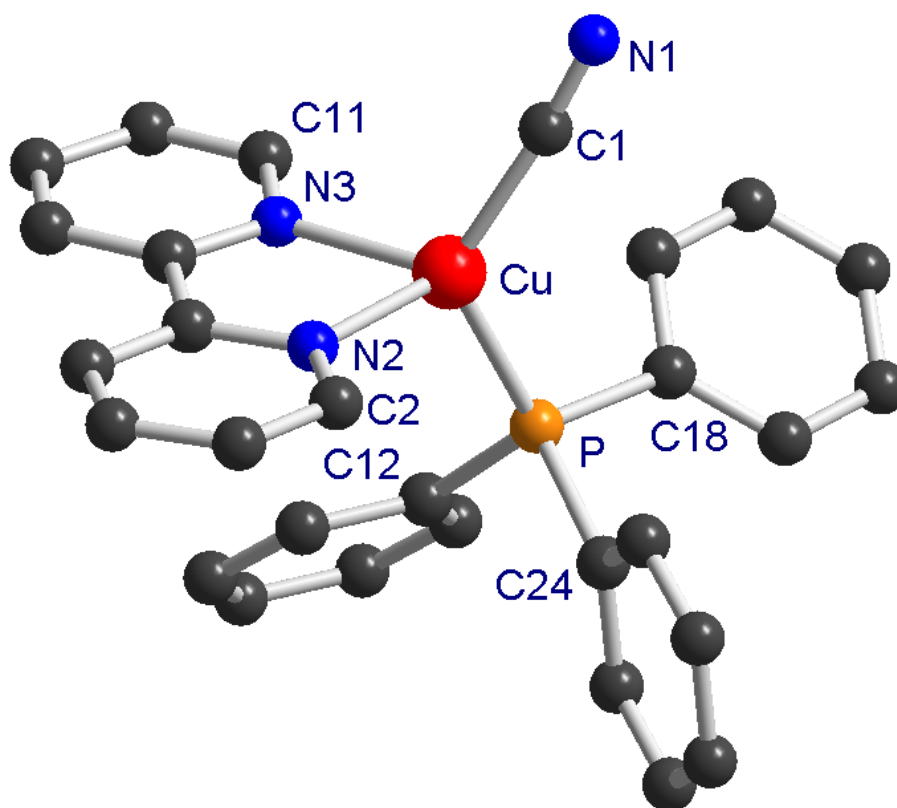


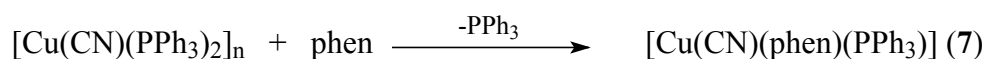
Fig. 49 Molecular structure of [Cu(CN)(bipy)(PPh₃)] (**6**) with selected atomic labeling (Hydrogen atoms are omitted for clarity).

Table 10 Selected bond lengths (Å) and angles (°) of **6**

Bond lengths		Bond angles	
Cu-C1	1.936(2)	C1-Cu-P	123.66(6)
Cu-N2	2.0975(2)	N2-Cu-P	112.29(5)
Cu-N3	2.0944(2)	N3-Cu-P	105.43(6)
Cu-P	2.2384(8)	N2-Cu-N3	78.59(7)
C1-N1	1.142(3)	N1-C1-Cu	174.81(2)
		C1-Cu-N2	112.89(8)
		C1-Cu-N3	114.93(8)

3.3.2.3. Synthesis of (Cyano-C)(1,10'-phenanthroline-N,N')(triphenylphosphane)copper(I) [Cu(CN)(phen)(PPh₃)] (7)

The complex **7** has been achieved by a reaction of $\{[\text{Cu}(\text{CN})(\text{PPh}_3)_2] \cdot \text{CH}_3\text{CN}\}_n$ with 1,10-phenanthroline, in a ratio 1:1, which leads to a substituted neutral mononuclear copper(I) complex received as yellowish crystals (Scheme 26):



Scheme 26

The single crystal X-ray structure analysis reveals that **7** is monomeric with a terminal cyano group C – coordinated to copper atom. The molecular structure of **7**, with the selected atom numbering scheme, is depicted in Fig. 50. Selected bond lengths and angles are given in Table 11. Fig. 50 shows that the copper atom is bonded to the carbon atom of the cyano, to the phosphorous atom of the triphenylphosphane and is finally chelated by two nitrogen atoms of the 1,10-phenanthroline ligand.

The solid-state structure consists of a distorted tetrahedron geometry around the copper with an N₂P donor set. The deviation arises from the geometrical constraints imposed by the bond angle N2-Cu-N3 of 80.41(10)° which differs significantly from the ideal value of 109.5°. The steric bulk of PPh₃ and phen ligands compare to the cyano group is explained by the N2-Cu-P and N3-Cu-P angles of 116.25(7)° and 108.22(7)° compared to 111.07(11)° and 108.68(11)° for the C1-Cu-N3 and C1-Cu-N2 and 123.78(9)° for C1-Cu-P angles. The cyano group is almost linear (Cu-C1-N1 175.70(3)°). The Cu-P distance of 2.218 (9) Å and the Cu-N distances of 2.087 (2) and 2.100 (2) Å are in good agreement with the literature [100]. Also the value of the C1-N1 bond length of 1.150 (4) Å is closely compared with that expected for a terminal CN triple bond [100].

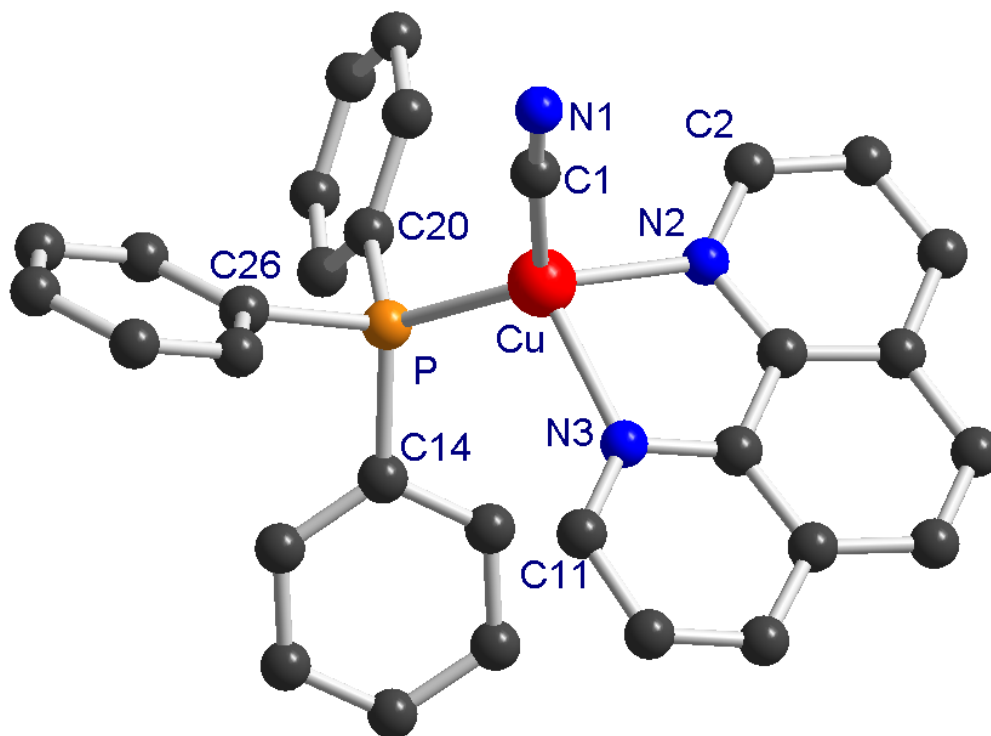


Fig. 50 Molecular structure of $[\text{Cu}(\text{CN})(\text{phen})(\text{PPh}_3)]$ (**7**) with selected atomic labeling (Hydrogen atoms are omitted for clarity).

Table 11 Selected bond lengths (Å) and angles (°) of **7**

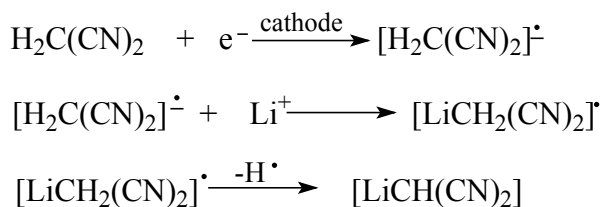
Lengths		Angles	
Cu-C1	1.935(4)	C1-Cu-P	123.78(9)
Cu-N2	2.087(2)	N2-Cu-P	116.25(7)
Cu-N3	2.100(2)	N3-Cu-P	108.22(7)
Cu-P	2.218(9)	N2-Cu-N3	80.41(10)
C1-N1	1.150(4)	N1-C1-Cu	175.70(3)
		C1-Cu-N2	108.68(11)
		C1-Cu-N3	111.07(11)

3.3.2.4. Discussion

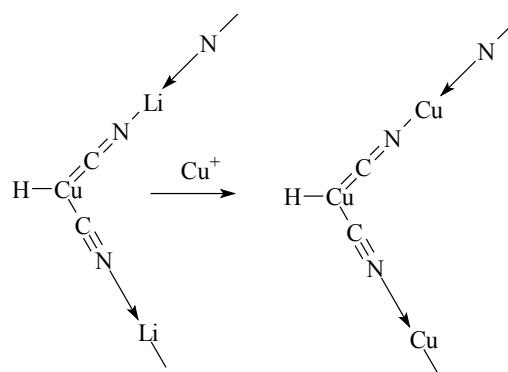
The synthesis of **5** has revealed to be an efficient way towards a simple and efficient one-step route to copper(I) cyanide mixed ligand complexes which are obtained by conventional method after many reaction steps have been involved [103-107].

The strong influence of synthesis conditions on the complex formation is to be noted. Potentiostatically, *Günther* [22b] achieved ionic binuclear Cu(I) compounds built up by $[\text{Cu}_2(\mu\text{-CN})(\text{PPh}_3)_4]^+$ cation and non-coordinated $[\text{HC}(\text{CN})_2]^-$ anion. However, *Ryabova* [22a] prepared galvanostatically, mononuclear Cu(I) compounds $[\text{Cu}(\text{NCC}(\text{H})\text{CN})(\text{PPh}_3)]_n$ in the presence of lithium tetrafluoroborate. In similar conditions as *Ryabova* [22a] and in the presence of Bu_4NBF_4 , electro-synthesis leads to $\{[\text{Cu}(\text{CN})(\text{PPh}_3)_2]\cdot\text{CH}_3\text{CN}\}_n$.

It appears that, galvanostatically, the size of cation of the supporting electrolyte plays an important role with regard to the mechanism of the complex formation whereas the anion, BF_4^- is known as a weakly coordinating anion (like PF_6^- and ClO_4^-) [111, 112]. The Li^+ ion, with a smaller radius of 0.68 Å than Bu_4N^+ ion (4.0 Å), reacts strongly with radical anion $[\text{H}_2\text{C}(\text{CN})_2]^-$ and the reaction is followed by a cleavage of C–H bond with the formation of a neutral Li(I)-complex as indicated in scheme 27 [22a]. Thus the $[\text{LiCH}(\text{CN})_2]$ complex in the presence of Cu^+ ion undergoes a transmetalation reaction according to scheme 28 [22a].



Scheme 27



Scheme 28

However, in the presence of the Bu_4N^+ cation, the radical anion generated at the cathode undergoes further chemical reaction which results in a cleavage of the C–CN bond with formation of a cyanide ion as suggested previously by *Schäfer et al.* [23]. Then Cu(I), soft acid, binds easily CN^- , soft base, according to the Pearson's concept [113].

In **5**, **6** and **7** Cu(I) is bonded to PPh_3 which is a stronger σ -donor than π -acceptor and consequently a strong back-donation is expected from Cu(I) to the cyanide group [104]. This could explain the terminal cyano group C – coordinated to copper atom.

3.3.3. Phenylacetonitrile as starting material

The electrosynthesis of copper(I) compounds with TCP and MDN ($pK_a = 11.1$ [21e]), two alkyl groups substituted by more than one cyanide group, has revealed that both ligands undergo an electroreductive cleavage in AN / Bu_4NBF_4 . The direct electrosynthesis of organocopper(I) with a lesser acidic nitrile arouses interest with regard to the mechanism of its reduction. For this proposal, phenylacetonitrile (PhAN, $pK_a = 21.9$ [21c]) has been selected and the electrosynthesis has been carried galvanostatically in a solvent which does not contain CN group, THF / Bu_4NBF_4 system.

3.3.3.1. Electrosynthesis of (1-benzyl-2-cyano-2-phenylvinylamine)bis(triphenylphosphane)copper(I) [Cu(BPVA)(PPh₃)₂] (**8**)

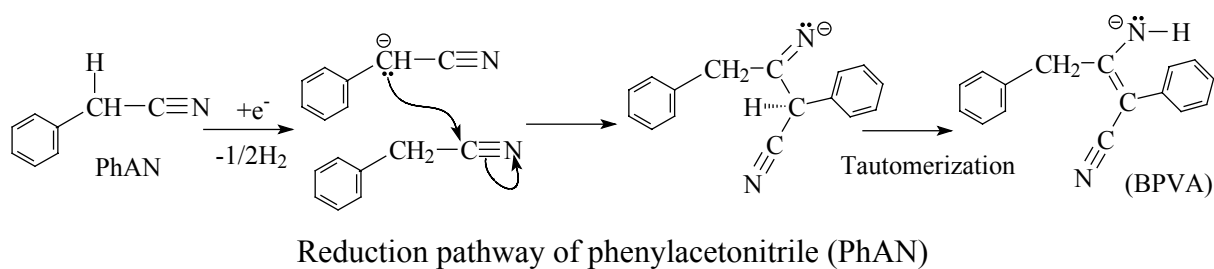
The compound **8** has been achieved by anodic dissolution of copper metal, at a constant current of 10 mA (current density 0.44 mA cm^{-2}), in THF / Bu_4NBF_4 , PhAN, PPh₃. The reaction was carried out smoothly at 0°C and stopped after a charge of 1 Faraday, which corresponds to $1 e^- / \text{mol}$, has passed through the solution. When the power supply is switched on, the colorless solution changes to dark-yellow after 45 min of electrolysis and to a black solution at the end of the synthesis. No precipitate is isolated immediately at the end of experiment but within one month, colorless crystals are collected. Unfortunately, these crystals were not suitable for X-ray analysis. Thus, **8** is characterized by satisfactory C, H, N elemental analysis, FAB⁺-MS, ¹H-, ¹³C-, ³¹P-NMR and IR-spectroscopies.

The elemental analysis (Table 12) reveals that **8** crystallizes with the supporting electrolyte and corresponds to a molecular formula of $\{[(C_4H_9)_4N][Cu(BPVA)(PPh_3)_2][BF_4]\}$.

Table 12 Analytical data of **8** $CuC_{68}H_{79}N_3P_2BF_4$: $1149.55 \text{ g mol}^{-1}$.

Elements	C (%)	H(%)	N(%)
Found / Calculated	70.28 / 70.98	5.80 / 6.87	3.29 / 3.65

The analyses reveal that phenylacetonitrile (PhAN) undergoes an electrolytic reductive coupling at the cathode (Scheme 29) meantime the galvanostatic dissolution of copper at the anode occurs followed by the formation of $\{[(C_4H_9)_4N][Cu(BPVA)(PPh_3)_2][BF_4]\}$.



Overall reaction

Scheme 29

The IR (in KBr) spectrum of **8** shows a weak band at 3309 cm^{-1} (Fig. 51) attributable to $\nu N-H$ and a strong $\delta N-H$ band at ca. 1518 cm^{-1} [116]. Two $\nu C\equiv N$ bands occurs at 2161 and 2125 cm^{-1} . The $\nu C=C-Ph$ bands are observed at 1632 , 1593 , 1585 and 1571 cm^{-1} . All the characteristic bands due to the phenyl rings are found in their spectral region.

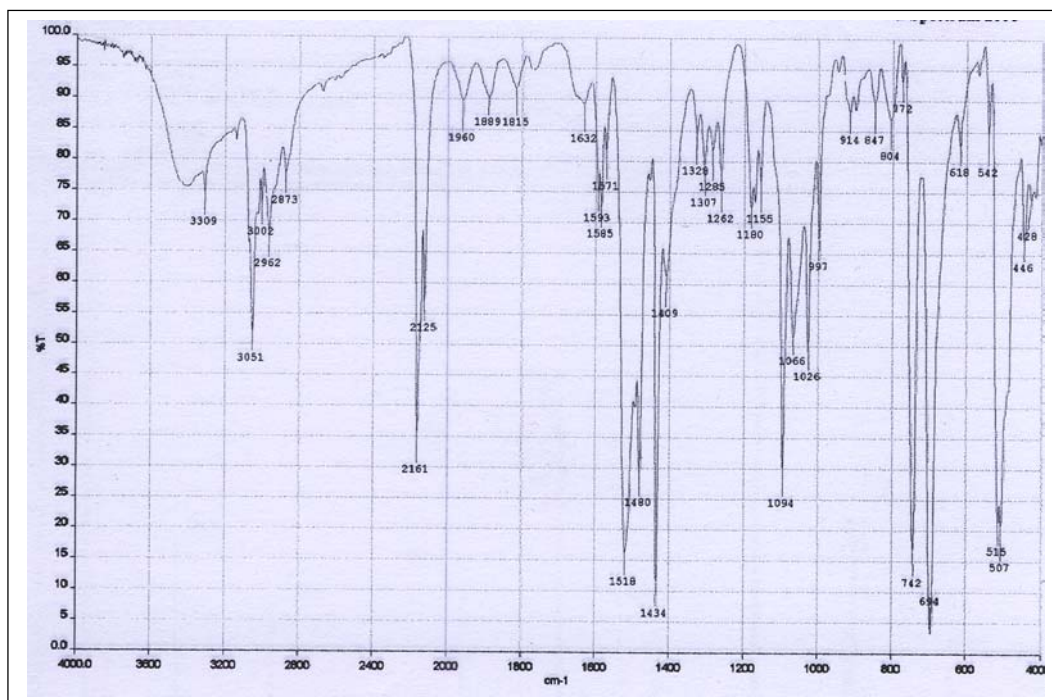


Fig. 51 Vibrational spectrum of **8**.

The mass spectrum of **8** is shown in Fig.52 and data are given in Table 13. The most important mass peaks appear at $m/z = 242$, 325 , 414 , 587 , 676 and 856 . The mass peak at 242 corresponds to the most abundant one and is derived from the supporting electrolyte. The

assignment of the others are reported in Table 13. All copper fragments $[\text{CuX}]^+$ are followed by a small packet of peaks, $M+16$, which could correspond to XCu-O , where X represents substituents. The peaks at m/z 587 correspond to $[\text{Cu}(\text{PPh}_3)_2]^+$, m/z 676 to (587+benzyl), m/z 767 to (587+2benzyl), m/z 856 to $[\text{Cu}(\text{PPh}_3)_2(\text{CH}_2\text{PPh})_2\text{BF}_4]^+$, m/z 947 to (856+benzyl), m/z 1038 to (856+2benzyl) and m/z 1129 to (856+3benzyl).

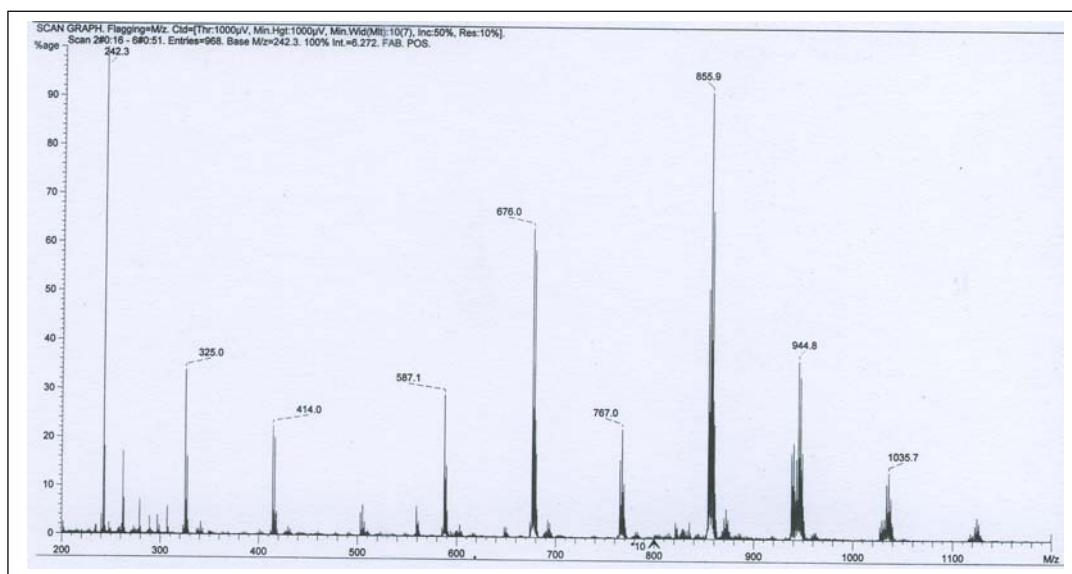


Fig. 52 FAB-MS spectrum of **8**.

Table 13 Mass spectrum data of **8**.

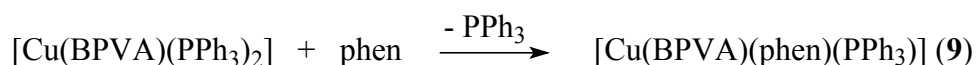
m/z	%	Fragments	m/z	%	Fragments
242	100	$[(\text{C}_4\text{H}_9)_4\text{N}]^+$	587	29	$[\text{Cu}(\text{PPh}_3)_2]^+$
262	17	$[\text{PPh}_3]^+$	678	63	$[\text{Cu}(\text{PPh}_3)_2(\text{CH}_2\text{Ph})]^+$
297	4	$([\text{Cu}(\text{BPVA})]^+ + 2\text{H})$	769	22	$[\text{Cu}(\text{PPh}_3)_2(\text{CH}_2\text{Ph})_2]^+$
325	34	$[\text{Cu}(\text{PPh}_3)]^+$	856	9	$[\text{Cu}(\text{PPh}_3)_2(\text{CH}_2\text{PPh})_2\text{BF}_4]^+$
414	23	$([\text{Cu}(\text{PPh}_3)(\text{BF}_4)]^+ + 2\text{H})$			

The results of the ^1H NMR of a solution of **8** in CD_3CN show the aromatic protons between 7.2 and 7.8 ppm as broad multiplets and a singlet at 3.66 ppm assigned to CH_2 group. Due to very low intensities, signal assigned to N–H could not be observed, such signal was found at around 9.8 and 9.6 ppm for azomethinic ligands [114].

The proton decoupled ^{13}C NMR of **8** exhibits a doublet at 134.28 ppm ($\text{C}_{\text{ortho}}\text{-PPh}_3$), a singlet at 130.54 ppm ($\text{C}_{\text{para}}\text{-PPh}_3$), another doublet at 129.47 ppm assigned to $\text{C}_{\text{meta}}\text{-PPh}_3$. The

singlet at 118.07 ppm was assigned to CN and the assignment of the singlet at 24.32 ppm to CH₂. Only one ³¹P NMR signal was observed at 13.10 ppm and assigned to Cu-PPh₃.

The compound **8** decomposes for a time when exposure to air. A reaction of [Cu(BPVA)(PPh₃)₂] with 1,10-phenanthroline leads to a substituted neutral mononuclear copper(I) complex (scheme 30). This reaction was carried out in the intention to stabilize **8** in the solid state. The crystals are received as stable red-violet compounds.



Scheme 30

3.3.3.2. Structure of (1-benzyl-2-cyano-2-phenylvinylaminate)(1,10-phenanthroline-N1, N10)(triphenylphosphane)copper(I) [Cu(BPVA)(Phen)(PPh₃)] (9)

The crystal structure of **9** has been investigated to uniquely determine the composition of the product of reaction in scheme 30, especially with respect to the determination of the structure of BPVA. The first results present a flack parameter of 0.3 and consequently, a possible twinned crystals. The orientation matrix for the single crystal was successfully obtained.

The structure of **9** consists of a monomeric unit as shown in Fig. 53. The copper atom is coordinated by the N atom of the BPVA ligand, by the phosphorous atom of the PPh₃ and chelated by two nitrogen atoms of the 1,10-phenanthroline ligand. Selected geometrical bond parameters are reported in Table 14. The coordination geometry about Cu(I) is described as distorted tetrahedral CuN₃P coordination sphere. This deviation is shown by the bond angles N4-Cu-N3 with 79.98(9)°. The bond length P-Cu of 2.205(8) Å is in good agreement with the average values of 2.252(44). Also the bond length C1-C2 being 1.406(4) Å agree with the value of literature 1.436(15) Å for C=C double bond length [100]. The two Cu-N(phen) bond lengths N3-Cu of 2.101(2) Å and N4-Cu of 2.099(2) Å are equal within experimental error and agree well with our previous experiences using phen as coligand.

It was not possible to improve the refinement beyond an *R*-value of 0.081. Nevertheless, this analysis do not permit a complete structural determination, but has served to identify the complex **9** and BPVA ligand beyond any doubt.

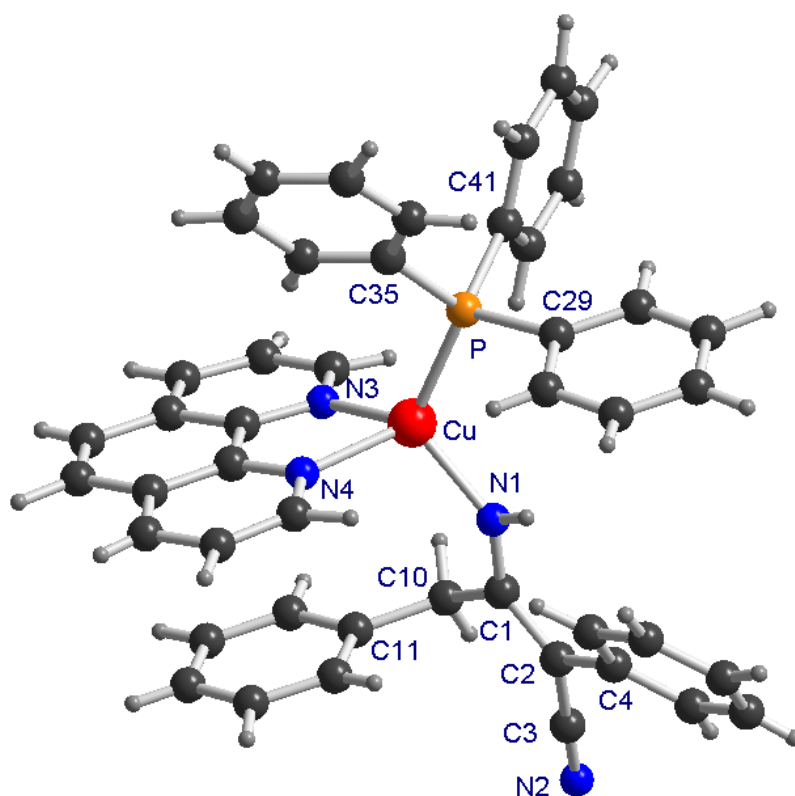


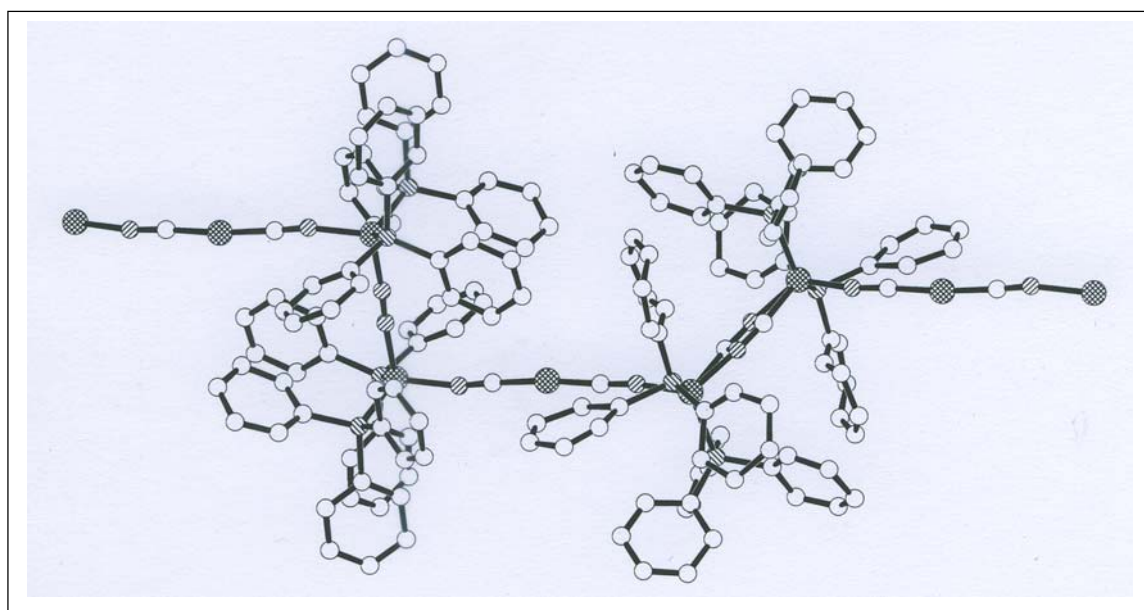
Fig. 53 Molecular structure of [Cu(BPVA)(phen)(PPh₃)] (**9**).

Table 14 Selected bond lengths (Å) and angles (°) of (**9**)

Bond lengths		angles	
P-Cu	2.205(8)	N1-C1-C2	126.8(2)
N1-Cu	1.977(2)	N1-C1-C10	114.3(2)
C1-N1	1.317(3)	C2-C1-C10	118.8(2)
C1-C2	1.406(4)	C1-C2-C3	118.6(2)
C1-C10	1.524(4)	C1-C2-C4	125.7(2)
C3-N2	1.159(4)	C3-C2-C4	115.5(2)
N3-Cu	2.101(2)	N2-C3-C2	179.2(4)
N4-Cu	2.099(2)	C11-C10-C1	114.1(2)
N1-Cu-P	112.07(7)	N1-Cu-N4	103.6(10)
N4-Cu-P	113.68(6)	N1-Cu-N3	123.6(9)
N3-Cu-P	117.47(6)	N4-Cu-N3	79.98(9)
C1-N1-Cu	135.8(2)		

3.3.3.3. Structure of $[\text{Cu}_9(\text{CN})_9(\text{PPh}_3)_8]_n$ (**10**)

The complex **8** is dissolved in CD_3CN in which it recrystallizes after standing for two weeks at room temperature. Single colorless crystals are collected for X-ray analysis which reveals a decomposition of **8** followed by a self-organization of Cu(I) and CN groups. Preliminary results shows that the crystal is twinned but it has been decided to proceed with the X-ray analysis in order to gain a fuller insight with regard to its structure. The crystal structure presents a neutral one-dimensional infinite polymer of composition $[\text{Cu}_9(\text{CN})_9(\text{PPh}_3)_8]_n$ (**10**) as depicted in scheme 31. The experiments are quite reproducible but unfortunately no improvements with regard to the quality of the crystals. **10** presents different interaction modes with Cu(I) centers and CN groups are σ, π -bonded. An uncommon coordination mode of CN occurs by $\mu\text{-}\eta^2\text{-NC}$ bonding. The copper atoms in this structure present three types of coordination environments; bi-, tetra- and penta-coordinated.



Scheme 31 A possible structure of a fragment of the chain in **10**.

An IR spectrum of **10** (Fig. 54) shows νCN stretching frequency bands occurring at 2123 and 2185 cm^{-1} which is typical for bridging cyanide groups [104,115].

Electrospray mass spectrum (Fig. 55) includes two main peaks at $m/z = 603$ and 676 corresponding to the most abundant ions. The peaks at m/z 676 corresponds to $[\text{Ph}_3\text{PCuCNCuPPh}_3]^+$, m/z 764 to $[(\text{Ph}_2\text{P})_2\text{Cu}(\mu\text{-}\eta^2\text{-CN})_2\text{Cu}(\text{PhP})_2]^+$ and at m/z 1200 to $[(\text{Ph}_3\text{P})_2\text{CuCNCu}(\text{PPh}_3)_2]^+$.

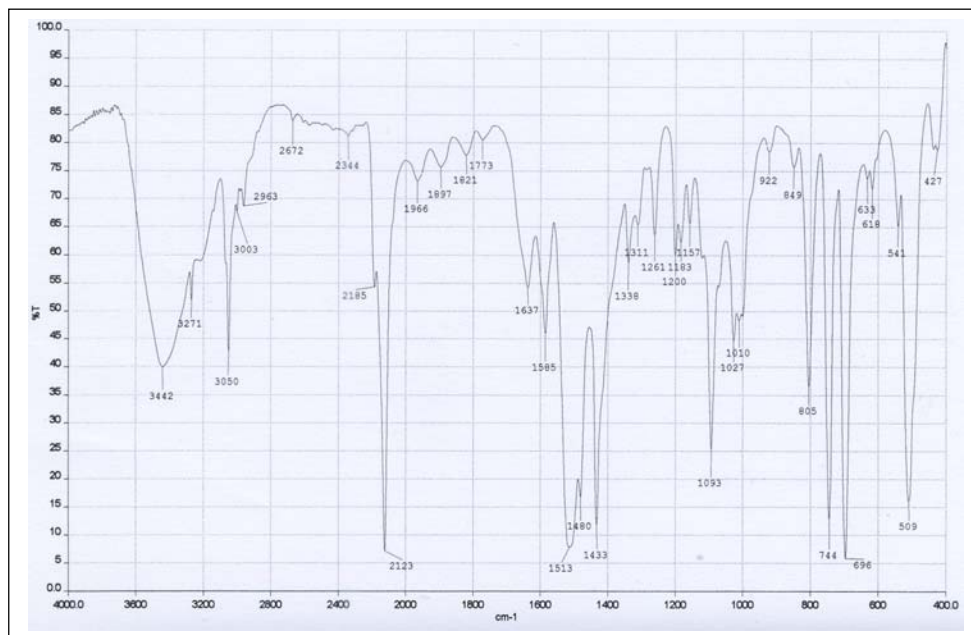


Fig. 54 Vibrational spectrum of **10**.

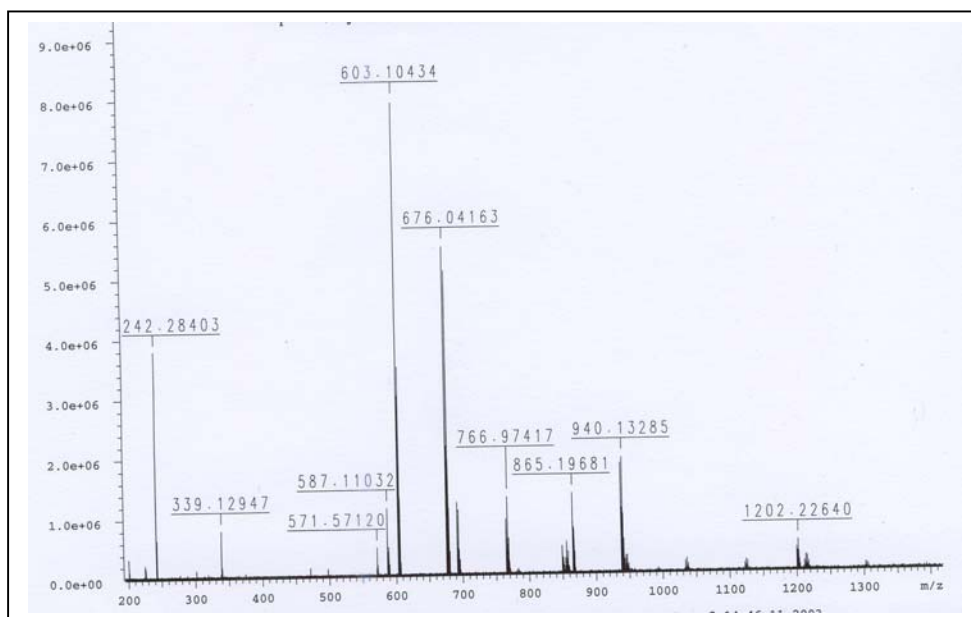


Fig. 55 ESI-MS spectrum of **10**.

3.3.3.4. Synthesis of $[\text{Cu}_3(\mu\text{-CN})_2(\text{phen})_3(\text{PPh}_3)_2][\text{BF}_4]$ (**11**)

The complex **11** has been achieved by adding 1,10-phenanthroline in excess to 10 ml of the electrolytic solution obtained by anodic dissolution of a copper metal, at a constant current of 10 mA, in THF / Bu_4NBF_4 , PhAN, PPh_3 at 0°C . **11** is received as orange crystals and characterized by elemental analysis, IR spectroscopy and X-ray crystal structure analysis.

The IR spectrum shows two bands at 2079 and 2178 cm^{-1} . This agrees with the observation of *Darensbourg et al.* [116] who found two $\nu(\text{CN})$ bands for similar compounds possessing tetrahedral copper. *Zhu and Vahrenkamp* [117] observed similar absorption bands for some trinuclear complexes and concluded that upon the formation of CN bridges the $\nu(\text{CN})$ bands move by 20-40 cm^{-1} to higher wave numbers.

The X-ray crystal structure of **11** reveals a one-dimensional copper(I) coordination with a bent $[(\text{phen})(\text{PPh}_3)\text{Cu}(\text{CN})\text{Cu}(\text{NC})(\text{phen})\text{Cu}(\text{phen})(\text{PPh}_3)]$ arrangement. The molecular structure of **11** consists of $[\text{Cu}_3(\text{CN})_2(\text{phen})_3(\text{PPh}_3)_2]^+$ cation with a non-coordinated $[\text{BF}_4]^-$ anion (Fig. 56). Selected bond lengths and angles are given in Table 15. Each copper(I) is tetra-coordinated and adopts a distorted tetrahedron. This deviation arises from the geometrical constraints imposed by the small bite angles N-Cu-N with a mean of $79.8(4)^\circ$. The Cu-C-N bond angles (mean $172.8(10)^\circ$) indicate an approximately linear CN coordination. The C1-N1 and C2-N2 bond lengths are 1.214(13) and 1.201(12) respectively. The Cu1-P1 and Cu3-P2 bond lengths (2.203(3) and 2.240(3) Å respectively) are comparable with those found in this work. Similar compounds exhibiting the characteristic of one dimensional $\{\text{Cu}(\text{CN})\}$ zigzag chain with chelating ligands side arms, are reported [117-121].

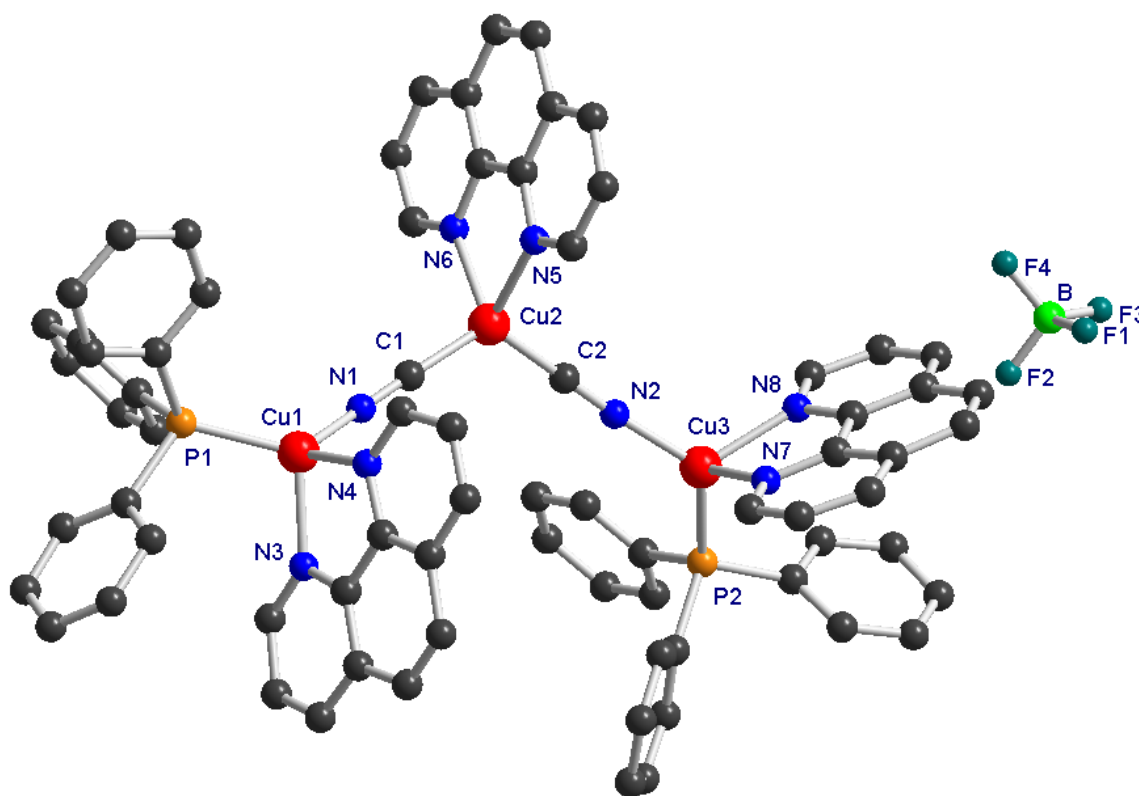


Fig. 56 Molecular structure of **11** (Hydrogen atoms are omitted for clarity).

Table 15 Selected bond lengths (Å) and angles (°) of **11**

Bond lengths		Bond angles	
C1-N1	1.214(13)	N1-C1-Cu2	177.4(10)
C2-N2	1.201(12)	N2-C2-Cu2	174.2(10)
C1-Cu2	1.917(10)	C1-N1-Cu1	165.3(10)
C2-Cu2	1.889(11)	C2-N2-Cu3	174.2(10)
C3-N3	1.332(14)	C3-N3-Cu1	132.3(9)
N1-Cu1	1.910(10)	N1-Cu1-N4	103.2(4)
N2-Cu3	1.920(11)	N1-Cu1-N3	114.2(3)
N3-Cu1	2.075(9)	N4-Cu1-N3	81.0(4)
N4-Cu1	2.061(9)	N1-Cu1-P1	123.4(3)
N5-Cu2	2.140(10)	N4-Cu1-P1	121.1(2)
N6-Cu2	2.117(9)	N3-Cu1-P1	106.5(3)
N7-Cu3	2.109(10)	C2-Cu2-C1	120.0(4)
N8-Cu3	2.124(10)	C2-Cu2-N6	114.8(4)
P1-Cu1	2.203(3)	C1-Cu2-N6	113.0(4)
P2-Cu3	2.240(3)	C2-Cu2-N5	111.0(4)
B-F3	1.263(18)	C1-Cu2-N5	111.9(4)
B-F4	1.280(19)	N6-Cu2-N5	78.9(3)
B-F2	1.308(19)	N2-Cu3-N7	105.8(4)
B-F1	1.357(18)	N2-Cu3-N8	119.4(4)
		N7-Cu3-N8	79.4(4)
		N2-Cu3-P2	125.7(3)
		N7-Cu3-P2	115.4(2)
		N8-Cu3-P2	102.2(2)

3.3.3.5. Synthesis of [Cu(CN)(phen)(PPh₃)₂·H₂O (**12**)

The complex **12** has been synthesized, in a similar way as **11**, by a reaction between 1,10-phenanthroline monohydrate (phen·H₂O) in excess with 10 ml of the electrolytic solution obtained by anodic dissolution of a copper metal, at a constant current of 10 mA, in THF / Bu₄NBF₄, PhAN, PPh₃ at 0°C. Slow evaporation at room temperature resulted in the

formation of green-yellowish crystals which are characterized by elemental analysis, IR spectroscopy, TG / DTG / DSC and X-ray crystal structure analyses.

The IR spectrum of **12** shows two main bands at 2079 and 2188 cm^{-1} due to $\nu(\text{CN})$ stretching vibrations.

The molecular structure of **12** consists of an asymmetric unit with two independent mononuclear molecules $[\text{Cu}(\text{CN})(\text{phen})(\text{PPh}_3)]$ and a non-coordinated H_2O molecule as shown in Fig. 57 with selected atom labeling. Selected bond lengths and angles are given in Table 16. The copper atoms are in a distorted tetrahedral environment defined by N_2P donor set and one cyano group. The deviation from ideal tetrahedral geometry is shown by the chelating angles $\text{N}2\text{-Cu}1\text{-N}3$ ($80.07(15)^\circ$) and $\text{N}5\text{-Cu}2\text{-N}6$ ($80.47(15)^\circ$). The terminal cyanide are close to ideally linear with Cu-C-N angle of $176(4)^\circ$. The $\text{Cu-N}(\text{phen})$ distances ranging from 2.084(4)-2.103(4) Å are within the normal range for copper complexes with N,N -chelating ligands [100,121,123,124]. The Cu-P distances which lie in the range 2.214(16) to 2.225(16) Å are in good agreement with those found previously.

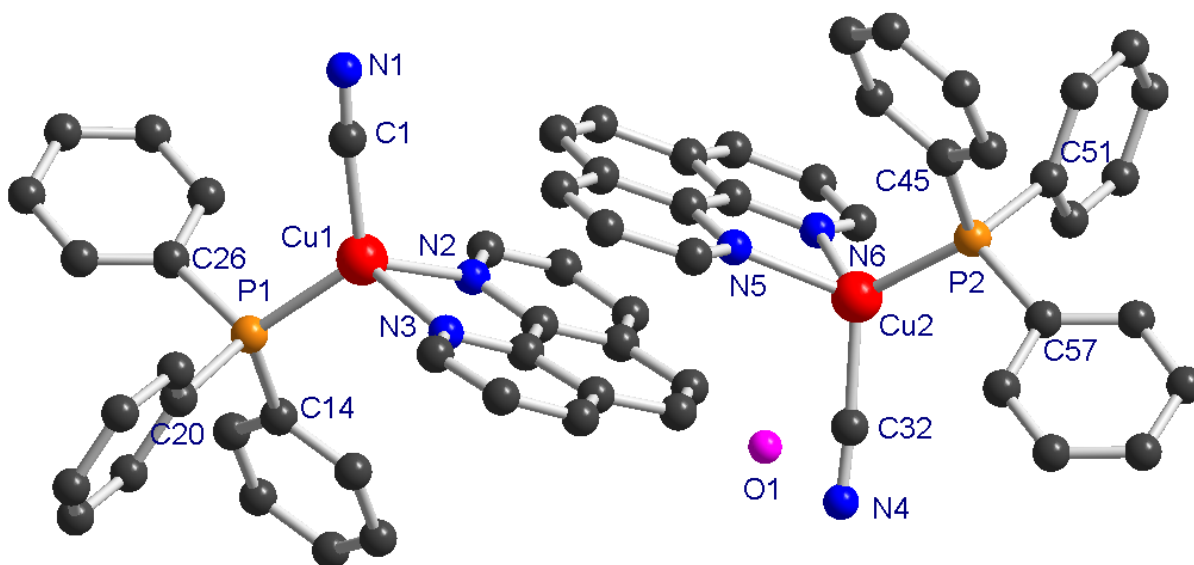


Fig. 57 Structure of $[\text{Cu}(\text{CN})(\text{phen})(\text{PPh}_3)]_2 \cdot \text{H}_2\text{O}$ (**12**) (Hydrogen atoms are omitted for clarity).

Table 16 Selected bond lengths (Å) and angles ($^\circ$) of **12**

Bond lengths					
C1-N1	1.123(7)	C32-Cu2	1.955(5)	N2-Cu1	2.084(4)
C32-N4	1.135(7)	P1-Cu1	2.225(16)	N3-Cu1	2.103(4)
C1-Cu1	1.957(6)	P2-Cu2	2.214(16)	N5-Cu2	2.084(4)
				N6-Cu2	2.086(4)

Bond angles					
N1-C1-Cu1	175.9(4)	C1-Cu1-P1	122.2(13)	N5-Cu2-N6	80.5(15)
N4-C32-Cu2	176.1(4)	N2-Cu1-P1	106.9(12)	C32-Cu2-P2	119.1(13)
C1-Cu1-N2	115.2(17)	N3-Cu1-P1	116.5(10)	N5-Cu2-P2	113.7(13)
C1-Cu1-N3	108.3(18)	C32-Cu2-N5	109.7(16)	N6-Cu2-P2	115.6(11)
N2-Cu1-N3	80.07(15)	C32-Cu2-N6	111.9(17)		

Within the crystal structure, the complex molecules are arranged in an alternating way with the oxygen atom and CN groups sandwiched by phenanthroline. A projection of the crystal packing is showed in Fig. 58.

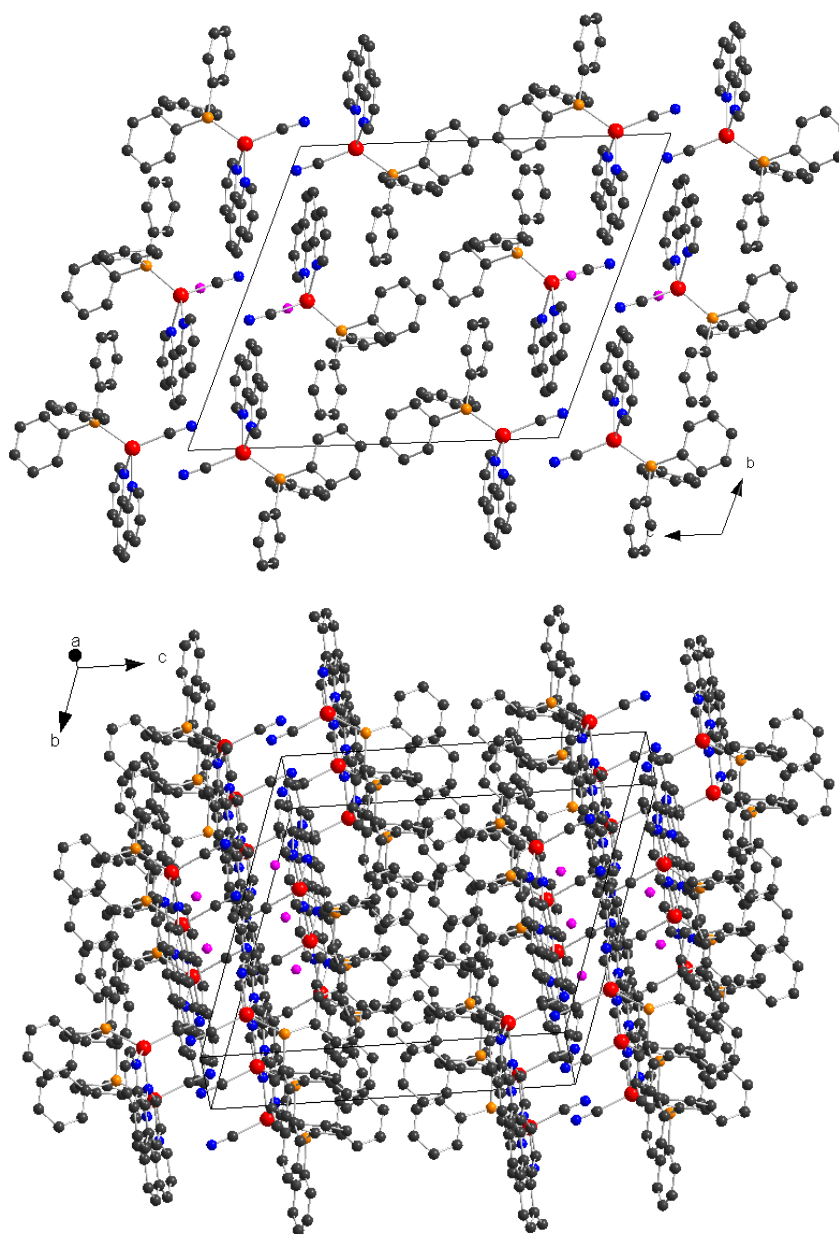


Fig. 58 Projection of the crystal packing of **12** (H atoms omitted for clarity)

The hydrogen atoms of water molecule could not be characterized by X-ray structure analysis. Therefore, it has been decided to proceed with thermal analysis.

Thermal analysis of 12

The combined TG / DTA / DSC curves of the complex **12** is presented in Fig. 59. Thermogravimetric curve shows that **12** decomposes in two steps. The first starts at about 70 °C and finishes at around 150 °C and corresponds to a weight loss of 1.67 % which is due to the dehydration. This weight loss corresponds well to the calculated value of 1.67 % for one mole of H₂O per formula unit and confirms that the non-coordinated H₂O observed in **12** derives from phenanthroline monohydrate (phen·H₂O).

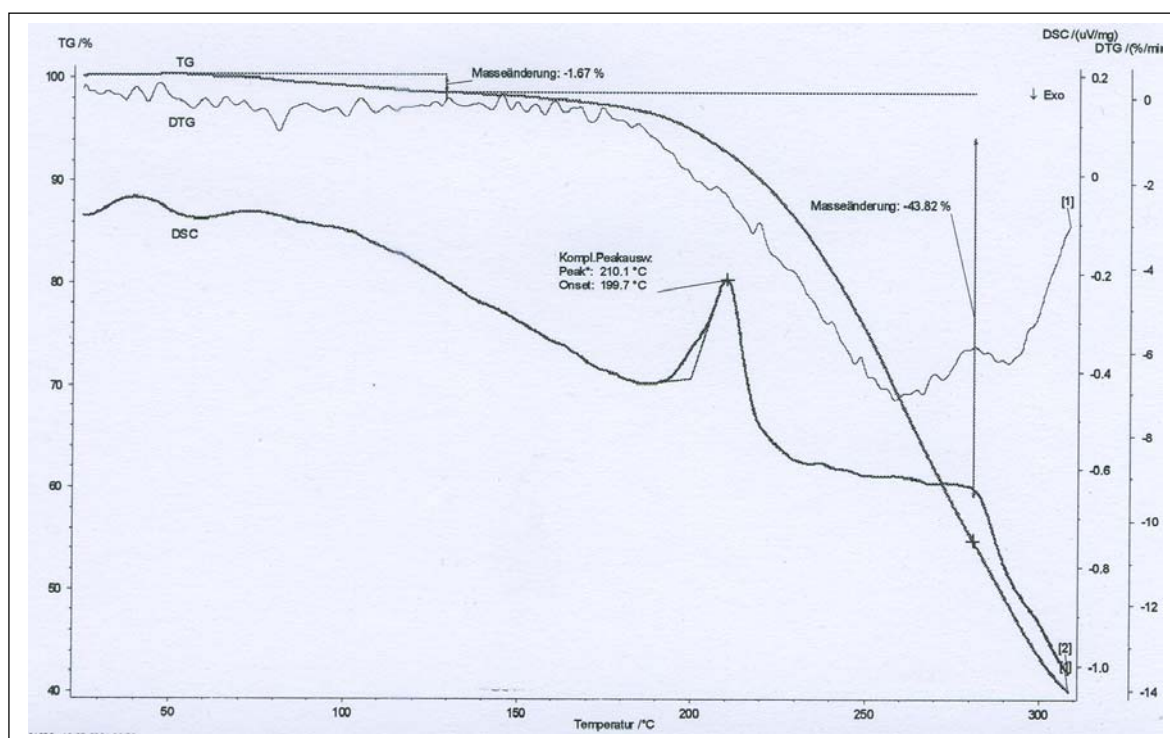


Fig. 59 TG / DTG / DSC curves for **12**.

The second step, over the temperature ranging from 150 °C to 280 °C and corresponds to a pronounced weight loss of 43.82 % attributed to the liberation of one phen, one PPh₃ and one CN molecules which was found to be 43.38 % after calculation. Differential scanning calorimetry (DSC) give the denaturation temperature of 210.1 °C.

Electrochemical behavior of 12

The electrochemical behavior of **12** has been investigated by cyclic voltammetry at a platinum and at a copper working electrodes in AN / Bu₄NBF₄. At the platinum electrode (Fig. 60) the cyclic voltammogram involves four distinguishable redox processes labeled R1 (−0.330 V), R2 (−1.250 V), O1 (−0.800 V) and O2 ($E_{1/2} = +1.166$ V). The irreversible process R1 is assigned to the reduction of **12**. *Leschke et al.* [80] explain such behavior by the fact that after being reduced the metal is released from the complexing environment. R2 is attributed to the reduction of free phenanthroline ligand [125]. Two oxidation peaks of the same height (O1 and O2) are observed during the backward scan. The second oxidation process is a reversible one-electron process with I_{pc}/I_{pa} close to unity (0.86) and almost slow electron transfer ($\Delta E = 97$ mV). Due to the difficulties to establish a base line for the counter part of O1, nothing could be said about its chemical reversibility. Nevertheless, O1 and O2 are assigned to Cu(I)/Cu(0) and Cu(II)/Cu(I) respectively. Such redox system, Cu(II)/Cu(I) with high potential was also found in Cu(I) complexes of substituted phenanthroline ligand [125].

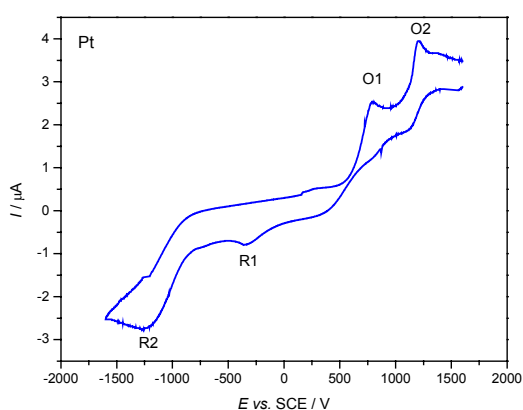


Fig. 60 CV of **12** at the platinum electrode (AN, 0.1M Bu₄NBF₄, 0.1 V s⁻¹).

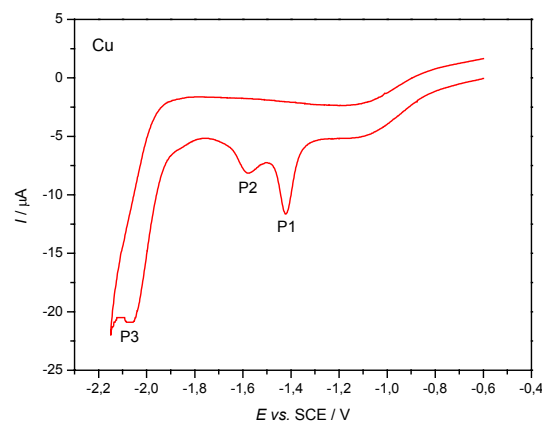


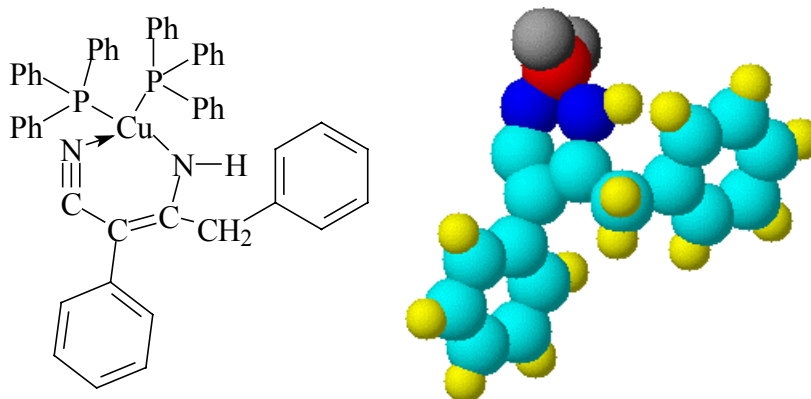
Fig. 61 CV of **12** at the copper electrode (AN, 0.1M Bu₄NBF₄, 0.1 V s⁻¹).

At the copper electrode (Fig. 61), three redox processes P1 (−1.416 V), P2 (−1.580 V) and P3 (−2.065 V) are observed. P1 and P2 are assigned to the reduction of Cu(I)/Cu(0) whereas P3 to the reduction of free phenanthroline.

3.3.3.6. Discussion

The direct electrosynthesis of PhAN-Cu(I) in THF / Bu₄NBF₄ has revealed that PhAN undergoes an electrolytic reductive coupling. The compound **8** is quite soluble in acetonitrile

and dimethylsulfoxide and could be represented as a monomer which can form through an intra molecular bonding six-membered atoms ring (CuN_2C_3) as shown in scheme 32.



Scheme 32 Proposed structure of $[\text{Cu}(\text{BPVA})(\text{PPh}_3)_2]$ (**8**)

The addition of phen in the one hand and $(\text{phen}\cdot\text{H}_2\text{O})$ in the other hand, to the solution of the electro-synthesis of $\text{Cu}(\text{I})$ -PhAN reveals that during the reduction of phenylacetonitrile, a splitting off of the CN group should be taken in consideration. This is confirmed by the molecular structure of **11** and **12**. It would be possible that **12** derives from **11** by breaking it up with the removal of a $\text{Cu}(\text{phen})$ unit.

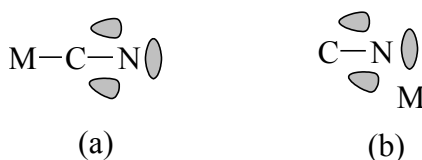
3.3.4. Discussion on the coordination mode of electrogenerated cyanide

Electrochemical synthesis of copper(I)-nitrile compounds has yielding a variety of products. In all cases examined electroreduction of nitriles occurs with C–CN bond cleavage as subsidiary reaction. The cyanide CN^- generated possesses the ability to act either as a terminal or as a bridging ligand. Question to be addressed should be its coordination mode. *Vinogradov et al.* [126] wrote that the metal–CN bonding in transition metal cyanides is usually described in terms of σ electron donation from the highest filled molecular orbital, lone-pair of CN^- ($\text{CN}^- \rightarrow \text{metal}$) and π -back-donation of metal 3d electrons into the first unfilled antibonding $2\pi(\pi^*)$ orbital of the ligand ($\text{metal} \rightarrow \text{CN}$). The $\text{Cu}(\text{I})$ center has a d^{10} electronic configuration and therefore is capable of back-donation to appropriate π -acid ligands such as CN^- , CO and alkenes [127]. *Vinogradov et al.* [126] demonstrated that CN^- is not only a good donor but also a reasonable π -acid ligand.

In this work, compounds with different coordination modes have been prepared successfully and characterized by X-ray structure analysis. Unfortunately, X-ray was not able to give

information about the coordination mode of cyanide. *Grotjahn et al.* [105] reported recently on the first precise molecular structure of a monomeric copper(I) cyanide, they found a Cu–C distance averaged 1.92 ± 0.03 Å. The Cu–C distances of Cu(I)-cyanide compounds obtained in this work are very closed to this value.

The degrees of bending of M–C–N and M–N–C is also informative about the coordination mode of cyanide [111,119,122, 128-130]. *Vahrenkamp et al* [128-130] discussed the metal-nitrogen interaction in the M–C≡N–M' bridge and reported that this interaction is in essence a σ -bond. They explain that the electron withdrawal from the CN⁻ ligand is compensated by enhanced π -back-donation to the C-bond metal. Thus there is a balance of σ -donation from the N atom and π -back-donation to the C atom which seems to be always the same in the case of CN bridge [129]. Generally, the π -back-donation from the metal (M) to cyanide causes a close-to-linear M–C–N [130]. However, the considerable deviation from linearity of the M–N–C angle is an indication of the absence or small magnitude of any π -interaction between metal and cyanide [129]. In this case the M–N bond is longer than the related M–C bond (π bonding) [131]. Consequently, M–C–N is characterized by the "linearizing" effect and M–N–C, the "bending" effect [131] as represented in scheme 33 [132] and which represents the molecular orbital description of the electron density in the nitrogen region of the C≡N group.



Scheme 33 Metal–cyanide bonding model [132].

As observed in this work, the CN bridges, Cu–CN–Cu, are usually linear and this could be explained by the fact that there is less π electron density distal to the N atom of the CN group [132]. It has been demonstrated that the CN ligand has less tendency to form bent bridges than CO in which exists more electron density in the vicinity of the O atom than in the analogous N atom in CN group [133]. In the most cases, the bridging CN group is required to be disordered as it lies on a centre of symmetry [23, 101].

3.4. Electrosynthesis of copper(I) complexes with non-nitrile ligands

The direct electrosynthesis of PhAN-copper(I) complex has shown that phenylacetonitrile ($pK_a = 21.9$ [21c]) undergoes an electroreductive coupling. As an extension of these studies, the synthesis of copper(I) complexes incorporating less acidic non-nitrile compounds has worth attention. For this achievement, fluorene ($pK_a = 22,6$ [134]) and triphenylmethane ($pK_a = 31.0$ [21h]) have been selected.

It has been pointed out and confirmed that copper(I)chloride complexes containing bidentate bridging diphosphine ligands exhibit antitumor activities [40]. The aim of this section is to make a contribution to the synthesis of such compounds by electrochemical procedure. To this end, the preparation of copper(I)chloride complex with 1,2-bis(diphenylphosphino)ethane (dppe) ligand has been attempted.

3.4.1. Electrosynthesis of fluorenylbis(triphenylphosphane)copper(I)-diacetonitrile $[\text{Cu}(\text{Flu})(\text{PPh}_3)_2] \cdot 2\text{CH}_3\text{CN}$ (**13**)

The electrochemical synthesis of **13** has been carried out as a one-step reaction in an undivided cell with a copper anode and a platinum cathode in AN / Bu_4NBF_4 at a constant current of 50 mA at 0 °C. Fluorene ($pK_a = 22,6$ [134]) is used as starting material and triphenylphosphane as coligand. A white precipitate is received as product after a charge of 1 Faraday, which corresponds to $1 e^- / \text{mol}$, has passed through the solution. **13** is quite soluble in DMSO and difficultly soluble in THF. No single crystals have been isolated therefore, the complex **13** has been characterized by C, H, N elemental analysis, EDX (Fig. 62), ESI-MS, ^1H -, ^{13}C -, ^{31}P -NMR and IR-spectroscopies.

The ESI mass spectrum of **13** presents the main peak at m/z 675 which corresponds to the most abundant ion $[\text{Cu}(\text{Flu})(\text{PPh}_3)(\text{PPh}_2)]^+$. Also, another important peak is found at m/z 603 and assigned to $[\text{Cu}(\text{Flu})(\text{PPh}_3)(\text{PPh})]^+$.

The IR spectrum of **13** exhibits two bands at 2120 and 2185 cm^{-1} attributable to CN group.

The ^1H NMR shows a sharp singlet signal at around 2.1 ppm which could correspond to a C–H proton of the fluorenyl. The proton of phenyl groups appear in the range of 7.2 – 7.9 ppm as broad multiplets.

In the ^{13}C spectrum, all peaks of the phenyl groups appear in the expected region, 128 – 135 ppm. The peak observed at 23.1 ppm could be assigned to C–H (fluorenyl).

The ^{31}P NMR signal was observed at 26.6 and -165.6 ppm and indicating that all phosphorus atoms are not chemically equivalent.

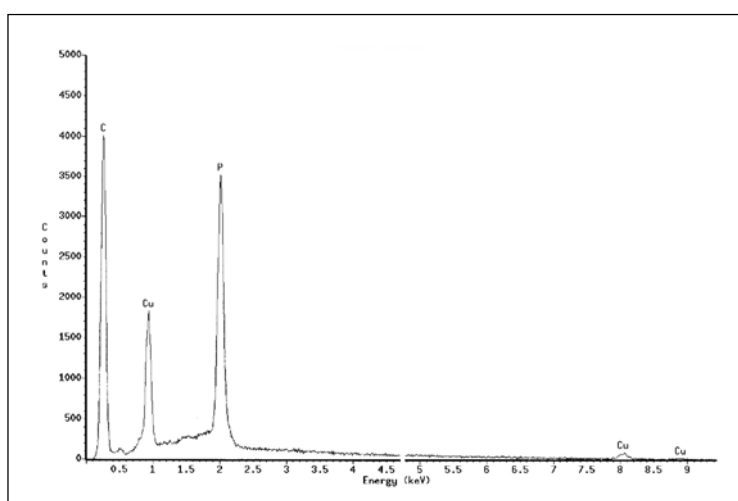
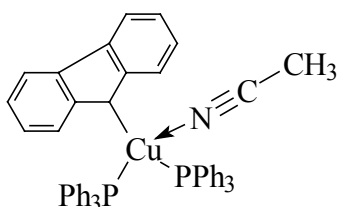


Fig. 62 Energy dispersive X-ray spectrum of **13**.

Based on these investigations the following structure is proposed as a possible structure for the complex **13** (scheme 34):

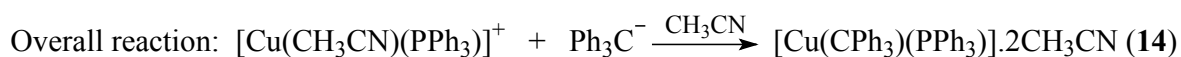
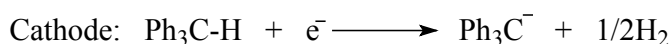


Scheme 34 The proposed structure for **13**.

The electrochemistry of fluorene is already reported in the literature [135,136]. That why it is not necessary to repeat it here.

3.4.2. Electrosynthesis of triphenylmethyl(triphenylphosphane)copper(I)-diacetonitrile $[\text{Cu}(\text{CPh}_3)(\text{PPh}_3)] \cdot 2\text{CH}_3\text{CN}$ (**14**)

The complex **14** has been prepared by galvanostatic dissolution of a sacrificial copper anode and simultaneous cathodic reduction of triphenylmethane in AN / Bu_4NBF_4 , PPh_3 at 50 mA and 0 °C. **14** is received as a greenish precipitate after 2 h 40 min of electrolysis. The electrochemical efficiency (E_f), found to be close to 1 mol F^{-1} , suggests the following reactions taking place at the electrodes:



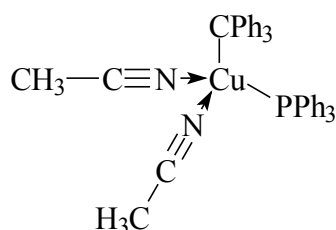
Scheme 35

The characterization of the complex **14** was done by C, H, N elemental analysis, EDX and FAB-MS.

The positive-ion fast atom bombardment (FAB) mass spectrum shows some significant mass peaks for species of $m/z = 142$ (56.34%), 185 (29.84%), 242 (100%) and 243 (54.77%). The mass peak at $m/z = 242$ corresponds to the base peak and is assigned to $[(\text{CPh}_3)\text{-H}]$. The peaks at $m/z = 140$ (5.21%), 171 (1.97%), 185 and 243 are attributed to $[\text{CuPh}]^+$, $[\text{Cu}(\text{PPh})]^+$, $[\text{PPh}_2]^+$ and $[\text{CPh}_3]^+$ respectively.

Energy dispersive X-ray (EDX) confirms the presence of carbon, copper and phosphor in the complex (Fig. 63).

A possible structure of **14** is represented as (scheme36):



Scheme 36 The proposed structure for **14**.

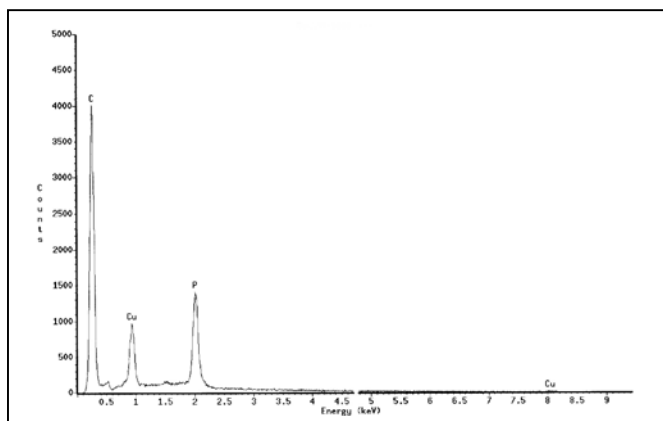
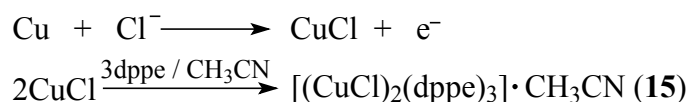


Fig. 63 Energy dispersive X-ray spectrum of **14**.

The mechanisms of the electrosynthesis of copper(I) complexes incorporating less acidic organic compounds (non-nitriles) are determined based only on the electrochemical efficiency.

3.4.3. Electrosynthesis of $[(\text{CuCl})_2(\mu\text{-dppe})(\eta^2\text{-dppe})_2] \cdot \text{CH}_3\text{CN}$ (**15**) and $[(\text{CuCl})_2(\mu\text{-dppe})(\eta^2\text{-dppe})_2] \cdot (\text{CH}_3)_2\text{SO}$ (**16**)

The complex **15** has been prepared at 0 °C by galvanostatic dissolution of a copper anode (50 mA) in the presence of 1,2-bis(diphenylphosphino)ethane (dppe) and lithium chloride (LiCl). The electrochemical cell is represented as: $\text{Cu}_{(+)} / \text{CH}_3\text{CN} + \text{LiCl} + \text{dppe} / \text{Pt}_{(-)}$. The complex formation occurs with an excess of chloride and 1,2-bis(diphenylphosphino)ethane (dppe). The reaction pathway of the synthesis is summarized as in scheme 37 which schematically corresponds to the anodic reaction (with an electrochemical efficiency of $E_F = 0.96$).



Scheme 37

A yellowish precipitate occurs during electrolysis. The synthesis is stopped after a charge of 1 Faraday has passed through the solution. Two weeks later, single brown crystals suitable for X-ray analysis have been collected and characterized. C, H and N elemental analysis was not possible because **15** seems to be hygroscopic.

The complex **15** is soluble in DMSO in which it recrystallizes leading to a substitution of solvent molecule, $[(\text{CuCl})_2(\mu\text{-dppe})(\eta^2\text{-dppe})_2]\cdot(\text{CH}_3)_2\text{SO}$ (**16**). Both complexes are characterized by EDX and X-ray.

Crystal structure of 15 and 16

The molecular structures of complexes **15** and **16** are depicted in Fig. 64. The solid-state consists of a neutral centrosymmetric molecular unit with the center of symmetry lying between the methylene carbons of the bridging 1,2-bis(diphenylphosphino)ethane (dppe) ligand. Each copper atom is in a distorted tetrahedral environment and terminally bounded by a single chloride and dppe in a η^2 fashion. **15** and **16** crystallize with one molecule of solvent in a ratio of 1:1.

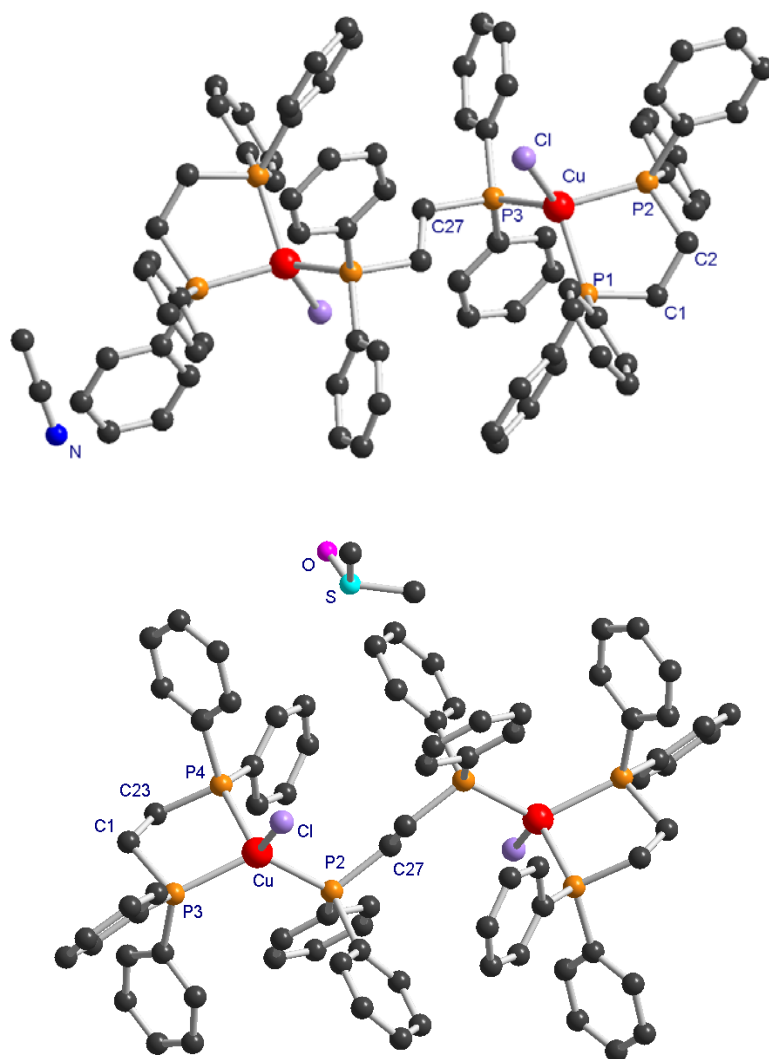


Fig. 64 Structure of $[(\text{CuCl})_2(\mu\text{-dppe})(\eta^2\text{-dppe})_2]\cdot\text{CH}_3\text{CN}$ (**15**) (top) and $[(\text{CuCl})_2(\mu\text{-dppe})(\eta^2\text{-dppe})_2]\cdot(\text{CH}_3)_2\text{SO}$ (**16**) (bottom) with selected atom numberings (Hydrogen atoms are omitted for clarity).

A projection of the crystal packing is presented in Fig. 65. Selected geometrical bond parameters have been compiled in Table 17. The main difference is that the P3-Cu-P1 angle, $123.6(7)^\circ$, in **16** is greater than in **15** ($115.0(3)^\circ$). The Cu-P distances are comparable with those found in the literature [95,100,138,139]. The bond lengths and angles reported in Table 17 are quite similar to those obtained by *Albano et al.* [139] by a reaction of a trimeric $[\text{Cu}(\text{halide})(\text{dppe})]_3$ with an excess of dppe in benzene and recrystallized from acetone.

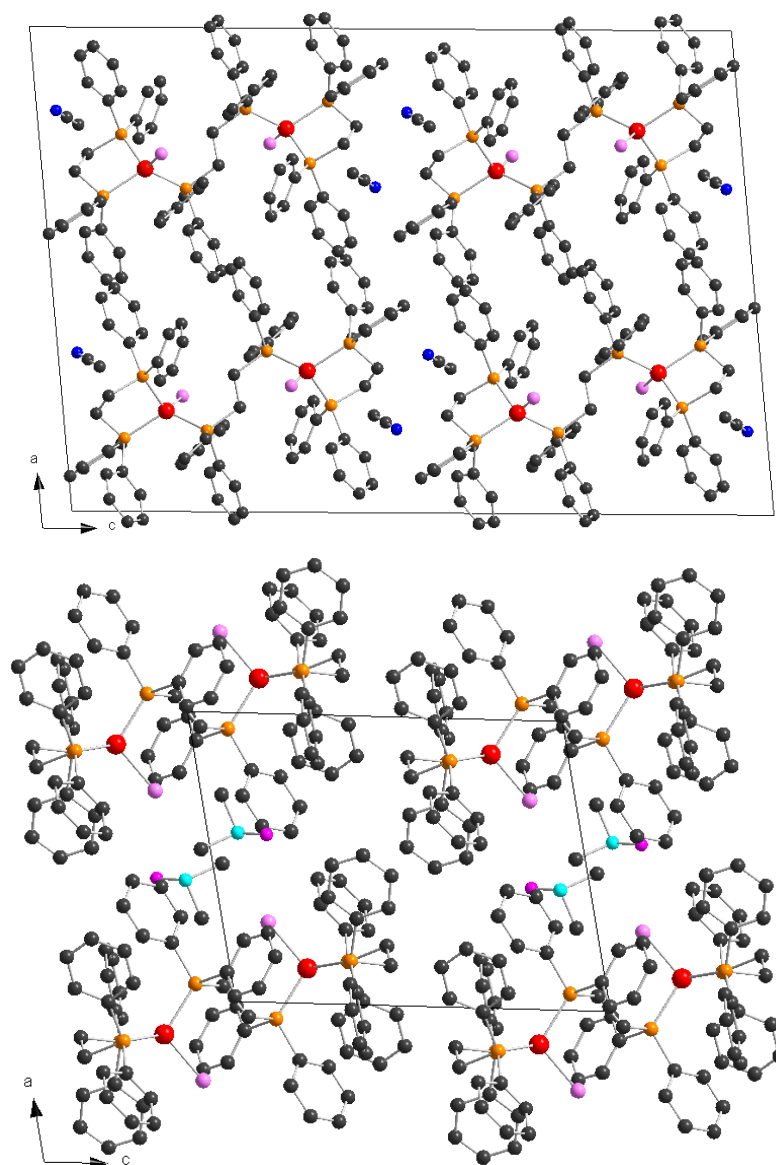


Fig. 65 Projection of the structure of $[(\text{CuCl})_2(\mu\text{-dppe})(\eta^2\text{-dppe})_2]\cdot\text{CH}_3\text{CN}$ (**15**) (top) and $[(\text{CuCl})_2(\mu\text{-dppe})(\eta^2\text{-dppe})_2]\cdot(\text{CH}_3)_2\text{SO}$ (**16**) (bottom) along b axis (Hydrogen atoms are omitted for clarity).

The molecular structure of tris-[1,2-bis(diphenylphosphino)ethane]dicopper(I) complexes prepared by classical routes, revealed that such compounds crystallize with two molecules of solvent [138-140] whereas those obtained by electrochemical way crystallize with only one

molecule of solvent. The structural differences between the results obtained in this work and the previously reported have been established and compiled in Table 18.

Table 17 Selected bond lengths (Å) and angles (°) of **15** and **16**.

Bond lengths	15	16	Bond angles	15	16
C1-C2	1.533(4)	1.535(9)	C1-C2-P2	110.9(2)	110.9(5)
C1-P1	1.851(3)	1.836(23)	C1-P1-Cu	102.5(9)	102.1(2)
C2-P2	1.845(3)	1.853(35)	C2-P2-Cu	103.1 (9)	102.0(2)
C27-P3	1.849(3)	1.832(24)	C27-P3-Cu	112.0 (8)	112.3(3)
P1-Cu	2.287(8)	2.319(40)	P3-Cu-P1	115.0(3)	123.6(7)
P2-Cu	2.290(9)	2.312(33)	P3-Cu-P2	119.5(3)	111.9(7)
P3-Cu	2.267(8)	2.288(39)	P1-Cu-P2	90.4(3)	90.2(6)
Cu-Cl	2.307(7)	2.308(27)	P3-Cu-Cl	103.8(3)	107.9 (2)
			P1-Cu-Cl	116.6(3)	109.7(1)
			P2-Cu-Cl	112.0(3)	112.5(1)

Table 18 Important structural features of [(CuCl)₂(μ-dppe)(η²-dppe)₂] (A) complexes.

Parameters	Value			
	A·CH ₃ CN	A·(CH ₃) ₂ O	A·2(CH ₃) ₂ O [139]	A·2CH ₂ Cl ₂ [140]
Crystal system	monoclinic	triclinic	monoclinic	monoclinic
Space group	I2/a	P $\bar{1}$ (No 2)	P2 ₁ /c (No 14)	P2 ₁ /n
Cell dimensions				
a [Å]	22.046(5)	11.264(2)	12.57(1)	12.608(9)
b [Å]	10.611(17)	12.439(2)	22.09(2)	21.729(7)
c [Å]	31.988(7)	14.372(3)	16.42(1)	14.473(8)
α [°]	90	94.21(3)	90	90
β [°]	95.40(3)	100.48(3)	121.28(12)	105.34(5)
γ [°]	90	96.03(3)	90	90
Volume [Å ³]	3725	1960.32	3896.5	3823.6

The electrochemical methodology has proved to be an efficient alternative and a very simple procedure for the preparation of copper(I)chloride complexes with 1,2-bis(diphenylphosphino)ethane ligand, [(CuCl)₂(μ-dppe)(η²-dppe)₂]. This compound exhibits antifungal activity against three strains of *C. albicans*, P388 leukemia, M5076 reticulum cell sarcoma and B16 melanoma [40,141] and exhibits tumouricidal properties [142].

4. Introduction to micro- and nanostructuring of metal surfaces

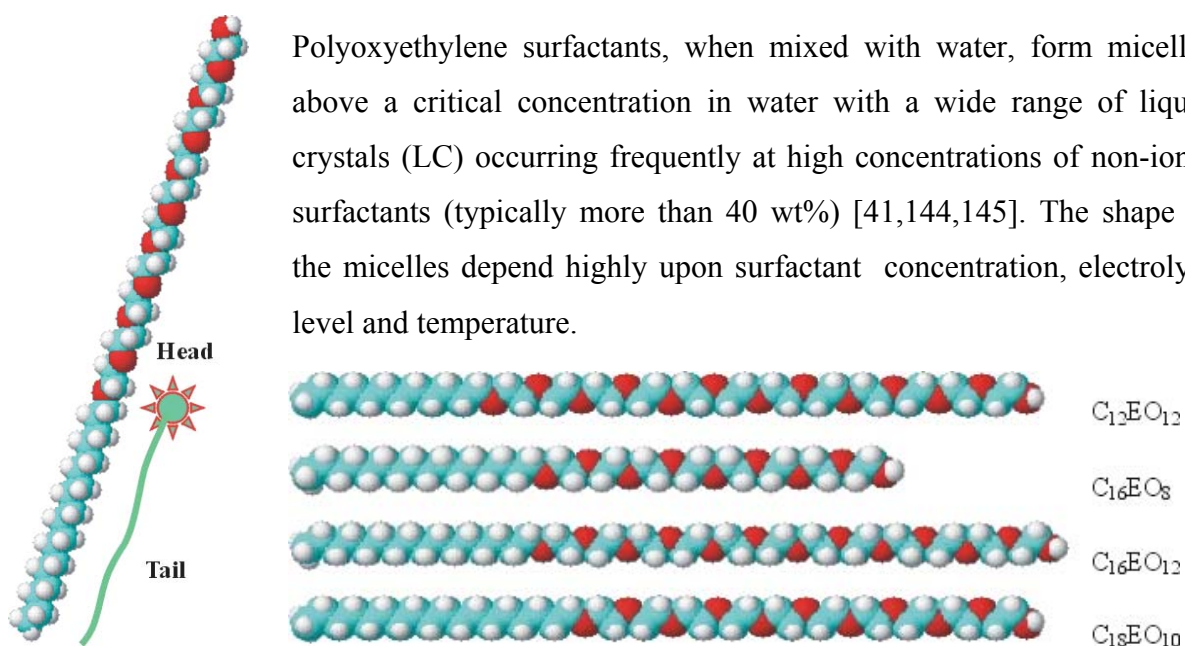
The modification of surfaces at micrometer and sub-micrometer scales is considered to be a key future technology. This has led in recent years to an interest in the generation of micro- and nanometer sized structures on surfaces [143]. Nanostructured materials may adopt various shapes which are critical factors in determining their basic properties and are of much current interest for extensive potential applications in electronic, mechanical and optical devices.

A variety of methods for the fabrication of micro- and nanostructured materials have been proposed and applied, such as molecular beam epitaxy, microlithography, vapor-liquid-solid growth, solution-liquid-solid growth and template-mediated methods. The latest entails synthesizing the desired material within the pores of a nanoporous material.

In this order of idea, a working place has been developed to modify the metallic surfaces with organocopper(I) complexes through coordinative interaction at micro and nanometer scales. To test the operating of the experimental setup, mesoporous platinum films (with a defined nanostructure) should be electrodeposited from lyotropic liquid crystal phases onto a gold surface under galvanostatic control. The templated electrodeposition was introduced by *Attard et al.* [41,42,144,145] to produce under potentiostatic control porous nanostructured metals from lyotropic liquid crystal [146-148]. Such modified materials found applications ranging from catalysts, molecular sieves to batteries and electronics [149-153].

4.1. Surfactant templating

Non-ionic surfactants, *n*-alkylpolyethylene glycol ethers commonly known as polyoxyethylene surfactants, are widely used as emulsifying agents, as detergents [154] and as template to produce mesoporous and/or mesostructured material [155-159]. They have the general chemical formula $C_nH_{2n+1}(CH_2CH_2O)_mOH$ [156], $CH_3CH_{(n-1)}(CH_2CH_2O)_mOH$ [155] or $n-C_nH_{2n+1}(OCH_2CH_2)_mOH$ [154] and denoted as C_nEO_m ; by alteration of *m* and *n* it is possible to change systematically their chemical structure. The templating aggregates arise because surfactants are bifunctional molecules which contain a polar head group (*m*) (water loving or hydrophilic) and a non-polar chain (tail) group (*n*) (solvent hating or hydrophobic) as drawn in scheme 38.



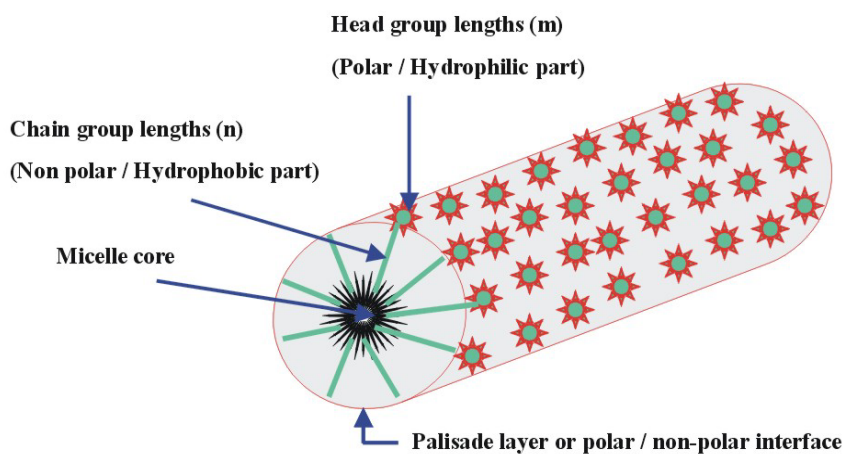
Scheme 38 The chemical structure of a non-ionic surfactants.

The amphiphilic nature of non-ionic surfactants results in molecular aggregation forming usually a lyotropic liquid crystalline (LLC) mesophase with a well-defined structure. This occurs because the alkyl group C_nH_{2n+1} (oil like) of the C_nEO_m molecule tends to minimize the interaction with water and also the polar EO head group $-(CH_2CH_2O)_mOH$ tends to stay outside to form diluted water solutions. Thus the liquid crystalline phase is formed by water molecules through polar-apolar interactions [156].

The topology of the structure can be varied in a predictable fashion. *Attard et al.* [144,146] have used at high concentration, the non-ionic surfactant, octaethyleneglycol monodecyl ether ($C_{16}EO_8$) to produce three liquid crystalline phases: hexagonal (H_I), cubic ($Ia3d$) and lamellar (L_α). Among these three phases, the hexagonal one, which exists over a wide range of composition and temperature is the most reported.

The hexagonal phase is consisted of long cylindrical micelles of surfactants packed into a hexagonal array with a uniform radius determined by the length of the surfactant molecules (scheme 39). The size of pores and the thickness of metal walls can be modified by varying the alkyl chain length of the surfactant and/or by adding a co-solvent as n-heptane to swell the micellar surfactant rods in lyotropic liquid crystalline phase. So, the range of radii was varied from 1.7 to 3.5 nm by using a variety of non-ionic surfactants (scheme 38) and added hydrocarbon swelling agents, suggesting the dispersion of alkane molecules between the surfactant micellar aggregates [160,161].

The cubic phase does not exist at room temperature. At high concentration of surfactant the lamellar (L_α) phase predominates and consists of surfactant molecules aggregated to form infinite continuous planes separated by water layers [160,161].



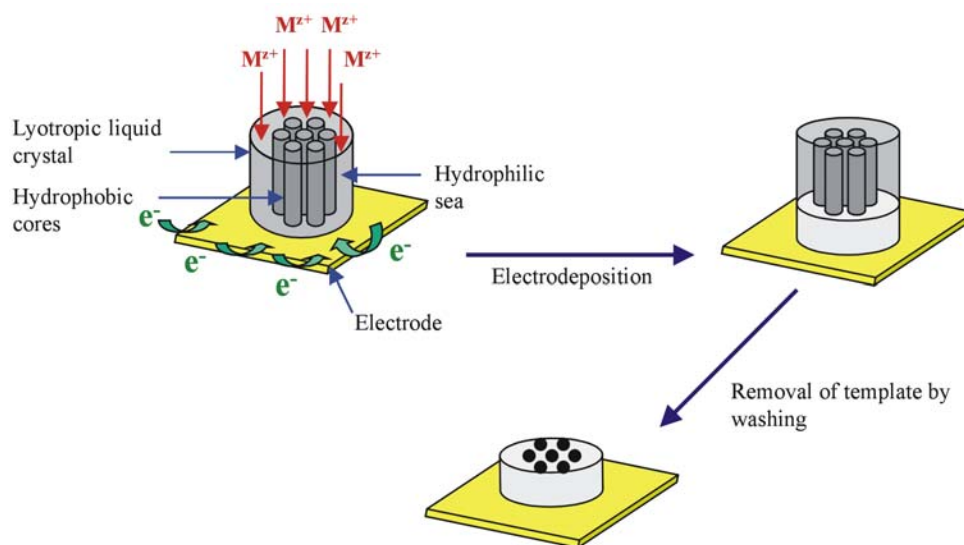
Scheme 39 Long cylindrical micelles of surfactants.

Consequently, the nanostructures of the metal films deposited from LLC phases depend on the structure of the lyotropic phase used. In the cases of $C_{12}EO_6-H_2O$, $C_{12}EO_8-H_2O$, $C_{12}EO_{10}-H_2O$, $C_{16}EO_8-H_2O$ and $C_{16}EO_{11}-H_2O$ systems, the sequence of the mesophase follows the hexagonal (H1) \rightarrow cubic (V1) \rightarrow lamellar (L_α) order with increasing surfactant concentration at room temperature. The hexagonal phase is the most stable and appears in a range of 40-70 wt% surfactant concentrations [42,144,154,158,162].

4.2. The principle of templated electrodeposition

The principle of the templated electrodeposition consists of dissolving the metal precursor in the hydrophilic domains of the mixture around the hexagonally packed cylindrical surfactant micelles. In these domains the metal salts are solvated by water in the vicinity of the polar EO head groups of the non-ionic surfactant molecules. Upon application of the potential, metal is electrodeposited within these aqueous domains, producing a metal film around the surfactant micelles. Once the metal deposition is complete, the electrochemical cell is disassembled and the surfactant is removed by soaking the film in water to leave an adherent nanostructured metal film with a hexagonal array of cylindrical pores as a direct cast of the lyotropic liquid crystalline phase (scheme 40 analog to [149,160,163,164]). Several prerequisites are required for using this method to prepare nanostructured materials: water, choice of surfactant,

precursor molecule and additive. Under the right conditions the precursor molecules react, only within the aqueous domains, to build up a solid mass of product.

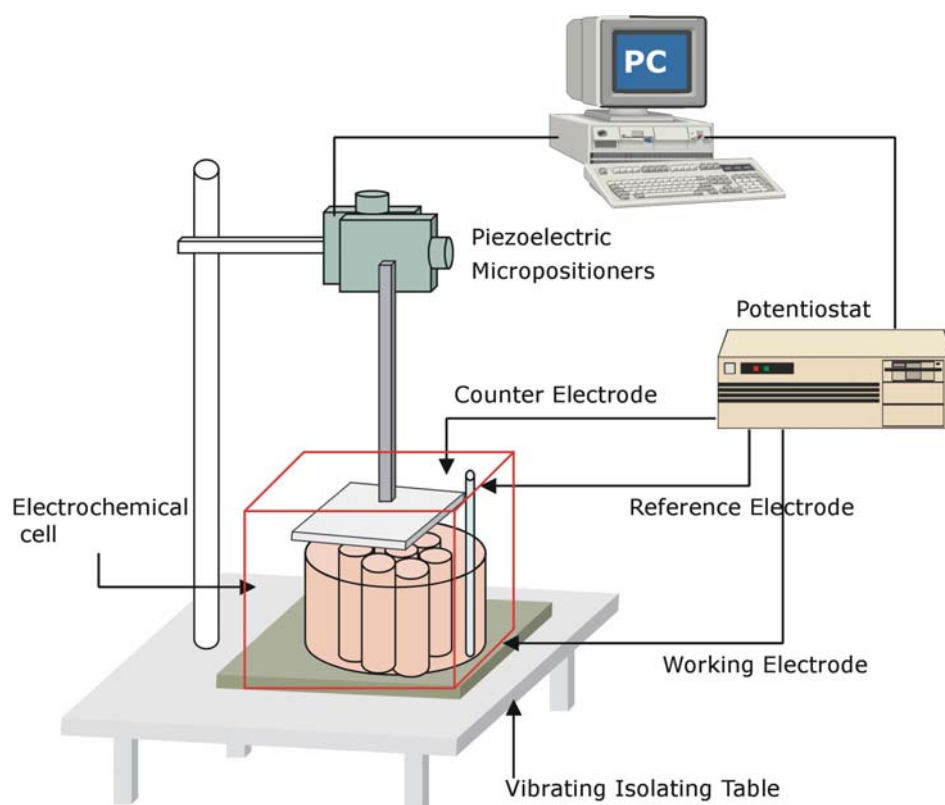


Scheme 40 The principle of the liquid crystal templating method.

The electrodeposition of metal by templating method usually occurs at a constant potential where the rate of deposition is controlled by the kinetics of the process and not by mass transport. So, the thickness of the deposited film is controlled by varying the total charge passed during the electroplating process [164].

4.3. Schematic representation of the working station

The first goal of this work is to achieve galvanostatically microstructures which exhibit a well defined nanostructures. These nanostructured surfaces will be used later for the fixation of metal complexes. For this achievement, the basic of apparatus for metal electrodeposition is shown in scheme 41. The working electrode is attached to the bottom of electrochemical cell which is mounted on a stable platform. The counter electrode is fixed on a Motor Controller which can drive up to 4 DC-motors directly from a PC with C-842 WinMove[®] programming software. The electrodes are connected to a Potentiostat / Galvanostat which operates remotely from a PC via a IEEE-488 interface port with 352 SoftCorr[®] III software. The distance between both electrodes (WE and CE) is maintained constant during the experiment by piezoelectric micropositioners which can move in two dimensions (y,z).



Scheme 41 Block diagram of the apparatus for metal electrodeposition.

4.4. Potentiostatic deposition of the platinum film from the liquid crystalline plating mixture

The first series of experiments in this part is devoted to the electrodeposition of mesoporous platinum film from the liquid crystalline plating mixture onto gold electrode. The plating mixture used consists of a commercially available non-ionic surfactant, Brij[®]76 that nominally corresponds to decaethyleneoxide monoctadecyl ether ($C_{18}EO_{10}$), a precursor salt such as hexachloroplatinic acid (HCPA) and water. The first step consists to identify the texture of the ternary salt/water/surfactant system by polarized optical microscopy (POM).

Thin films of the liquid crystals were prepared by sandwiching the mixture between a glass microscope slide and cover slide, and cooling them from 83-85°C to room temperature. The POM image of the mixture displays a typical texture which corresponds to a columnar phase and was found to be stable up to 85°C (Fig. 66). By pressing on the sample sandwiched between glass slides, large dark region are developed which could be refer to hexagonal phases. Unfortunately, images could not be possible from the X-ray, consequently nothing could be said about the mesophase.

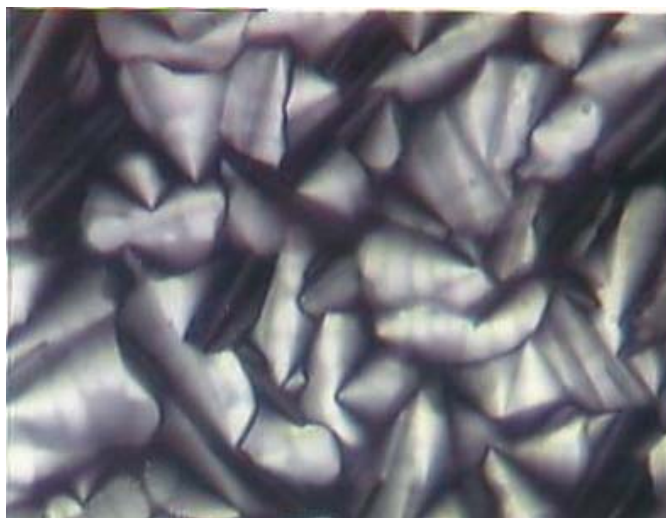


Fig. 66 Polarized optical microscopy image of the liquid crystal phase of $C_{18}EO_{10}/H_2O/H_2PtCl_6$ system (ratio 2:1:1 by weight) at room temperature.

The electrodeposition of the platinum film from the liquid crystalline plating mixture is carried out under thermostatic and potentiostatic control. The temperature is maintained constant at 40°C and the potential at -0.1 V for 30 min. After the deposition, the electrode is soaked in water, after the deposition, for at least 48 h to remove the surfactant. The resulting film was adherent, gray and shiny. Atomic force microscopy (AFM) was employed to visualize the structure of the deposited platinum film. The morphology of the deposited film is presented in Fig. 67.

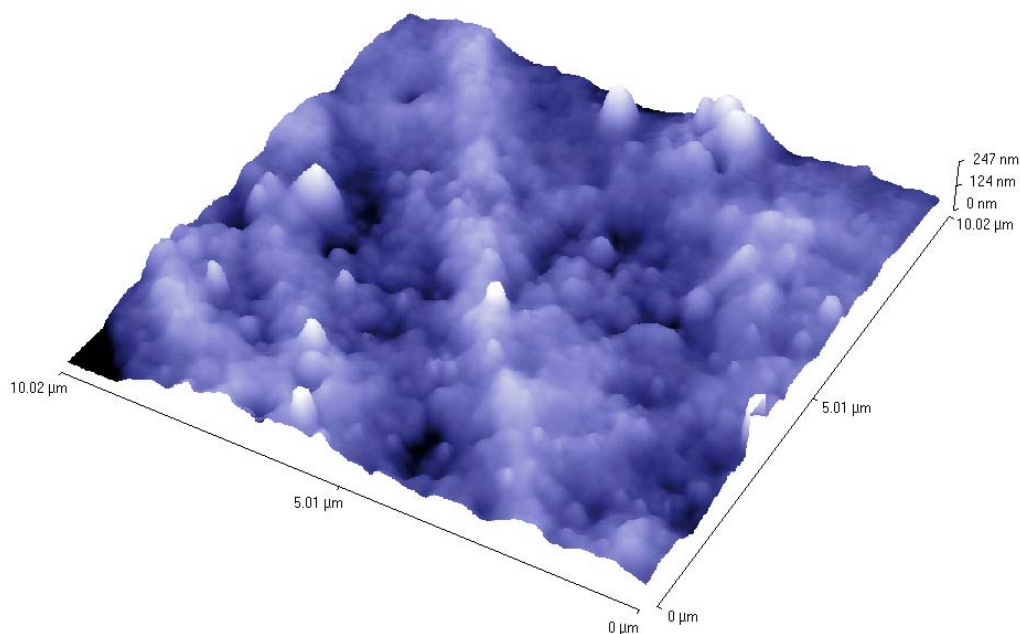


Fig. 67 AFM image of nanostructured platinum (3-dimensional view).

As it is shown, AFM reveals that the deposits were not uniform and present large pores which could not be comparable with that found *Attard et al.* [41] for mesoporous platinum films electrodeposited from the hexagonal phase of a nonionic surfactant octaethyleneglycol monohexadecyl ether ($C_{16}EO_8$). The pore diameters are estimated ranging 220 – 316 nm. The use of the working place presented in the previous paragraph is more complicated for the electrodeposition under potentiostatic control.

4.5. Galvanostatic deposition of the platinum film from the plating mixture

The galvanostatic deposition of the platinum film from the templating liquid crystal has been carried out from the hexagonal phase formed by a mixture of a non-ionic surfactant, $C_{18}EO_{10}$ denoted Brij[®] 76, and an aqueous solution of HCPA.

In this part, the structure and the morphology of the electrodeposited platinum films is established by AFM. Fig. 68 represents the 3-dimensional view of the gold working electrode without the deposit.

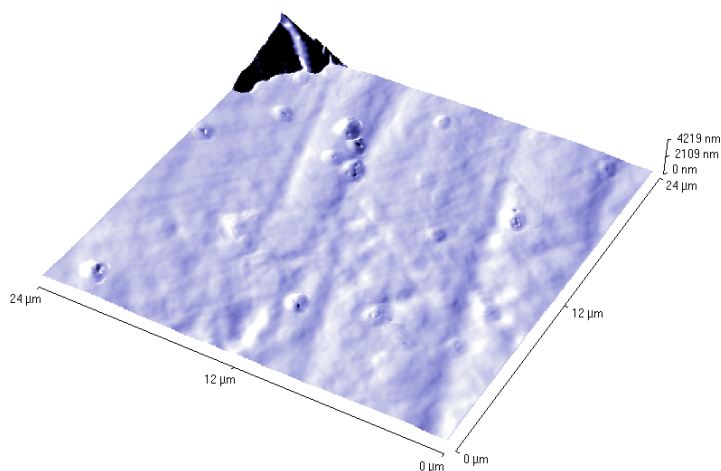


Fig. 68 AFM image of the gold electrode without deposit (3-dimensional view).

The ternary plating mixture is prepared from an aqueous solution of 2M HCPA which is mixed, in a ratio 1:1, with 50 wt% of Brij[®] 76 in water. The platinum films are deposited at a constant current of 9 μ A (Fig. 69A) and 50 μ A (Fig. 69B) for about 45 min and 3 hours respectively on a polished gold electrode. The morphology of the deposited films is investigated over a range of length scales reported in Fig. 69. The AFM studies show a porosity in the structure although nothing could be said presently about its regularity. It appears that the time of deposition could play an important role with regard to the

morphology of the film electrodeposited. The deposit obtained within a short time scale seems to be more structured and flat (Fig 69A) than the long time deposition which present large pores (Fig. 69B).

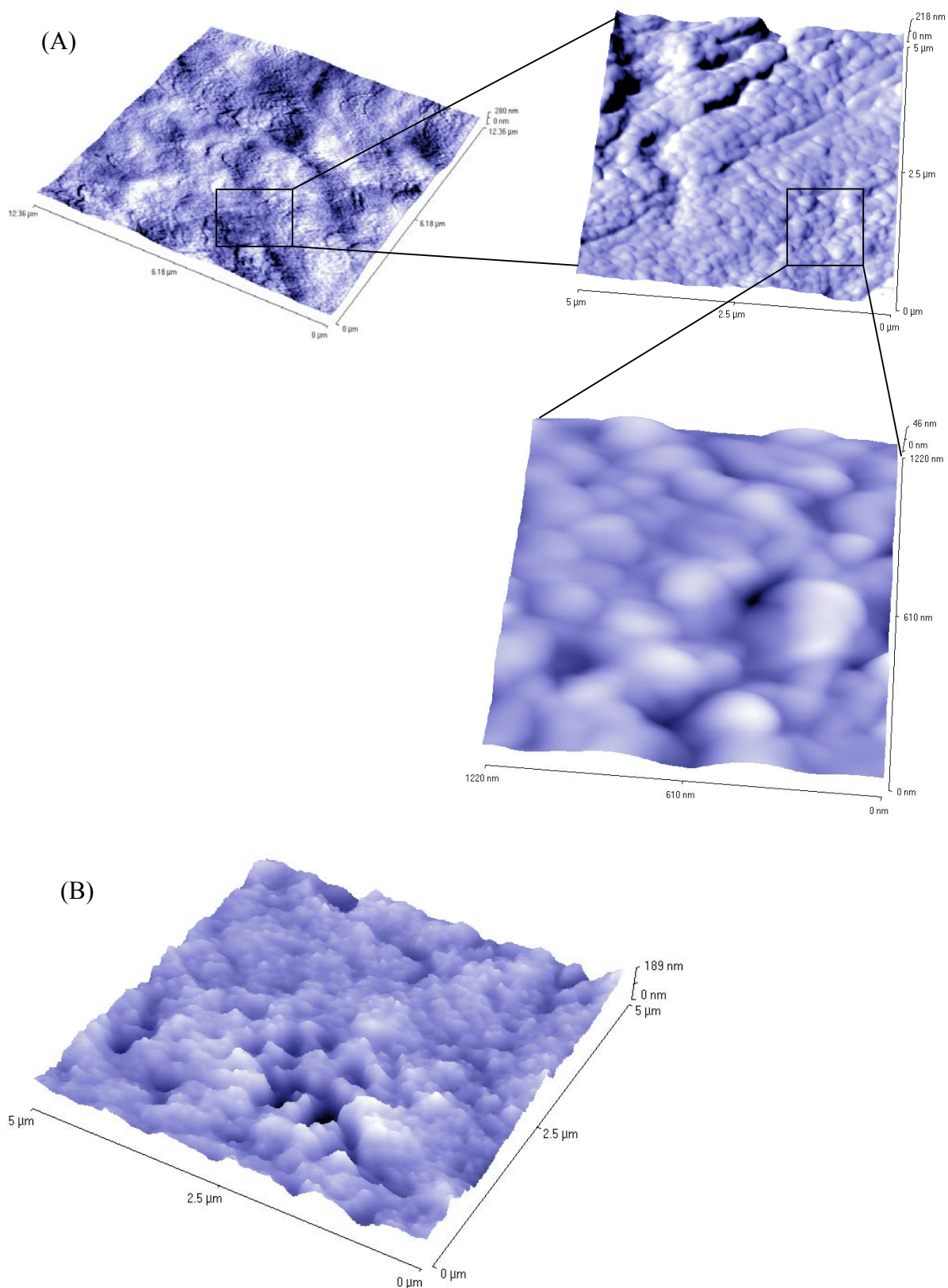


Fig. 69 AFM image of the electrodeposited platinum films: (A) 9 μA , 45 min and (B) 50 μA , 3 h.

The diameter of pores are estimated in the range of 115 – 121 nm with a deepness of 4.2 nm for short time deposition (Fig. 69A) and 360 – 365 nm with a deepness of 5.6 nm for long time deposition (Fig. 69B). These values are very different of the theoretical value of 4.5 nm calculated assuming that the diameter of micelle is $2.5n$ for C_nEO_m surfactant [154]. Up to now this difference remains non clarified. A possible explanation may be arise from the composition mixture of the ternary system used.

4.6. Conclusion

The work described in this part, as mentioned before is an introductive work devoted to the testing of a new working place built up for molecular architectures and nanostructures on metal surfaces. The first test was devoted to the electrodeposition of mesoporous platinum films from lyotropic liquid crystalline phases. The plating mixtures consist of non-ionic surfactant Brij[®] 76 ($C_{18}EO_{10}$), hexachloroplatinic acid and water in a ratio 2:1:1. The morphology of the electrodeposited platinum film investigated only by atomic force microscopy (AFM) presents a porous structure. The AFM studies of the thin films deposited galvanostatically reveal to be in sharp contrast to those achieved potentiostatically. The deposits seem to be uniform and flat over the electrode area but the diameter of pores remains large than expected and could not be compared with the results reported in the literature. Nevertheless, the new workstation can be use to produce porous platinum films from lyotropic liquid crystalline phase. Thus, this porous electrode could be use for microstructuring of metal complexes onto its surface.

5. Experimental part

5.1. Reagents

Analytical grade acetonitrile (Merck) was used without further purification. THF (Acros) was distilled over Na/Ph₂CO. Malononitrile (Acros), 2,2'-bipyridine (Gliwice Poland), hexachloroplatinic acid (Aldrich), Brij[®] 76 (Aldrich), 1,1,3,3-tetracyanopropane (Aldrich), triphenylphosphane (Merck), fluorine (Acros), triphenylmethane (Acros), 1,2-bis(diphenylphosphino)ethane (Merck) and 1,10-phenanthroline (Lancaster) were reagent grade and used as received.

Tetrabutylammonium tetrafluoroborate (Fluka), Tetrabutylammonium hexafluorophosphate, Tetraethylammonium perchlorate (Merck), lithium chloride (Merck) and lithium perchlorate (Merck) used as supporting electrolyte were dried under vacuum.

5.2. Instrumentation

Electrochemical measurements

Electrochemical measurements were performed at room temperature. Voltammetric experiments were carried out using a VersaStatTM Potentiostat / Galvanostat Model 270 (EG&G Princeton Applied Research, Princeton, NJ, USA) connected to a computer for data acquisition with Echem Software. A conventional three-electrode electrochemical glass cell was used. A saturated aqueous calomel electrode (SCE), served as a reference electrode, was connected via a Haber-Luggin capillary with an outside diameter of 1.1 mm. The capillary was filled with the same solution as in the cell (all potentials are referred to the SCE). The counter electrode consisted of a sheet of platinum (11×11 mm²). The working electrodes were copper wire (1.2 mm of diameter) and platinum wire (1 mm of diameter). Solutions were deaerated with argon for at least 10 min prior to undertaking experiments.

Rotating disc voltammetry measurements were conducted with a rotator EUROSTAR (IKA LaborTechnik, Germany) connected to the previous potentiostat. Potentiodynamic measurements were performed using an EG&G Model 366 Bi-potentiostat and a multimeter Keithley Instruments Inc. Model 2001 (USA) in connection with a PC using Test Point Software Version 4.0. The setup of the Double Segment Electrode is described in detail in appendix (A1). All data were exported and the curves drawn with Microcal Origin[®].

Micro and nanostructuration

The working station consists of a vibration-free table (Newport, USA) used in order to provide adequate vibration isolation. DC-Motor Controllers (Physik Instrumente, Germany) consist of C- 842.20 DC- Motor Controller model M-126.DG (DC-motor, gear head) which can drive up to 4 DC-motors directly from a PC with C-842 WinMove software. This model has the following features:

- 25 mm travel range
- XY stages
- 118.6 c/ μm linear transmission ratio
- 0.0085 μm linear resolution
- 0.1 μm minimum incremental motion
- velocity of motor: minimal 8.432 $\mu\text{m/s}$ and maximal 1012 $\mu\text{m/s}$

These equipments are used concomitantly with a potentiostat (EG&G Instruments) Model 273 A Potentiostat / Galvanostat which operates remotely from a PC via the IEEE-488 interface port (National Instruments, USA).

Spectroscopic studies

Infrared spectral were recorded on a Perkin-Elmer System 2000 FT-IR spectrometer scanning between 400 and 4000 cm^{-1} using KBr disks.

^1H , ^{13}C and ^{31}P NMR spectra were recorded on an AVANCE DRX 400 spectrometer (Bruker). Chemical shifts for ^1H and ^{13}C NMR spectra are reported in parts per million (ppm) at 400.13 MHz and 100.63 MHz with tetramethylsilane as external standard. Chemical shifts for ^{31}P NMR spectra are reported in parts per million (ppm) at 161.97 MHz (with 85% H_3PO_4 external standard).

Mass spectra were recorded on a VG 12-250 EI mass spectrometer (70 eV), on a FT-ICR-MS Bruker-Daltonics ESI mass spectrometer (APEX II, 7 Tesla), and on a Ltd. ZAB-HSQ-VG for FAB mass spectra, with 3-nitrobenzyl alcohol as matrix.

Simultaneous thermoanalysis (TG, DTG, DSC) with STA 409, Netzsch .

Elemental Analyses

C, H and N elemental analyses were performed with CHNS 932 (Leco). Other elements like Cu, P, F, B were analyzed by energy dispersive X-ray (EDX). In this way, the samples were investigated with Digital Scanning Microscope 982 Gemini (Zeiss).

X-Ray Crystal Structure Analyses

Crystals were mounted on a Stoe Stadi4 diffractometer. All measurements were done at ambient temperature using graphite-monochromatized $\text{CuK}\alpha$ radiation. Intensity data were collected in ω - 2θ scan technique with variable scan speed. Monitoring of three control reflections every hour revealed an intensity loss of 17.9 % during data collection due to crystal decay resulting in the comparatively low precision of the structure analysis. The structure was solved by direct methods and the positional and anisotropic displacement parameters of the non-hydrogen atoms were refined by least-squares calculations on F^2 . Hydrogen atom positions were geometrically determined and treated according to the riding model. Calculations and drawings were done using the programs SHELXS-97 [165], SHELXL-97 [166], and Siemens XP/PC [167]. The crystallographic data are reported in appendix. Diamond 2.1 [168] software was also used for drawings.

Polarizing microscopy

The texture of the liquid crystal template mixtures was investigated using polarizing microscope Leitz (Laborlux 12 Pol S, Germany). The sample sandwiched between two glass plates was put in a temperature controlled oven (Linkam TMS 92, England). A CCD-color camera (Hitachi, Model KP-C 551, Japan) allows to save the image of the texture on the video tape. Another camera (Leica, Model Wild MPS 52, Germany) make the photo print possible.

Atomic force microscopy (AFM) measurements

The electrodeposited platinum films were investigated by atomic force microscopy (AFM). AFM measurements were performed at room temperature and under ambient conditions at approximately 60% relative humidity using the TMX 2010 Explorer of TopoMetrix in the non-contact mode (Si tips with a resonance frequency of about 300 kHz). The maximal scan rate was 2 Hz. The image processing used was a third-order plane levelling.

5.3. Electrosynthesis



Fig. 70 The electrochemical cell.

The electrochemical cell (Fig.70) consists of a glass (approx. 250 ml) with 4 cross section openings. The copper anode (23 cm^2) and the platinum cathode (23 cm^2) are held by an open-top cap equipped with a joint. Side-arms allow the introduction of electrolyte and a permanent supply of argon. A magnetic stirring system was also used. All operations were performed under argon atmosphere using Schlenk techniques.

5.3.1. Electrosynthesis with nitriles as starting materials

1,1,3,3-Tetracyanopropane as starting material

5.3.1.1. Electrosynthesis of $[\text{Cu}(\mu\text{-C}(\text{CN})_3)(\text{PPh}_3)_2]_2$ (**1**)

2.305 g (7.00 mmol) of Bu_4NBF_4 , 3.672 g (14.00 mmol) of PPh_3 and 1.44 g (10.00 mmol) of 1,1,3,3-tetracyanopropane are electrolyzed in 70 ml of acetonitrile. The reaction mixture was stirred up during the synthesis. Galvanostatic oxidation of the copper anode in the electrolytic medium results in a deeper red solution (Fig. 73). At the end of experiment two phases were formed, a liquid phase and an oil-like. Both phases were separated and the complex **1** was received from the liquid phase at 0°C after four days. m.p. $> 135^\circ \text{C}$.

Current yield: 98 % (0.320g, 4.9 mmol of copper dissolved); *Chemical Yield:* 4.974g (75%) based on copper dissolution.

Elemental analysis for $C_{80}H_{60}Cu_2N_6P_4$ (1356 g.mol⁻¹); C 69.30 (Calc. 70.70); H 4.11 (4.40); N 5.69 (6.19) %.

IR (KBr): 3056w, 2173s, 1626w, 1479m, 1434s, 1309w, 1260w, 1182w, 1158w, 1095m, 1027w, 998w, 802w, 746s, 694s, 560m, 517s, 506s, 493m cm⁻¹.

In order to identify traces of acrylonitrile in the electrolytic solution, we have developed a small unit cell which can contain 2 ml of solution (Fig. 71). It consists of a glass with three cross section openings. The anode or the cathode are held by an open-top cap equipped with a joint. Side-arm allows a permanent supply of argon.

This cell was used to carried out in the same molar ratio and in CD₃CN the synthesis of **1**. At the end of synthesis, the solution was poured in the NMR-tube and analyzed by GC-MS, ¹H NMR spectroscopy.

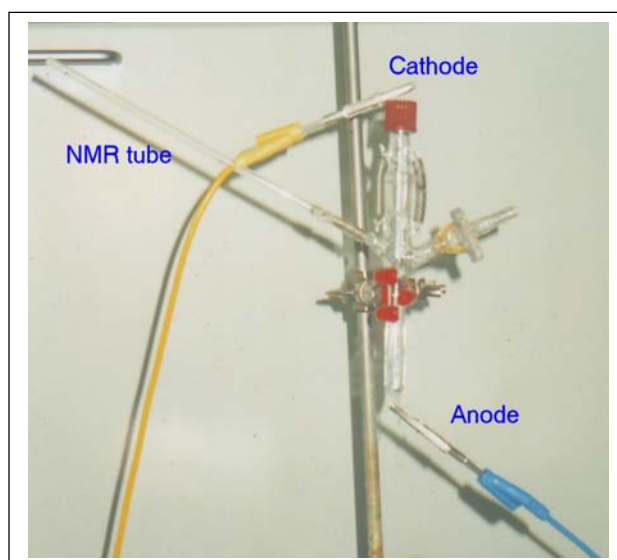


Fig. 71 Small unit electrochemical cell.

The acrylonitrile electropolymerized and grafted was scraped off at the cathode and characterized by infrared spectroscopy and fast atom bombardment mass spectrometry.

IR (KBr): 3417vs, 2960w, 2850vw, 2523m, 2205s, 1635vs, 1570vs, 1437vs, 1262w, 1239w 1089s, 937w, 914vw, 856m, 812w, 756vw, 628m, 531m, 435w, 445w, 413m cm⁻¹.

FAB-MS: m/z(%) 107.1(22.06), 120.1(12.46), 136(73.79), 137(63.07), 138(32.26), 139(12.43), 154(100), 155(28.79), 160.1(65.83), 161.1(10.23), 289(13.58), 307(27.86), 313.1(50.51), 314(14.23), 466.1(5.02).

5.3.1.2. Preparation of $\text{cis-}[\text{Cu}_2(\mu\text{-CN})(\text{PPh}_3)_2(\text{Phen})_2]_2 [\text{C}(\text{CN})_3][\text{BF}_4]\cdot 2\text{CH}_3\text{CN}$ (**2**)

Compound **2** was isolated from the solution of **1** containing oil phase, by addition of 0,216 g (1,2 mmol) of 1,10-phenanthroline previously dissolved in 12 ml of CH_3CN . Single orange-yellow crystals suitable for X-ray characterization were collected after three days at $0\text{ }^\circ\text{C}$. The compound **2** was not soluble in AN and THF but partially soluble in DMSO. m.p. $> 200\text{ }^\circ\text{C}$. Yield: 21 % with regard to the copper dissolution.

IR (KBr): 3053m, 2963w, 2160s, 1622w, 1585w, 1479s, 1434s, 1310w, 1260w, 1183w, 1158w, 1123w, 1084s, 1026m, 998m, 856w, 748s, 695s, 618w, 561m, 518s, 504s, 445w, 418 cm^{-1} .

5.3.1.3. Preparation of $[\text{Cu}_2(\mu\text{-CN})(\text{PPh}_3)_6][\text{BF}_4]$ (**3**)

Complex **3** was received by dissolving the oil phase (reported in 4.3.1) in 10 ml of THF. Single colorless crystals suitable for X-ray characterization were collected after three months at $+5\text{ }^\circ\text{C}$. **3** was also characterized by EDX (Fig. 72).

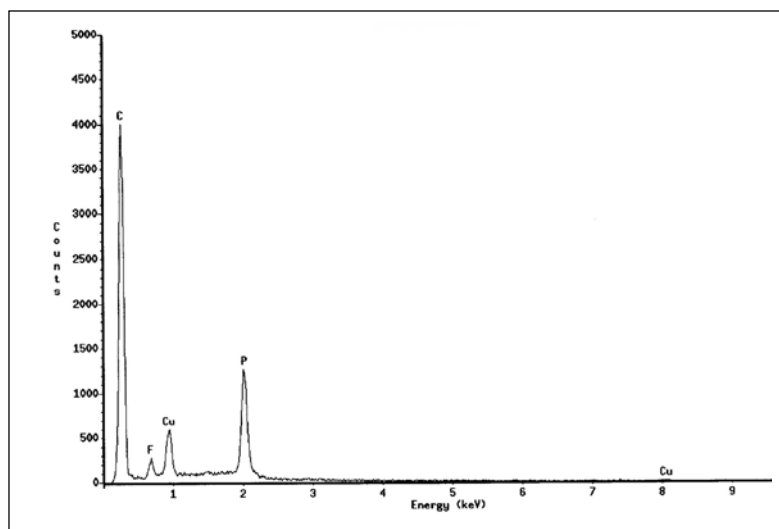


Fig. 72 EDX of $[\text{Cu}(\mu\text{-CN})(\text{PPh}_3)_6][\text{BF}_4]$ (**3**)

5.3.1.4. Preparation of $\text{trans-}[\text{Cu}_2(\mu\text{-CN})(\text{PPh}_3)_2(\text{bipy})_2][\text{BF}_4]\cdot \text{THF}$ (**4**)

Complex **4** was received by dissolving 0,30 g (1,2 mmol) of 2,2'-bipyridine in 10 ml of THF containing the oil phase. Single green-yellowish crystals suitable for X-ray characterization were collected after a few days at $+5\text{ }^\circ\text{C}$. m.p.: $140 - 145\text{ }^\circ\text{C}$.

Elemental analysis for $\text{C}_{61}\text{H}_{50}\text{BCu}_2\text{F}_4\text{N}_5\text{O}_2\text{P}_2$ ($1144.93\text{ g mol}^{-1}$); C 65.22 (Calc. 63.99); H 4.01 (4.40); N 6.89 (6.12) %.

IR (KBr): 2856w, 2120m, 1593m, 1478s, 1436s, 1311w, 1172m, 1155w, 1093vs, 904w, 767s, 697s, 623w, 561m, 517s, 503s, 413w cm^{-1} .

Malononitrile as starting material

5.3.1.5. Electrosynthesis of $[\text{Cu}(\text{CN})(\text{PPh}_3)_2] \cdot \text{CH}_3\text{CN}$ (5)

Electrosynthesis of $[\text{Cu}(\text{CN})(\text{PPh}_3)_2] \cdot \text{CH}_3\text{CN}$ has been achieved in an undivided electrochemical cell by galvanostatic dissolution of copper metal and cathodic reduction of malonodinitrile (0.896 g, 13,56 mmol) in 70 ml of acetonitrile in the presence of 2.256 g (8.60 mmol) of triphenylphosphane and 2.305 g (7.00 mmol) of Bu_4NBF_4 used as supporting electrolyte. Once the current reaction (50 mA which corresponds to a current density of 4.2 mA cm^{-2}) is set, the hydrogen gas began to evolve. After few minutes an insoluble white compound became visible. The electrolysis was stopped after 160 minutes and the white product was filtered, washed with acetonitrile and diethyl ether and then dried under vacuum. *Current yield*: 99.46 % (0.316g, 4.973 mmol of copper dissolved); *Chemical Yield*: 56.18% (2.794 g, 2.8 mmol) based on the copper dissolution.

Elemental analysis for $\text{C}_{39}\text{H}_{33}\text{N}_2\text{P}_2\text{Cu}$ (655.2 g mol^{-1}): C 70,42(Calc. 71.49); H 5.03(5.03); N 4.68(4.68) %.

IR (KBr): 3052m, 3003vw, 2962vw, 2874vw, 2329w, 2187m, 2104vs, 1650w, 1584w, 1479s, 1433s, 1348m, 1182w, 1141w, 1093s, 1027m, 997w, 743vs, 695vs, 618w, 508vs, 429w cm^{-1} .

ESI-MS: m/z 197.55 $[\text{Cu}(\text{CN})(\text{PPh}_2)]^+$, 587.111 $[\text{Cu}(\text{PPh}_3)_2]^+$, 587.55 $[\text{Cu}(\text{PPh}_3)_2]^+$, 613.55 $[\text{Cu}(\text{CN})(\text{PPh}_3)_2]^+$, 849.55 $[\text{Cu}(\text{PPh}_3)_3]^+$, 875.55 $[\text{Cu}(\text{CN})(\text{PPh}_3)_3]^+$.

$^1\text{H-NMR}$ (400 MHz, $\text{THF-}d_8$, [ppm]): $\delta = 7.2\text{--}7.8$ (m, H-Ph).

$^{13}\text{C-NMR}$ (50 MHz, $\text{THF-}d_8$, [ppm]): $\delta = 129.92\text{--}135.47$ (C-PPh₃), 138.32 (s, CN).

$^{31}\text{P-NMR}$ (81 MHz, $\text{THF-}d_8$, [ppm]): $\delta = 24.72$ (s, Cu-PPh₃), -2.83 (s, PPh₃).

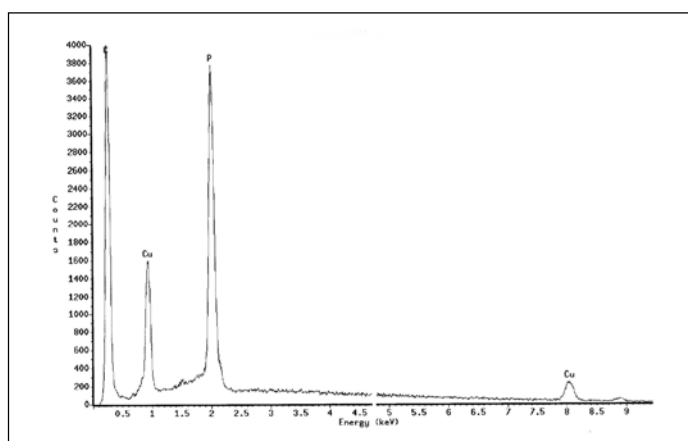


Fig. 73 EDX of $[\text{Cu}(\text{CN})(\text{PPh}_3)_2] \cdot \text{CH}_3\text{CN}$ (5)

5.3.1.6. Preparation of [Cu(CN)(bipy)(PPh₃)] (6)

To a solution containing [Cu(CN)(PPh₃)₂] \cdot CH₃CN (0.549 g, 1.08 mmol) in AN (10 ml) was added 10 ml of AN containing 2,2'-bipyridine (bipy) (0,469 g, 3 mmol). Some yellow single crystals suitable for X-ray characterization were collected after a few days at 0°C. m.p.: 180 – 185°C

Chemical Yield: 12.07% (0.52 g, 0.593 mmol) based on the copper dissolution.

IR (KBr): 3056w, 2173vs, 1626w, 1479m, 1434s, 1309w, 1260w, 1182w, 1158w, 1095s, 1027m, 998w, 802w, 746s, 694vs, 560m, 517s, 506s, 493m cm⁻¹.

5.3.1.7. Preparation of [Cu(CN)(phen)(PPh₃)] (7)

Similar to **6**, complex **7** was prepared by adding 0,216 g (1,2 mmol) of 1,10-phenanthroline, dissolved in 10 ml of AN to 10 ml of acetonitrile containing [Cu(CN)(PPh₃)₂] \cdot CH₃CN (0,469g, 3 mmol). Some yellowish single crystals suitable for X-ray characterization were collected after a few days.

m.p.: 189 – 193°C.

Elemental analysis for C₃₁H₂₃CuN₃P (532.03 g.mol⁻¹); C 70.18 (Calc. 69.98); H 4.11 (4.36); N 7.69 (7.90) %.

Phenylacetonitrile as starting material

5.3.1.8. Electrosynthesis of {[C₄H₉]₄N}[Cu(BPVA)(PPh₃)₂][BF₄] (8)

The compound **8** was prepared by anodic dissolution of copper metal, at a constant current of 10 mA (current density 0.44 mA cm⁻²), in THF (70 ml) / Bu₄NBF₄ (2.305g, 7 mmol), PAN (1,15 ml, 10 mmol) and PPh₃ (3.672 g, 14 mmol). The reaction was carried out smoothly at 0 °C for 13 h 25 min which corresponds to 1 e⁻ / mol. When the power supply is switched on, the colorless solution change from yellow-dark after 45 min. Any precipitate was isolated immediately but, within one month, crystals were collected. Unfortunately, these crystals were not suitable for X-ray analysis. **8** was characterized by satisfactory C, H, N elemental analysis, FAB⁺-MS, ¹H-, ¹³C-, ³¹P-NMR and IR-spectroscopies. m.p.: 175 – 180 °C.

Current yield: 55.39 % (0.176 g, 2.77 mmol) copper dissolution.

Elemental analysis for $C_{68}H_{79}N_3P_2CuBF_4$ (1149.55 g mol⁻¹): C 70,28 (Calc. 70.98); H 5.80(6.87); N 3.29(3.65) %.

IR (KBr): 3309w, 3051m, 3002vw, 2962w, 2873w, 2161s, 2125m, 1960w, 1889w, 1815w, 1632w, 1593w, 1585w, 1571w, 1518vs, 1480s, 1434vs, 1409m, 1328w, 1307w, 1285w, 1262w, 1180w, 1155w, 1094s, 1066m, 1026m, 914w, 847w, 804w, 772vw, 742vs, 694vs, 618w, 542w, 515s, 507s, 446w, 428w cm⁻¹.

FAB-MS: m/z(%) 242.3(100), 243.3(18.08), 262.1(17.06), 325(33.89), 327(16.10), 414(22.42), 415.9(20.04), 587.1(29.18), 676(63.35), 677.1(26.66), 678(58.90), 679.1(24.27), 765(16.07), 767(22.36), 769(11.16), 855.9(9.17).

¹H-NMR (400 MHz, THF-*d*₈, [ppm]): δ = 7.2-7.8 (m, H-Ph), 3.66 (s, CH₂).

¹³C-NMR (50 MHz, THF-*d*₈, [ppm]): δ = 129.47 - 134.28(C-PPh₃), 118.07 (s, CN), 24.32 (CH₂).

³¹P-NMR (81 MHz, THF-*d*₈, [ppm]): δ = 13.10 (s, Cu-PPh₃).

5.3.1.9. Preparation of [Cu(PAN)₂(Phen)(PPh₃)] (9)

The complex **9** was prepared by reacting {[C₄H₉]₄N}[Cu(PAN)₂(PPh₃)₂][BF₄]_n (0.21 g, 0.183 mmol) in 10 ml of THF with 0.450 g (2.50 mmol) of 1,10-phenanthroline. The reaction led to red-violet crystals within a couple of months. Yield: 3.46 % (0.127 g, 0.172 mmol) m.p.: 155 – 160 °C.

5.3.1.10. Preparation of [Cu₉(CN)₉(PPh₃)₈]_n (10)

The polymeric compound [Cu₉(CN)₉(PPh₃)₈]_n (**10**) was received from **8** two weeks its dissolution in CD₃CN. Colorless single crystals were collected and characterized by X-ray structure analysis. Unfortunately, the structure of **10** is not yet fully investigated.

IR (KBr): 3271w, 3050m, 3002vw, 2962w, 2185m, 2123vs, 1637m, 1585m, 1513vs, 1480s, 1434vs, 1338w, 1311w, 1261w, 1202w, 1182w, 1156w, 1093s, 1027m, 1010m, 805s, 744vs, 695vs, 509vs, 428w cm⁻¹.

ESI-MS: m/z 603.104, 339.129, 676.05, 766.97, 12002.23.

5.3.1.11. Preparation of $[\text{Cu}_3(\text{CN})_2(\text{phen})_3(\text{PPh}_3)_2][\text{BF}_4]$ (**11**)

The complex **11** was prepared by adding 0.450 g (2.50 mmol) 1,10-phenanthroline to 10 ml of the electrolytic solution obtained in 5.3.1.8. **11** was received as orange crystals and characterized by elemental analysis, IR spectroscopy and X-ray crystal structure analysis.

Elemental analysis for $\text{C}_{74}\text{H}_{54}\text{N}_8\text{P}_2\text{Cu}_3$ (1307.86 g mol⁻¹); C 69,60(Calc. 67.96); H 4.55(4.16); N 7.98(8.57) %.

IR (KBr): 3069m, 2976w, 2868vw, 2204m, 2096m, 1615vw, 1585w, 1524w, 1477m, 1430s, 1305vw, 1328w, 1091m, 1028w, 904w, 858m, 750s, 688vs, 517s, 425vw cm⁻¹.

5.3.1.12. Preparation of $[\text{Cu}(\text{CN})(\text{o-phen})(\text{PPh}_3)]_2 \cdot \text{H}_2\text{O}$ (**12**)

The complex **12** was achieved similarly to **11** by reacting 0.450 g (2.27 mmol) 1,10-phenanthroline monohydrate (o-phen) with 10 ml of the electrolytic solution obtained in 5.3.1.8. Slow evaporation at room temperature resulted in the formation of green-yellowish crystals. m.p.: 223 – 225 °C.

Elemental analysis for $\text{C}_{62}\text{H}_{48}\text{N}_6\text{P}_2\text{CuO}$ (1082.124 g mol⁻¹); C 69.47 (Calc. 68.81); H 4.64(4.47); N 7.97(7.77) %.

IR (KBr): 3410w, 3069w, 2961m, 2868w, 2172m, 2096m, 1708w, 1570w 1477m, 1430m, 1074s, 858m, 750s, 689vs, 487s cm⁻¹.

5.3.2. Electrosynthesis with non nitrile ligands

5.3.2.1. Electrosynthesis of $[\text{Cu}(\text{Flu})(\text{PPh}_3)_2] \cdot 2\text{CH}_3\text{CN}$ (**13**)

The fluorenyl copper(I) complex **13** was prepared by galvanostatic dissolution of copper metal ($I = 50\text{mA}$) and cathodic reduction of 1.622 g (10 mmol) of fluorene in 70 ml of acetonitrile containing 2.305 g (7.00 mmol) of Bu_4NBF_4 and 3.672 g (14.00 mmol) of PPh_3 used as supporting electrolyte and coligand respectively at 0 °C. After a few minutes of electrolysis the solution changes from colorless to red brown and then to brown; green powder was received as product.

Current yield: 104 % (0.33 g, 5.20 mmol of copper dissolved); *Chemical Yield*: 52.85 % (2.296 g, 2.748 mmol) based on the copper dissolution.

Elemental analysis for $C_{53}H_{45}N_2P_2Cu$ (835.43 g mol⁻¹); C 70,28(Calc. 76.20); H 5.48(5.43); N 3.72(3.35) %.

ESI-MS: m/z 571.57, 603.11, 676.04, 692.04, 6.94.04.

IR (KBr): 3033w, 3064m, 2185s, 2120w, 1634vs, 1586vs, 1495s, 1454s, 1082m, 1030m, 939w, 914w, 803w, 762m, 738m, 700s, 616w cm⁻¹.

¹H-NMR (400 MHz, DMSO-*d*₆, [ppm]): δ = 7.1-7.9 (m, H-Ph), 2.1 (s, CH-fluorenyl).

¹³C-NMR (50 MHz, DMSO-*d*₆, [ppm]): δ = 128.45 - 135.11(C-Ph), 118.07 (s, CN), 23.1 (s, CH-fluorenyl).

³¹P-NMR (81 MHz, DMSO-*d*₆, [ppm]): δ = 26.58 (s, Cu-PPh₃), -165.6 (s, Cu-PPh₃).

5.3.2.2. Electrosynthesis of [Cu(CPh₃)(PPh₃)]·2CH₃CN (**14**)

The triphenylmethyl copper(I) complex **14** was prepared by galvanostatic dissolution of a copper metal ($I = 50$ mA) and concomitantly cathodic reduction of 2.443 g (10 mmol) of triphenylmethane in 70 ml of acetonitrile containing 2.305 g (7.00 mmol) of Bu₄NBF₄ and 3.672 g (14.00 mmol) of PPh₃ used as supporting electrolyte and coligand respectively at 0 °C. During the electrolysis the solution changes from colorless to yellow. **14** was received at the end as brown precipitate.

Current yield: 95.40 % (0.303 g, 4.77 mmol of copper dissolved); *Chemical Yield*: 73.82 % (2.293 g, 3.521 mmol) based on the copper dissolution.

Elemental analysis for $C_{41}H_{36}N_2PCu$ (651.26 g mol⁻¹); C 72.9 (Calc. 75.61); H 5.69(5.57); N 4.40(4.30) %.

FAB-MS: m/z(%) 142.2 (56.34%), 184.2 (29.84%), 242 (100%), 571.6 (6.29%) and 637.6(3).

5.3.2.3. Electrosynthesis [(CuCl)₂(μ-dppe)(η²-dppe)₂]·CH₃CN (**15**)

The complex **15** was electrosynthesized by galvanostatic dissolution of a copper metal in 70 ml of acetonitrile in the presence of 3.985 g (10 mmol) of 1,2-bis(diphenylphosphino)ethane (dppe) and 2.97 g (7.00 mmol) of LiCl used as supporting electrolyte and source of chloride. The reaction mixture is stirred up during the synthesis, then the anodic dissolution of copper metal is followed by a reaction with excess of chloride and dppe. The current reaction was set as previously at 50 mA and the electrolysis stopped after 2 hours 41 minutes. A white-grey product was collected, washed with acetonitrile and diethyl ether and dried under vacuum.

Also, the anode was washed, dried and weighted in order to calculate the electrochemical efficiency. The compound **15** was hygroscopic non-homogeneous and consequently the C, H, N elemental analysis was not successful, only EDX (Fig. 74) was possible.

m.p.: 305 – 310 °C.

Current yield: 94.10 % (0.299 g, 4.705 mmol of copper dissolved); *Chemical Yield:* 20.70 % (1.397 g, 0.974 mmol) based on the copper dissolution.

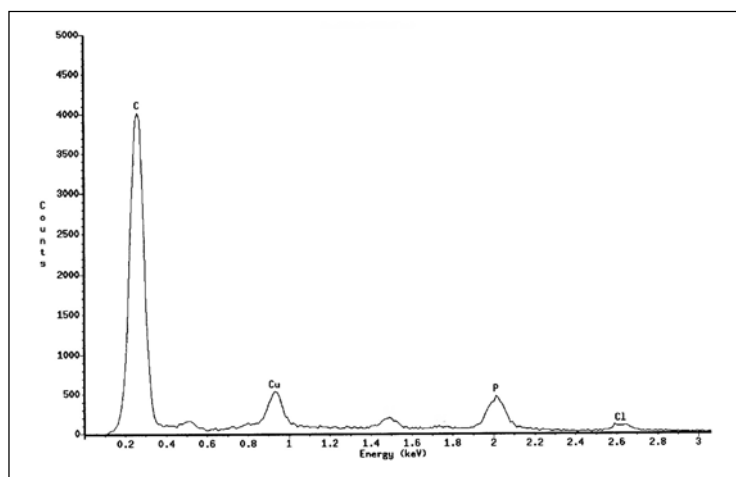


Fig. 74 EDX of $[(\text{CuCl})_2(\mu\text{-dppe})(\eta^2\text{-dppe})_2]\cdot\text{CH}_3\text{CN}$ (**15**)

5.3.2.4. Preparation of $[(\text{CuCl})_2(\mu\text{-dppe})(\eta^2\text{-dppe})_2]\cdot(\text{CH}_3)_2\text{SO}$ (**16**)

The compound **16** was received by dissolution of 0.22 g of **15** in 2 ml $\text{DMSO-}d_6$. Colorless single crystals were collected and characterized by X-ray structure analysis and EDX (Fig.75).

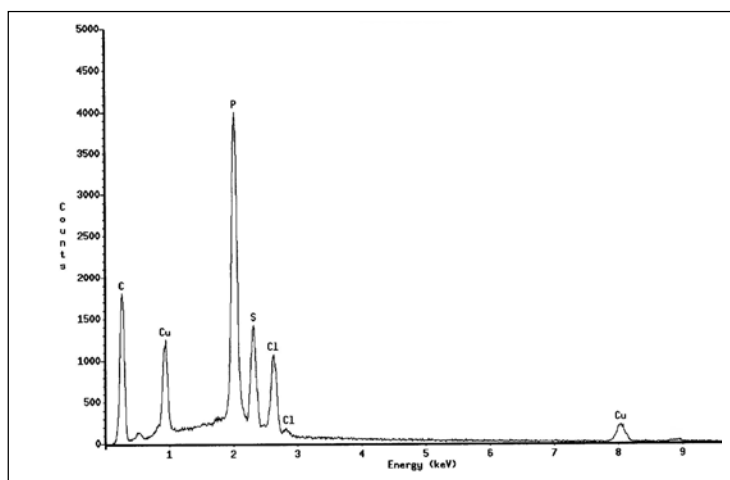


Fig. 75 EDX of $[(\text{CuCl})_2(\mu\text{-dppe})(\eta^2\text{-dppe})_2]\cdot(\text{CH}_3)_2\text{SO}$ (**16**)

5.4. Electrodeposition from lyotropic liquid crystalline phases

The plating mixture used consisted of a non-ionic surfactant, Brij[®]76 that nominally corresponds to decaethyleneoxide mono-octadecyl ether and denoted C₁₈EO₁₀ (50 wt. %), 2M of hexachloroplatinic acid (HCPA) and water in ratio of 2:1:1 in weight. The preparation of this ternary system was based on procedures described by *Attard et al.* [41,42,144,145]. The texture of the mixture was examined under a polarizing light optical microscope. The platinum films were electrodeposited from lyotropic liquid crystalline phases onto gold sheet electrode (1×1 cm²) in a portion area of about 0.00385 cm² both potentiostatically (at -0.1 V at 40 °C) and galvanostatically (at room temperature, density of charge 6.37 C cm⁻²). The surfactant was removed after the deposition by soaking the electrode in distilled water for at least 24 h and during this time the water was replaced every 3 h.

The working electrode was polished using alumina in three grades: 1, 0.3 and 0.05 μm (Struers, Denmark) or silicon carbide paper (Struers, Denmark) and finally polishing cloths (Struers, Denmark). Then, the electrode was cleaned electrochemically by cycling in 2M aqueous sulfuric acid between -0.7 and +0.8 V at 200 mV s⁻¹ and allowed to dry under ambient condition.

6. Summary / Zusammenfassung

Summary

In the context of this work the direct electrosynthesis of some selected organonitrilecopper(I) compounds and the electrochemical reaction mechanisms by which these compounds can be achieved are investigated.

It was important, first of all, to examine the electrochemical behavior of the electrolytic solution at a copper electrode, used as the working electrode, in different systems and in the presence of some nitriles possessing hydrogen in α -position of the nitrile group.

These investigations concerned with the negative potential range and was carried out in acetonitrile (AN) and a non-nitrile solvent, tetrahydrofuran (THF). The cyclic voltammetry (CV) of AN / Bu₄NBF₄, AN / LiClO₄, AN / Et₄NClO₄ and THF / Bu₄NPF₆ systems at a copper electrode, presented similar behaviors and two well defined irreversible cathodic peaks (labelled I and II) were observed. The solvated Cu(I) was reduced at more negative potential (peak I) in AN / Bu₄NBF₄ (−0.346 V) and in AN / LiClO₄, Et₄NClO₄ (−0.409 V) whereas the reduction of the less solvated Cu(I) occurred at more positive potential in THF / Bu₄NPF₆ (+0.341 V). The peak current of the process (II) was dependent on the concentration of the anion (X[−]) of the supporting electrolyte and the order of the reaction closed to unity. Therefore, this process was ascribed to the reduction of the complex (CuX), formed between the solvated Cu(I) and the anion (X[−]), and appeared at −1.437, −1.600 and −1.712 V in AN / Bu₄NBF₄, AN / LiClO₄, Et₄NClO₄ and THF / Bu₄NPF₆ systems, respectively. The kinetic parameters of the reaction involved in process (II) was determined using copper rotating disk electrode (RDE) in acetonitrile. It has been proved by mean of chronopotentiometry, chronoamperometry and Double Segment Electrode (DSE) that the complex CuX diffuses through the electrolytic solution where it is reduced at more negative potential.

The electrochemical behaviors of three nitriles {1,1,3,3-tetracyanopropane (TCP), malononitrile (MDN) and phenylacetonitrile (PhAN)} with different acidities ($pK_a > 10$) have also been investigated at a platinum and at a copper working electrodes. The results of the reduction revealed that the electron transfer reactions are coupled with chemical reactions. Thus, TCP is reduced according to an ECEC mechanism, the first electron transfer reaction is

coupled with an irreversible, second order, chemical reaction and the second electron transfer reaction is coupled with an irreversible, first order, chemical reaction. However, MDN and PhAN are reduced according to an EC mechanism, the electron transfer reaction is coupled with an irreversible, first order, chemical reaction. At the copper electrode, the cyclic voltammograms present an irreversible peak between -0.8 V and -1.0 V which was assigned unambiguously to the reduction of Cu(I)-nitrile complex.

These nitriles have been used to prepare electrochemically organonitrilecopper(I) compounds and their derivatives, in the presence of different donors, in non-aqueous media by galvanostatic dissolution of a copper metal and concomitantly their reduction at the cathode in an undivided electrochemical cell.

The first attempt of experiments was devoted to the preparation of TCP–Cu(I) complex. The electroynthesis of this compound was already investigated potentiostatically in our laboratory and the product of the reaction was a cuprate complex with the general formula $\{(C_4H_9)_4N[Cu(TCP)BF_4]\}_n$. However, due to the complexity of the compound, it was impossible to know the real molecular structure of this cuprate and consequently, the mechanism of the reaction was not possible to describe fully. In an effort to elucidate the structure and the mechanism of the reaction by which TCP–Cu(I) can be prepared, the electroynthesis has been carried out by the galvanostatic procedure in AN / Bu_4NBF_4 . As results, no TCP–Cu(I) was achieved rather two phases (liquid and oil-like) were obtained and separated. From the liquid phase, colorless single crystals suitable for X-ray analysis were collected and characterized as a neutral dimeric binuclear copper(I) complex, $[Cu(\mu-C(CN)_3)(PPh_3)_2]_2$ (**1**). A reaction between 1,10-phenanthroline (phen) and the solution containing the oil phase afforded orange single crystals characterized as an ionic binuclear copper(I) compound $\{cis-[Cu_2(\mu-CN)(Phen)_2(PPh_3)_2]\}_2[C(CN)_3][BF_4] \cdot 2CH_3CN$ (**2**).

In order to shed some light on the structure of oil phase, it has been dissolved in THF in which colorless single crystals were collected and characterized as $[Cu_2(\mu-CN)(PPh_3)_6][BF_4]$ (**3**).

A reaction between **3** and 2,2'-bipyridine (bipy) in THF gave green-yellowish crystals identified by X-ray structure determination as $[Cu_2(CN)(bipy)_2(PPh_3)_2][BF_4] \cdot THF$ (**4**).

The electrosynthesis of TCP-Cu(I) complex has been carried out at different temperatures (0, -35 °C and at room temperature). The X-ray crystal structure analysis of single crystals received revealed the reaction product to be the complex **1**.

Further investigations on the electrolysis of TCP revealed that the carbanion generated was not stable and initiated a decomposition pathway. This decomposition yielded acrylonitrile, tricyanomethanide and cyanide anions, and eventually MDN. The acrylonitrile was grafted and electropolymerized at the cathode.

The second attempt of the direct electrosynthesis was devoted to the preparation of MDN-Cu(I) compounds and its derivatives. It was shown in an earlier work that, depending of experimental conditions, malononitrile (MDN) can be use to achieve electrochemically different Cu(I) compounds. By potentiostatic dissolution of Cu anode, in AN / Bu₄NBF₄, PPh₃ at room temperature, [(PPh₃)₂Cu(μ-CN)Cu(PPh₃)₂][HC(CN)₂] and its derivatives, have been received. Galvanostatically, a polymeric Cu(I) compound [Cu(NCC(H)CN)(PPh₃)_n] and its derivative had been generated in AN / LiBF₄, PPh₃ at 0 °C. As an extension of these studies, MDN-Cu(I) has been attempted galvanostatically in AN / Bu₄NBF₄, PPh₃ at 0 °C. As result no MDN-Cu(I) complex was formed rather the cyano copper(I) complex which was received as white precipitate and characterized by C, H, N elemental analysis, EDX, ESI-MS, ¹H-, ³¹P-NMR and IR-spectroscopies as a polymer with the general formula {[Cu(CN)(PPh₃)₂]·CH₃CN}_n (**5**).

A chemical reaction, between 2,2'-bipyridine (bipy) and **5** on the one hand, and between 1,10-phenanthroline (phen) and **5** on the other hand, afforded yellowish single crystals characterized by X-ray analysis as mononuclear copper(I) complexes with the formulae [Cu(CN)(bipy)(PPh₃)] (**6**) and [Cu(CN)(phen)(PPh₃)] (**7**) respectively.

It appeared that, galvanostatically, the size of cation of the supporting electrolyte plays an important role with regard to the mechanism of the MDN-Cu(I) formation. Thus, [Cu(NCC(H)CN)(PPh₃)_n] is favored in AN / LiBF₄ whereas **5** is favored in AN / Bu₄NBF₄.

The electrosynthesis of copper(I) compounds with TCP and MDN has revealed that both ligands undergo an electroreductive cleavage in AN / Bu₄NBF₄. Therefore, synthesis of nitrilecopper(I) complexes with a lesser acidic nitrile arouses interest with regard to the mechanism of its reduction.

For this proposal, phenylacetonitrile (PhAN) has been selected and the experiment was carried out galvanostatically in THF / Bu₄NBF₄ at 0 °C. Colorless crystals not suitable for X-ray analysis were collected and characterized by C, H, N elemental analysis, FAB⁺-MS, ¹H-, ¹³C-, ³¹P-NMR and IR-spectroscopies as {[C₄H₉)₄N][Cu(BPVA)(PPh₃)₂][BF₄]} (**8**) where BPVA stands for 1-benzyl-2-cyano-2-phenylvinylamine. The analyses revealed that PhAN undergoes an electrolytic reductive coupling at the cathode.

A reaction between **8** and 1,10-phenanthroline led to red-violet crystals which were characterized by X-ray analysis as a substituted neutral mononuclear copper(I) complex [Cu(BPVA)(phen)(PPh₃)] (**9**).

The complex **8** was dissolved in CD₃CN in which it recrystallized after standing for a time at room temperature and single crystals were collected for X-ray analysis which revealed a decomposition of **8** followed by a self-organization of Cu(I) and CN groups leading to a neutral one-dimensional infinite polymer of composition [Cu₉(CN)₉(PPh₃)₈]_n (**10**). The structure of **10** was drawn based on the preliminary results.

The addition of an excess of phen to the electrolytic solution obtained for **8** afforded orange crystals which were characterized by X-ray crystal structure analysis as an ionic trinuclear complex with a bent arrangement [Cu₃(CN)₂(phen)₃(PPh₃)₂][BF₄] (**11**).

A reaction between 1,10-phenanthroline monohydrate (phen·H₂O) in excess with the electrolytic solution obtained for **8** yielded green-yellowish crystals characterized by X-ray crystal structure analysis as monohydrated asymmetric unit with two independent mononuclear molecules [Cu(CN)(phen)(PPh₃)₂·H₂O] (**12**). The hydrogen atoms of the non coordinated water molecule could not be characterized by X-ray structure analysis but by thermal analysis.

These results revealed that PhAN has undergone not only an electrolytic reductive coupling at the cathode but also an electroreductive cleavage of C–CN bond as subsidiary reaction.

The direct electrosynthesis using a weak acidic PhAN has shown that it can undergo an electroreductive coupling. As an extension of these studies, some less acidic non-nitrile compounds, fluorine (FLU) and triphenylmethane (TPM), have been selected. The

electrochemical syntheses were carried out by galvanostatic methodology in AN / Bu₄NBF₄ at 0 °C.

The synthesis with FLU gave a white precipitate as product which were characterized by C, H, N elemental analysis, EDX, ESI-MS, ¹H-, ¹³C-, ³¹P-NMR and IR spectroscopies as [Cu(FLU)(PPh₃)₂] \cdot 2CH₃CN (**13**). However, with TPM, a greenish precipitate was received and characterized by C, H, N elemental analysis, EDX and FAB-MS as [Cu(CPh₃)(PPh₃)] \cdot 2CH₃CN (**14**).

It has been pointed out that copper(I)chloride complexes containing bidentate bridging diphosphine ligands exhibit antitumor activities. The electrochemical synthesis based on the galvanostatic dissolution of a copper electrode, in the presence of LiCl and 1,2-bis(diphenylphosphino)ethane (dppe), revealed to be an efficient alternative to achieve such compounds. Thus in AN / LiCl, dppe at 0 °C, single brown crystals suitable for X-ray analysis were collected and characterized as [(CuCl)₂(μ -dppe)(η^2 -dppe)₂] \cdot CH₃CN (**15**).

The complex **15** was soluble in DMSO in which it recrystallized as colorless crystal leading to a substitution of solvent molecule, [(CuCl)₂(μ -dppe)(η^2 -dppe)₂] \cdot (CH₃)₂SO (**16**).

The last part of this work was devoted to the modification of metal surfaces at micrometer and sub-micrometer scales. The work described in this part is an introductory work and devoted to the molecular architectures and nanostructures on metal surfaces. Therefore, a working place has been developed and the templating liquid crystalline method has been selected to test its operating.

The plating mixtures consist of non-ionic surfactant Brij[®] 76, hexachloroplatinic acid and water in a ratio 2:1:1. The electrodeposition of the platinum film from this mixture was carried out under galvanostatic control. The morphology of the electrodeposited platinum film was established only by atomic force microscopy (AFM) which revealed a porous structure on the gold surface.

Zusammenfassung

Im Rahmen der vorliegenden Arbeit wurde die Elektropräparation ausgewählter Kupfer(I)-nitrilkomplexe näher untersucht und es werden Aussagen zum elektrochemischen Reaktionsmechanismus dieser Synthesen gemacht.

Zunächst wurde das elektrochemische Verhalten von Nitrilen, die über Wasserstoff in α -Stellung zur Nitrilgruppe verfügen an einer Kupferelektrode sowohl in Acetonitril als auch in Tetrahydrofuren als nitrilfreiem Lösungsmittel untersucht. Die Cyclovoltammogramme der Systeme AN / Bu₄NBF₄, AN / LiClO₄, AN / Et₄NClO₄ und THF / Bu₄NPF₆ zeigen an der Kupferelektrode ein ähnliches Verhalten. Es werden zwei gut ausgebildete irreversible kathodische Peaks beobachtet (Peak I und II). Die Reduktion der solvatisierten Kupfer(I)-ionen (Peak I) erfolgt im System AN / Bu₄NBF₄ (-0.346 V) bei einem negativeren Potential als im System in THF / Bu₄NPF₆ (+0.341 V) und stimmt mit der starken Komplexbildungstendenz des Acetonitrils gegenüber Kupfer(I)-ionen überein.

Der Peakstrom des zweiten Prozesses hängt von der Konzentration der Anionen (X⁻) des Leitelektrolyten ab. Die Reaktionsordnung bezogen auf das Anion ist eins und zeigt, dass in diesem Potentialgebiet die Reduktion der Verbindung CuX stattfindet (bei -1.437 V in AN / Bu₄NBF₄, im System AN / LiClO₄, Et₄NClO₄ bei -1.600 V und in THF / Bu₄NPF₆ bei -1.712 V). Die kinetischen Parameter der Reaktion II an der rotierenden Kupfer-Scheibenelektrode in AN belegen einen diffusionskontrollierten Prozess. Die CuX-Spezies diffundieren durch die Elektrolytlösung und werden bei stärker negativen Potentialen reduziert, wie durch chronopotentiometrische und chronoamperometrische Messungen sowie Untersuchungen an der Doppelsegmentselektrode (DSE) nachgewiesen werden konnte.

Das elektrochemische Verhalten der drei Nitrile 1,1,3,3-Tetracyanopropan (TCP), Malonsäuredinitril (MDN) und Phenylacetonitril (PhAN)} mit unterschiedlicher Acidität ($pK_a > 10$) wurde sowohl am Kupfer als auch am Platin untersucht. Es konnte gezeigt werden, dass neben der Reduktion weitere chemische Reaktionen ablaufen. So wird 1,1,3,3-Tetracyanopropan nach einem ECEC-Mechanismus reduziert, wobei sich an den ersten Elektronentransfer eine irreversible chemische Reaktion zweiter Ordnung anschließt. Dem zweiten Elektronentransfer folgt eine irreversible chemische Reaktion erster Ordnung.

Malonsäuredinitril und Phenylacetonitril werden entsprechend einem EC-Mechanismus reduziert. Die Elektronentransferreaktion ist mit einer irreversiblen chemischen Reaktion erster Ordnung verknüpft. An der Kupferelektrode zeigt das Cyclovoltammogramm einen irreversiblen Peak zwischen $-0,8$ V und $-1,0$ V, der der Reduktion von Kupfer(I)-nitrilkomplexen zugewiesen werden kann.

Die genannten Nitrile wurden zur elektrochemischen Präparation von Organonitrilkupferverbindungen und deren Derivaten eingesetzt. Die Synthese erfolgte durch galvanische Auflösung von metallischem Kupfer in nichtwässrigen Medien in Gegenwart verschiedener Donatoren und gleichzeitiger kathodischer Reduktion der Nitrile in einer ungeteilten elektrochemischen Zelle.

Zunächst wurde ein Tetracyanopropan–Kupfer(I)-Komplex hergestellt. Mit Tetracyanopropan waren in unserem Labor schon potentiostatische Elektrosynthesen durchgeführt worden, bei denen wahrscheinlich der Kupratkomplex $\{(C_4H_9)_4N[Cu(TCP)BF_4]\}_n$ erhalten worden war. Es war jedoch bisher nicht gelungen, die Struktur und den Bildungsmechanismus eindeutig aufzuklären. Deshalb wurde die Elektrosynthese unter galvanostatischen Bedingungen im System AN / Bu_4NBF_4 genauer untersucht. Die Elektrolyse ergab ein Zweiphasensystem mit einer flüssigen und einer öligen Phase. Aus der flüssigen Phase wurden farblose Einkristalle erhalten, deren Röntgenstrukturuntersuchung ergab, dass es sich um einen neutralen, dimeren Zweikernkomplex der Zusammensetzung $[Cu(\mu-C(CN)_3)(PPh_3)_2]_2$ (**1**) handelt. Mit 1,10-Phenanthrolin (phen) konnten orange Kristalle isoliert werden, die durch Röntgenstrukturanalyse als $\{cis-[Cu_2(\mu-CN)(Phen)_2(PPh_3)_2]\}_2[C(CN)_3][BF_4] \cdot 2CH_3CN$ (**2**) identifiziert wurden.

Aus der in THF gelösten Ölphase wurden farblose Kristalle isoliert, hierbei handelt es sich um $[Cu_2(\mu-CN)(PPh_3)_6][BF_4]$ (**3**).

Die Reaktion zwischen **3** und 2,2'-Bipyridine (bipy) in THF lieferte grüngelbe Kristalle, deren Röntgenstrukturanalyse folgende Struktur ergab $[Cu_2(CN)(bipy)_2(PPh_3)_2][BF_4] \cdot THF$ (**4**).

Die Elektrosynthese des TCP-Cu(I)-Komplexes wurde bei verschiedenen Temperaturen durchgeführt ($-35^\circ C$, $0^\circ C$ und bei Raumtemperatur). Die Röntgenstrukturuntersuchungen zeigten, dass immer der Komplex **1** gebildet wird.

Weitere detaillierte elektrochemische Untersuchungen mit Tetracyanopropan ergaben, dass das generierte Carbanion nicht stabil ist, sondern einer Zersetzungsreaktion unterliegt. Der Zerfall liefert Acrylnitril, Tricyanomethanid und Cyanidanionen, eventuell bildet sich auch Malonsäuredinitril. Das entstehende Acrylnitril unterliegt einer Elektropolymerisation an der Kathode.

Der zweite Versuchskomplex der direkten Elektrosynthese widmete sich der Herstellung von Malonsäuredinitril-Cu(I)-Verbindungen und deren Derivaten. In einer früheren Arbeit war gezeigt worden, dass bei den Elektrosynthesen in Gegenwart von Malonsäuredinitril in Abhängigkeit von den experimentellen, elektrochemischen Bedingungen verschiedene Kupfer(I)-verbindungen entstehen. Durch potentiostatische Auflösung einer Kupferanode in AN / Bu₄NBF₄/ PPh₃ bei Raumtemperatur wurde [(PPh₃)₂Cu(μ-CN)Cu(PPh₃)₂][HC(CN)₂] erhalten. Galvanostatisch konnten in AN / LiBF₄, PPh₃ bei 0 °C die monomere Kupfer(I)-verbindung [Cu(NCC(H)CN)(PPh₃)] und deren Derivate synthetisiert werden. Wurde die galvanostatische Elektrolyse jedoch in AN / Bu₄NBF₄, PPh₃ bei 0 °C ausgeführt entstand kein Malonsäuredinitril-Cu(I)-komplex. Vielmehr bildete sich ein weißer, polymerer Niederschlag der Zusammensetzung {[Cu(CN)(PPh₃)₂·CH₃CN]_n (**5**), wie C-, H-, N-Elementaranalyse, EDX, sowie ¹H-, ³¹P-NMR- und IR-spektroskopische Untersuchungen ergaben.

Die chemischen Reaktionen von **5** mit 2,2'-Bipyridin (bipy) auf der einen Seite und 1,10-Phenanthrolin (phen) andererseits ergaben jeweils gelbliche Kristalle, die durch Röntgenstrukturanalyse charakterisiert wurden. Es handelt sich um die Komplexe [Cu(CN)(bipy)(PPh₃)] (**6**) und [Cu(CN)(phen)(PPh₃)] (**7**).

Bei der galvanostatischen Elektrolyse spielt die Art des Kations des Leitelektrolyten eine wichtige Rolle bezüglich des Mechanismus der Bildung der Kupfer(I)-komplexe.

Die Elektropräparation von Kupfer(I)-verbindungen mit Tetracyanopropan und Malonsäuredinitril zeigt, dass beide Liganden in AN / Bu₄NBF₄ einer reduktiven Bindungsspaltung unterliegen. Deshalb erschienen Synthesen mit einem weniger aciden Nitril bezüglich des Reduktionsmechanismus interessant. Zu diesem Zweck wurde Phenylacetonitril (PhAN) ausgewählt. Die Experimente wurden unter galvanostatischen Bedingungen in THF / Bu₄NBF₄ bei 0 °C durchgeführt. Bei der entstandenen farblosen Substanz handelt es sich um {[C₄H₉)₄N][Cu(BPVA)(PPh₃)₂][BF₄]} (**8**) (BPVA: 1-benzyl-2-cyano-2-phenylvinylamine)

wie C-, H-, N- Elementaranalyse, FAB⁺-MS, ¹H-, ¹³C-, ³¹P-NMR und IR-spektroskopischen Messungen ergaben. Die Kristalle waren nicht geeignet für eine Röntgenstrukturanalyse. Die Analyse zeigte, dass PhAN einer reduktiven Kupplung an der Kathode unterliegt.

Die Reaktion zwischen **8** and 1,10-Phenanthrolin liefert rotviolette Kristalle, die durch Röntgenstrukturanalyse als substituierter neutraler, mononuklearer Kupfer(I)-Komplex [Cu(BPVA)(phen)(PPh₃)] (**9**) charakterisiert wurden.

Der Komplex **8** wurde in CD₃CN gelöst und nach einiger Zeit kristallisierte eine Verbindung bei Raumtemperatur aus, die der Röntgenstrukturanalyse zugänglich war. Sie ist offensichtlich ein Zersetzungsprodukt von **8**, gefolgt von einer Selbstorganisation von Cu(I) und CN-Gruppen, die zu einem neutralen, eindimensionalen infiniten Polymer der Zusammensetzung [Cu₉(CN)₉(PPh₃)₈]_n (**10**) führen. Die Struktur von **10** wurde auf der Basis vorläufiger Ergebnisse konstruiert.

Die Zugabe von einem Überschuss an phen zu der Elektrolyselösung von **8** liefert orange Kristalle von [Cu₃(CN)₂(phen)₃(PPh₃)₂][BF₄] (**11**). Es handelt sich um einen Dreikernkomplex mit einer gewinkelten Struktur.

Die Reaktion der Elektrolyselösung **8** mit einem Überschuss an 1,10-Phenanthroline monohydrate (phen·H₂O) liefert grüngelbe Kristalle, deren Röntgenstrukturanalyse eine monohydratisierte asymmetrische Einheit zeigt mit zwei unabhängigen mononuklearen Molekülen [Cu(CN)(phen)(PPh₃)₂·H₂O] (**12**). Die Wasserstoffatome der nichtkoordinierten Wassermoleküle konnten nicht durch Röntgenstrukturanalyse nachgewiesen werden. Das Wasser wurde jedoch durch thermische Analyse konnte jedoch die Abspaltung einem Mol Wasser pro Mol Komplex eindeutig nachgewiesen werden.

Die direkte Elektrosynthese unter Verwendung des schwach aciden Phenylacetonitril zeigt, dass es nicht nur einer elektroreduktiven Kupplung an der Kathode, sondern auch einer reduktiven C-CN Bindungsspaltung unterliegt.

Aus diesem Grund wurden auch einige weniger acide nicht nitrilhaltige Verbindungen Fluoren (FLU) and Triphenylmethane (TPM) als Ausgangsstoffe ausgewählt. Die Elektrolysen wurden galvanostatisch in AN / Bu₄NBF₄ bei 0 °C ausgeführt.

Die Synthese mit FLU lieferte ein weißes Produkt, das durch C, H, N Elementaranalyse, EDX, ESI-MS, ^1H -, ^{13}C -, ^{31}P -NMR and IR-Spektroskopie als $[\text{Cu}(\text{FLU})(\text{PPh}_3)_2] \cdot 2\text{CH}_3\text{CN}$ (**13**) identifiziert wurde. Triphenylmethane entsteht ein grüner Niederschlag der Zusammensetzung $[\text{Cu}(\text{CPh}_3)(\text{PPh}_3)] \cdot 2\text{CH}_3\text{CN}$ (**14**), wie C, H, N Elementaranalyse, EDX- und FAB-MS-Untersuchungen zeigten.

Es ist bekannt, dass Kupfer(I)-chloridkomplexe mit zweizähligen Diphosphin-Brückenliganden Antitumoraktivität zeigen. Die elektrochemische Synthese derartiger Komplexe basiert auf der galvanostatischen Auflösung einer Kupferelektrode in Gegenwart von LiCl und 1,2-Bis(diphenylphosphino)ethan (dppe) als einer effektiven Präparationsmethode.

In AN/LiCl, dppe wurden bei $0\text{ }^\circ\text{C}$ braune Kristalle erhalten, die eine Röntgenstrukturanalyse erlaubten und bei denen es sich um $[(\text{CuCl})_2(\mu\text{-dppe})(\eta^2\text{-dppe})_2] \cdot \text{CH}_3\text{CN}$ (**15**) handelt. Der Komplex **15** ist in DMSO löslich. Beim Umkristallisieren in diesem Lösungsmittel werden farblose Kristalle erhalten, bei denen das Solvensmolekül CH_3CN gegen DMSO ausgetauscht wurde $[(\text{CuCl})_2(\mu\text{-dppe})(\eta^2\text{-dppe})_2] \cdot (\text{CH}_3)_2\text{SO}$ (**16**).

Der letzte Teil der Arbeit beschäftigt sich mit der Modifizierung von Metalloberflächen im Mikrometer- und Submikrometermaßstab. Von den verschiedenen bekannten Arbeitstechniken wurde die an der Universität Southampton entwickelte templating liquid crystalline method ausgewählt.

Deshalb war es notwendig, ein Verständnis für das System und das Herstellungsverfahren zu entwickeln, bei dem flüssigkristalline Substanzen als templates für die Synthese nanostrukturierter Materialien eingesetzt werden. Erste Ergebnisse der Nanostrukturierung durch galvanische Metallabscheidung von Platin auf Goldoberflächen werden mitgeteilt.

Das Galvanisierungsgemisch bestand aus den nichtionischen Tensid Brij[®] 76, Hexachloroplatinsäure und Wasser im Verhältnis 2:1:1. Die Elektroabscheidung eines strukturierten Platinfilms aus diesem Gemisch geschieht unter galvanostatischer Kontrolle. Die Morphologie der abgeschiedenen Platinfilme wurde bisher nur durch AFM-Untersuchungen charakterisiert, die eine poröse Struktur auf der Goldoberfläche zeigen.

7. References

- [1] N. Krause, *Modern Organocopper Chemistry*, Wiley-VCH, Weinheim, 2002.
- [2] a) C. Piazza, Ph.D. Thesis, LMU Univ. Munich 2002.
b) R. K. Gujadhur, Ph.D. Thesis, UMA Univ. Massachusetts 2003.
- [3] I. Omae, *Applications of Organometallic Compounds*, John Wiley and Sons, Chichester, New York, Weinheim, Brisbane, Singapore, Toronto, 1998.
- [4] R. J. K. Taylor, *Organocopper Reagents: A practical Approach*, Oxford University Press, Oxford, New York, Tokyo, 1994.
- [5] K. Nilsson, T. Andersson, C. Ullenius, A. Gerold, N. Krause, *Chem. Eur. J.* **1998**, *4*, 2051.
- [6] S. I. Murahashi, N. Komiya, Y. Hayashi, T. Kumano, *Pure Appl. Chem.* **2001**, *73*, 311.
- [7] P. Knochel, P. Jones, *Organozinc Reagents: A practical Approach*, Oxford University Press, Oxford, 1999.
- [8] A. N. Nesmeyanov, K. A. Kocheshkov, *Methods of Elemento-Organic Chemistry*, vol. 3, North-Holland Publishing Company, Amsterdam, The world Publishing Company, Cleveland, New York, 1967.
- [9] H. Gilman, R.G. Jones, L. A. Woods, *J. Org. Chem.* **1952**, *17*, 1630.
- [10] H. Gilman, L. A. Woods, *J. Am. Chem. Soc.* **1943**, *65*, 435.
- [11] A. D. Garnovskii, B. I. Kharisov, *Direct Synthesis of Coordination and Organometallic Compounds*, Elsevier, Amsterdam, Lausanne, New York, Oxford, Shannon, Singapore, Tokyo, 1999, pp. 72-134.
- [12] M. C. Chakravorti, G. V. B. Subrahmanyam, *Coord. Chem. Rev.*, **1994**, *135-136*, 65.
- [13] K. D. Moeller, *Tetrahedron Letters*, **2000**, *56*, 9527.
- [14] B. Gerdes, *J. Pract. Chem.*, **1882**, *26*, 257.
- [15] H. Lehmkuhl, *Synthesis*, **1973**, 377.
- [16] a) D. G. Tuck, *Pure Appl. Chem.* **1979**, *51*, 2005.
b) J. J. Habeeb, A. Osman, D. G. Tuck, *J. Organomet. Chem.* **1980**, *185*, 117.
c) F. F. Said, D. G. Tuck, *J. Organomet. Chem.*, **1982**, *224*, 121.
d) F. F. Said, D. G. Tuck, *Can. J. Chem.*, **1980**, *58*, 1673.
- [17] a) A. Castineiras, J. A. Castro, M. L. Duran, J. A. Garcia-Vazquez, A. Macias, J. Romero, A. Sousa, *Polyhedron*, **1989**, *8*, 2543.
b) E. Labisbal, A. De Blas, J. A. Garcia-Vazquez, J. Romero, M. L. Duran, A. Sousa, N. A. Bailey, D. E. Fenton, P. B. Leeson, R. V. Parish, *Polyhedron*, **1992**, *11*, 222.

- c) J. A. Castro, J. E. Vilasanchez, J. Romero, J. A. Garcia-Vazquez, M. L. Duran A. Sousa, E. E. Castellano, J. Zukerman-Schpector, *Z. Anorg. Allg. Chem.*, **1992**, 612, 83.
- d) J. A. Castro, J. Romero, J. A. Garcia-Vazquez, A. Macias, A. Sousa, U. Englert, *Polyhedron*, **1993**, 12, 1391.
- e) J. A. Castro, J. Romero, J. A. Garcia-Vazquez, A. Sousa, E. E. Castellano, J. Zukerman-Schpector, *Polyhedron*, **1993**, 12, 31.
- f) J. A. Castro, J. Romero, J. A. Garcia-Vazquez, M. L. Duran, A. Sousa, E. E. Castellano, J. Zukerman-Schpector, *Polyhedron*, **1992**, 11, 235.
- g) J. A. Castro, J. Romero, J. A. Garcia-Vazquez, A. Castineiras, M. L. Duran, A. Sousa, *Z. Anorg. Allg. Chem.*, **1992**, 615, 155.
- h) M. L. Duran, J. A. Garcia-Vazquez, A. Macias, J. Romero, A. Sousa, E. B. Rivero, *Z. Anorg. Allg. Chem.*, **1989**, 573, 215.
- [18] F. Battaglini, E. J. Calvo, F. Doctorovich, *J. Organomet. Chem.* **1997**, 547, 1.
- [19] G. A. Tedoradze, *J. Organomet. Chem.*, **1975**, 88, 1.
- [20] R. A. Michelin, M. Mozzon, R. Bertani, *Coord. Chem. Rev.*, **1996**, 147, 299.
- [21] a) W. S. Matthews, J. E. Bares, J. E. Bartness, F. G. Bordwelle, F. J. Cornforth, G. E. Drucker, Z. Margolin, R. J. McCallum, G. J. McCollum, *J. Am. Chem. Soc.*, **1975**, 97, 7006.
- b) F. G. Bordwell, N. R. Vanier, W. S. Matthews, J. B. Hendrickson, P. L. Skipper, *J. Org. Chem.*, **1976**, 41, 1885.
- c) F. G. Bordwell, J. E. Bares, J. E. Bartness, G. J. McCollum, M. Van der Puy, N. R. Vanier, W. S. Matthews, *J. Org. Chem.*, **1977**, 42, 321.
- d) F. G. Bordwell, X. Zhang, M. S. Mikhail, *J. Am. Chem. Soc.*, **1992**, 114, 7623.
- e) F. G. Bordwell, J. E. Bartness, J. A. Hautala, *J. Org. Chem.* **1978**, 43, 3095.
- f) F. G. Bordwell, J. C. Branca, J. E. Bares, R. Filler, *J. Org. Chem.* **1988**, 53, 780.
- g) N. S. Isaacs, *Physical organic chemistry*, 2nd ed. 1996, Longman, Singapore Publ. Ltd., 247.
- h) D. A. Bors, M. J. Kaufman, *J. Am. Chem. Soc.*, **1985**, 107, 6975.
- [22] a) V. Ryabova, Ph.D. Thesis, MLU Univ. Halle 2001;
b) M. Günther, Ph.D. Thesis, MLU Univ. Halle 1999.
- [23] M. Günther, W. Schäfer, A. Stettler, H. Hartung, *Z. Anorg. Allg. Chem.* **2000**, 626, 655.
- [24] W. Schäfer, V. Ryabova, M. Günther, M. M. Fotsing Kamte, 53rd Annual Meeting of ISE, Düsseldorf, **2002**, Preprints, 343.

- [25] J. Klunker, W. Schäfer, *J. Electroanal. Chem.*, **1999**, 466, 107.
- [26] A. H. Moreira, A. V. Benetti, P. L. Cabot, P. T. A. Sumodjo, *Electrochimica Acta*, **1993**, 38, 981.
- [27] R. L. Brossard, *Can. J. Chem.*, **1983**, 61, 2022.
- [28] R. L. Brossard, *Can. J. Chem.*, **1982**, 60, 616.
- [29] R. L. Brossard, *J. Electrochem. Soc.*, **1983**, 130, 403.
- [30] I. M. Kolthoff, J. F. Coetzee, *J. Am. Chem. Soc.*, **1957**, 79, 139.
- [31] S. E. Manahan, R. T. Iwamoto, *J. Electroanal. Chem.*, **1967**, 14, 213.
- [32] a) R. R. Bessette, J. W. Olver, *J. Electroanal. Chem.*, **1969**, 21, 525.
b) A. J. Parker, *Search*, **1973**, 14, 426.
- [33] S. N. Raicheva, *Electrochimica Acta*, **1984**, 29, 1067.
- [34] B. G. Cox, W. Jedral, J. Palou, *J. Chem. Soc., Dalton Trans.*, **1988**, 733.
- [35] P. Kamau, R. B. Jordan, *Inorg. Chem.*, **2001**, 40, 3879.
- [36] D. K. Padma, *J. Electrochem. Soc. India*, **1989**, 38, 67.
- [37] F. J. Hughes, I. M. Ritchie, P. Singh, *Aust. J. Chem.*, **1984**, 37, 903.
- [38] a) R. A. Couche, I. M. Ritchie, *Aust. J. Chem.*, **1984**, 37, 237.
b) I. D. MacLeod, D. M. Muir, A. J. Parker, *Aust. J. Chem.*, **1977**, 30, 1423.
- [39] R. A. Bell, B. E. Brown, M. Duarte, H. E. Howard-Lock, C. J. L. Lock, *Can. J. Chem.*, **1987**, 65, 261.
- [40] a) S. J. Berners-Price, P. J. Sadler, *Chem. Brit.*, **1987**, 23, 541.
b) S. J. Berners-Price, C. K. Mirabelli, R. K. Johnson, M. R. Mattern, F. L. McCabe, L. F. Faucette, C-M. Sung, S-M. Mong, P. J. Sadler, S. T. Crooke, *Cancer Res.*, **1986**, 46, 5486.
- [41] G. S. Attard, P. N. Bartlett, N. R. B. Coleman, J. M. Elliot, J. R. Owen, J. H. Wang, *Science*, **1997**, 278, 838.
- [42] J. M. Elliot, G. S. Attard, P. N. Bartlett, J. R. Owen, N. Ryan, G. Singh, *J. New. Mat. Electrochem. Systems*, **1999**, 2, 239.
- [43] J. Grobe, M. Keil, B. Schneider, H. Zimmerman, *Z. Naturforsch. Teil B*, **1980**, 35, 428.
- [44] A. D. Garnovskii, B. I. Kharisov, *Direct Synthesis of Coordination and Organometallic Compounds*, Elsevier, Amsterdam-Lausanne-New York-Oxford-Shannon-Singapore-Tokyo 1999, pp.81-82.
- [45] J. Wang, *Analytical Electrochemistry*, VCH, New York-Weinheim-Cambridge, 1994, p. 71.
- [46] Y. Zhao, F. G. Bordwell, *J. Org. Chem.*, **1996**, 61, 6623.

- [47] X.-M. Zhang, F. G. Bordwell, *J. Am. Chem. Soc.*, **1994**, *116*, 904.
- [48] a) K. J. Borhani, M. D. Hawley, *J. Electroanal. Chem.*, **1979**, *101*, 407.
b) A. Lagu, H. B. Jr. Mark, J. R. Jesorek, *J. Org. Chem.*, **1977**, *42*, 1603.
c) D. Casson, B. J. Tabner, *J. Chem. Soc. B*, **1969**, 887.
- [49] D. Griller, M. Simoes, J. A. Mulder, B. A. Sim, D. D. M. Wayner, *J. Am. Chem. Soc.*, **1989**, *111*, 7872.
- [50] X.-M. Zhang, F. G. Bordwell, *J. Am. Chem. Soc.*, **1992**, *114*, 9787.
- [51] V. Y. Kukushkin, A. J. L. Pombeiro, *Chem. Rev.*, **2002**, *102*, 1771.
- [52] a) R. M. Bullock, C. E. L. Headford, S. E. Kegley, J. R. Norton, *J. Am. Chem. Soc.*, **1985**, *107*, 727.
b) D. M. Hoffman, S. Lee, *Inorg. Chem. Rev.*, **1992**, *31*, 2675.
- [53] C. Colominas, M. Orozco, F. J. Luque, J. I. Borell, J. Teixidó, *J. Org. Chem.*, **1998**, *63*, 4947.
- [54] L. Ebersson, in: *Organic Electrochemistry*, M. M. Baizer (Eds), 1st Edn, Marcel Dekker, New York 1973, Chap. 10, p. 423.
- [55] S. E. Treimer, D. H. Evans, *J. Electroanal. Chem.*, **1998**, *455*, 1.
- [56] A. V. Bukhtiarov, V. N. Golyshin, A. P. Tomilov, O. V. Kuz'min, *Zh. Obshch. Khim.*, **1988**, *58*, 857.
- [57] P. H. Rieger, I. Bernal, W. H. Reinmuth, G. K. Fraenkel, *J. Am. Chem. Soc.*, **1963**, *85*, 683.
- [58] a) J. Volke, *Electrochemistry in organic synthesis: with 12 tables*, Springer Verlag 1994, pp.98-99.
b) J. Volke, V. Skála, *J. Electroanal. Chem.*, **1972**, *36*, 383.
- [59] A. C. Fisher, *Electrode Dynamics*, Oxford University Press, Oxford, New York, Tokyo, 1996, pp. 30-31.
- [60] A. Bard, L. Faulkner, *Electrochemical Methods: Principles and Applications*, Wiley: New York, 1980, p. 228.
- [61] F. Opekar and P. Beran, *J. Electroanal. Chem.*, **1976**, *69*, 1.
- [62] P. J. Kinlen, C. J. H. King, *J. Electroanal. Chem.*, **1991**, *304*, 133.
- [63] W. Schäfer, *Ger. Offen.*, **1994**, 4pp., DE 93-4303446.
- [64] W. Schäfer, A. G. Atanasjanz, V. A. Kornienko, *Z. phys. Chemie Leipzig*, **1990**, *3*, S. 495.
- [65] S. E. Manahan, R. T. Iwamoto, *J. Electroanal. Chem.*, **1967**, *14*, 213.
- [66] a) R. R. Bessette, J. W. Olver, *J. Electroanal. Chem.*, **1969**, *21*, 525.

- b) A. J. Parker, *Search*, **1973**, 4, 426.
- c) I. D. MacLeod, D. M. Muir, A. J. Parker, *Aust. J. Chem.*, **1977**, 30, 1423.
- d) F. J. Hughes, I. M. Ritchie, P. Singh, *Aust. J. Chem.*, **1984**, 37, 903.
- e) R. A. Couche, I. M. Ritchie, *Aust. J. Chem.*, **1984**, 37, 237.
- f) O. J. Parker, J. H. Espenson, *J. Am. Chem. Soc.*, **1969**, 91, 1968.
- [67] S. N. Raicheva, *Electrochimica Acta*, **1984**, 29, 1067.
- [68] B. G. Cox, W. Jedral, J. Palou, *J. Chem. Soc., Dalton Trans.*, **1988**, 733.
- [69] P. Kamau, R. B. Jordan, *Inorg. Chem.*, **2001**, 40, 3879.
- [70] I. M. Kolthoff, J. F. Coetzee, *J. Am. Chem. Soc.*, **1957**, 79, 139.
- [71] D. K. Padma, *J. Electrochem. Soc. India*, **1989**, 38, 67.
- [72] B. W. Rossiter, J. F. Hamilton, *Physical Methods of Chemistry Electrochemical Methods*, 2nd ed., vol. 2, John Wiley and Sons, New York-Chichester-Brisbane-Toronto-Singapore, 1986, pp. 318-321, 330.
- [73] R. S. Nicholson, I. Shain, *Anal. Chem.*, **1965**, 37, 178.
- [74] G. S. Alberts, I. Shain, *Anal. Chem.*, **1963**, 35, 1854.
- [75] D. S. Polyn, I. Shain, *Anal. Chem.*, **1965**, 37, 178.
- [76] K.-S. Jung, S. C. Sohn, Y. K. Ha, T. Y. Eom, *Bull. Korean Chem. Soc.*, **1991**, 12, 239.
- [77] S. M. A. Jorge, P. Maia de Campos, N. R. Stradiotto, *J. Braz. Chem. Soc.*, **1999**, 10, 176.
- [78] E. T. Seo, R. F. Nelson, J. M. Fritsch, L. S. Marcoux, D. W. Leedy, R. N. Adams, *J. Am. Chem. Soc.*, **1966**, 88, 3498.
- [79] A. C. Fisher, *Electrode Dynamics*, Oxford University Press, Oxford, New York. Tokyo, 1996, pp. 3-5.
- [80] M. Leschke, H. Lang, R. Holze, *Electrochimica Acta*, **2003**, 48, 919.
- [81] K. S. V. Santhanam, A. J. Bard, *J. Am. Chem. Soc.*, **1968**, 90, 1118.
- [82] R. E. Dessy, T. Chivers, W. Kitching, *J. Am. Chem. Soc.*, **1966**, 88, 467.
- [83] a) J. A. Davies, V. Uma, *J. Electroanal. Chem.*, **1984**, 179, 273.
b) J. M. Saveant, S. K. Binh, *J. Electroanal. Chem.*, **1978**, 88, 27.
c) H. Ohmori, S. Nakai, M. Masui, *J. Chem. Soc. Trans Perkin I.*, **1978**, 1333.
d) G. Schiavon, S. Zecchin, G. Cogoni, G. Bontempelli, *J. Electroanal. Chem.*, **1978**, 48, 425.
e) J. A. Carem, E. J. Vasini, *Electrochimica Acta*, **1994**, 39, 2395.
- [84] V. H. Matschiner, L. Krause, F. Krech, *Z. Anorg. Allg. Chem.*, **1970**, 373, 1
- [85] C. B. Lebrilla, T. Drewello, H. Schwarz, *Organometallics*, **1987**, 6, 2450.

-
- [86] K. E. Bessler, L. A. de P. Calzavara, V. M. Deflon, E. Niquet, *Acta Cryst.* **2001**, *E57*, m522.
- [87] L. Jäger, C. Tretner, H. Hartung, M. Biedermann, *Eur. J. Inorg. Chem.*, **1998**, 1051.
- [88] L. Jäger, C. Tretner, H. Hartung, M. Biedermann, *Z. Anorg. Allg. Chem.*, **1997**, *623*, 1299.
- [89] P. J. Kinlen, C. J. H. King, *J. Electroanal. Chem.*, **1991**, *304*, 133.
- [90] E. W. Ainscough, E. N. Baker, M. L. Brader, A. M. Brodie, *J. Chem. Soc., Dalton Trans.*, **1991**, 1243.
- [91] N. B. Colthup, L. H. Daly, S. E. Wiberley, *Introduction to infrared and Raman spectroscopy*, Academic Press, New York, 1961, pp. 278-290.
- [92] M. Mertens, C. Calberg, L. Martinot, R. Jerome, *Macromolecules* **1996**, *29*, 4910.
- [93] K. Sato, M. Ogasawara, K. Hayashi, *J. Polym. Sci., Polym. Lett. Ed.*, **1973**, *11*, 5.
- [94] O. R. Brown, E. R. Gonzalez, A. R. Wright, *Electrochim. Acta* **1973**, *18*, 555.
- [95] R.-N. Yang, Y.-A. Sun, Y.-M. Hou, X.-Y. Hu, D.-M. Jin, *Inorganica Chimica Acta* **2000**, *304*, 1.
- [96] C. Bureau, G. Deniau, P. Viel, G. Lecayon, *Macromolecules* **1997**, *30*, 333.
- [97] P. J. Kinlen, C. J. H. King, *J. Electroanal. Chem.* **1991**, *304*, 133.
- [98] G. Lecayon, Y. Bouizem, C. Le Gressus, C. Boiziau, C. Juret, *Chem. Phys. Lett.* **1982**, *91*, 506.
- [99] G. O. Morpurgo, G. Dessy, V. Fares, *J. Chem. Soc., Dalton Trans.* **1984**, 785
- [100] A. G. Orpen, G. Brammer, F. H. Allen, O. Kennard, D. G. Watson, R. Taylor, *J. Chem. Soc., Dalton Trans.* **1989**, 1.
- [101] M. M. Olmstead, G. Speier, L. Szabo, *J. Chem. Soc., Chem. Commun.*, **1994**, 541.
- [102] M. I. Bruce, B. W. Skelton, A. H. White, N. N. Zaitseva, *J. Chem. Soc., Dalton Trans.* **2001**, 3627.
- [103] Y. Zhao, M. Hong, W. Su, R. Cao, Z. Zhou and A. S. C. Chan, *J. Chem. Soc. Dalton Trans.*, **2000**, 1685.
- [104] R. Singh and S. K. Dikshit, *Polyhedron*, **1993**, *12*, 1697.
- [105] D. B. Grotjahn, M. A. Brewster and L. M. Ziurys, *J. Am. Chem. Soc.*, **2002**, *124*, 5895.
- [106] C. Pettinari, *Polyhedron*, **2001**, *20*, 2755.
- [107] J. Zhou, J. W. Raebiger, C. A. Crawford and R. H. Holm, *J. Am. Chem. Soc.*, **1997**, *119*, 6242.
- [108] R. C. Bott, P. C. Healy and D. S. Sagatys, *Chem. Commun.*, **1998**, 2403.
-

- [109] A. E. Mauro, C. C. Porta, S. R. Ananias, V. Sargentelli, R. H. D. A. Santos and M. T. D. P. Gambardella, *J. Coord. Chem.*, **1999**, *49*, 9.
- [110] M. Meyer, A.-M. Albrecht-Gary, C.O.Dietrich-Buchecker, J.-P. Sauvage, *Inorg. Chem.*, **1999**, *38*, 2279.
- [111] J. M. Knaust, D. A. Knight, S. W. Keller, *J. Chem. Crystallogr.*, **2003**, *33*, 813.
- [112] P. G. Jones, O. Crespo, *Act. Cryst.*, **1998**, *C54*, 18.
- [113] a) R. G. Pearson, *J. Chem. Educ.*, **1968**, *45*, 581.
b) R. G. Pearson, *J. Chem. Educ.*, **1968**, *45*, 643.
- [114] B. I. Kharisov, D. A. Garnovskii, L. M. Blanco, A. S. Burlov, I.S. Vasilchenko, A. D. Garnovskii, *Polyhedron* **1999**, *18*, 985.
- [115] E. Colacio, R. Kivekäs, F. Lloret, M. Sunberg, J. Suarez-Varela, M. Bardají, A. Laguna, *Inorg. Chem.*, **2002**, *41*, 5141.
- [116] D.J. Darensbourg, W. Z. Lee, M. J. Adams, D. L. Larkins, J. H. Reibenspies, *Inorg. Chem.*, **1999**, *38*, 1378
- [117] N. Zhu, H. Vahrenkamp, *J. organomet. Chem.*, **1999**, *573*, 67.
- [118] C. J. Shorrock, B.-Y. Xue, P. B. Kim, R. J. Batchelor, B. O. Patrick, D. B. Leznoff, *Inorg. Chem.*, **2002**, *41*, 6743.
- [119] C. J. Shorrock, H. Jong, R. J. Batchelor, D. B. Leznoff, *Inorg. Chem.*, **2003**, *42*, 3917.
- [120] D. J. Chesnut, A. Kusnetzow, R. Birge, J. Zubieta, *J. Chem. Soc., Dalton Trans.*, **2001**, 2581.
- [121] G. Dessy, V. Fares, P. Imperatori, G. O. Morpurgo, *J. Chem. Soc., Dalton Trans.*, **1985**, 1285.
- [122] V. Comte, H. Vahrenkamp, *J. organomet. Chem.*, **2001**, *627*, 153.
- [123] D. J. Chesnut, A. Kusnetzow, R. Birge, J. Zubieta, *Inorg. Chem.*, **1999**, *38*, 5484.
- [124] B. K. Koo, *Bull. Korean Chem.Soc.*, **2001**, *22*, 113.
- [125] M. T. Miller, P. K. Gantzel, T. B. karpishin, *Angew. Chem.*, **1998**, *110*, 1659 and references therein.
- [126] A. S. Vinogradov, A. B. Preobrajenski, A. Knop-Gericke, S. L. Molodtsov, S. A. Krasnikov, S. V. Nekipelov, R. Szargan, M. Hävecker, R. Schlögl, *J. Electron Spectrosc. Relat. Phenom.*, **2001**, *114-116*, 813.
- [127] G. van Koten, S. L. James, J. T. B. H. Jastrzebski, in: *Comprehensive Organometallic Chemistry II*, E. W. Abel, F. G. A. Stone, G. Wilkinson (eds) Vol. 3, Pergamon, Oxford 1995, pp. 57-133.
- [128] G. N. Richardson, U. Brand, H. Vahrenkamp, *Inorg. Chem.*, **1999**, *38*, 3070.
- [129] G. N. Richardson, H. Vahrenkamp, *J. Organomet. Chem.*, **2000**, *593-594*, 44.

- [130] V. Comte, Z.-N. Chen, M.-L. Flay, H. Vahrenkamp, *J. organomet. Chem.*, **2000**, 614-615, 131.
- [131] H. Vahrenkamp, G. N. Richardson, *J. Chem. Soc., Dalton Trans.*, **1997**, 3643.
- [132] I. Escorihuela, L. R. Falvello, M. Tomás, *Inorg. Chem.*, **2001**, 40, 636.
- [133] M. Y. Darensbourg, H. L. C. Barros, *Inorg. Chem.*, **1979**, 18, 3286.
- [134] X.-M. Zhang, F. G. Bordwell, *J. Am. Chem Soc.*, **1994**, 116, 904.
- [135] J. Rault-Berthelot, J. Simonet, *J. Electroanal. Chem.*, **1985**, 182, 187.
- [136] K. J. Borhani, M. Dale Hawley, *J. Electroanal. Chem.*, **1979**, 101, 407.
- [137] F. F. Said, D. G. Tuck, *Can.J. Chem.*, **1981**, 59, 62.
- [138] E. W. Ainscough, E. N. Baker, M. L. Brader, A. M. Brodie, S. L. Ingham, J. M. Waters, J. V. Hanna, P. C. Healy, *J. Chem. Soc., Dalton Trans.* **1991**, 1243.
- [139] V. G. Albano, P. L. Bellon, G. Ciani, *J. Chem. Soc., Dalton Trans.* **1972**, 1938.
- [140] C. Lin, L. L. Yongshou, *Jiegou Huaxue*. **1993**, 12, 286. CAN 120:337610
- [141] S. J. Berners-Price, R. K. Johnson, C. K. Mirabelli, L. F. Faucette, F. L. McCabe, P. J. Sadler, C. Birkbeck, *Inorg. Chem.*, **1987**, 26, 3383.
- [142] a) S. J. Berners-Price, R. K. Johnson, Al J. Giovenella, L. F. Faucette, C. K. Mirabelli, P. J. Sadler, *J. Inorg. Biochem.*, **1988**, 33, 285.
b) J. S. Lewis, J. Zweit, P. J. Blower, *Polyhedron* **1998**, 17, 513 and references therein.
- [143] a) J. V. Barth, J. Weckesser, N. Lin, A. Dmitriev, K. Kern, *Appl. Phys. A*, **2003**, 76, 645.
b) C. Minelli, N. Blondiaux, M. Losson, M. Liley, S. Jeney, C. Hinderling, R. Pugin, D. Joester, F. Diederich, J. Vancso, M. Hempenius, H. Heinzelmann, *Chimia*, **2003**, 57, 646.
c) G. Y. Tseng, J. C. Ellenbogen, *Science*, **2001**, 294, 1293.
d) R. Schuster, V. Kirchner, P. Allongue, G. Ertl, *Science*, **2000**, 289, 98.
e) D. M. Kolb, R. Ullmann, T. Will, *Science*, **1997**, 275, 1097.
- [144] G. S. Attard, J. C. Glyde, C. G. Göltner, *Nature*, **1995**, 378, 366.
- [145] G. S. Attard, C. G. Göltner, J. M. Corker, S. Henke, R. H. Templer, *Angew. Chem. Int. Ed. Engl.*, **1997**, 36, 1315.
- [146] G. S. Attard, S. A. A. Leclerc, S. Maniguet, A. E. Russell, I. Nandhakumar, B. R. Gollas, P. N. Bartlett, *Microporous and Mesoporous Materials*, **2001**, 44-45, 159.
- [147] G. S. Attard, M. Edgar, C. G. Göltner, *Acta Mater.*, **1998**, 46, 751.

- [148] G. S. Attard, N. R. B. Coleman, J. M. Elliot, in: *Mesoporous Molecular Sieves 1998*, L. Bonneviot, F. Béland, C. Danumah, S. Giasson, S. Kaliaguine (eds), Elsevier, *Studies in Surface Science and Catalysis*, **1998**, *117*, 89-94.
- [149] S. A. G. Evans, J. M. Elliot, L.M. Andrews, P. N. Bartlett, P. J. Doyle, G. Denuault, *Anal. Chem.*, **2002**, *74*, 1322.
- [150] P. A. Nelson, J. M. Elliot, G. S. Attard, J. R. Owen, *Chem. Mater.*, **2002**, *14*, 524.
- [151] P. R. Nelson, J. M. Elliot, Y. E. Watson, *Chem. Commun.*, **2000**, 1693.
- [152] J. M. Elliot, P. R. Birkin, P. N. Bartlett, G. S. Attard, *Langmuir*, **1999**, *15*, 7411.
- [153] J. M. Elliot, J. R. Owen, *Phys. Chem. Chem. Phys.*, **2000**, *2*, 5653.
- [154] D. J. Mitchell, G. J. T. Tiddy, L. Waring, T. Bostock, M. P. McDonald, *J. Chem. Soc., Faraday Trans. I*, **1983**, *79*, 975.
- [155] P. Sakya, J. M. Seddon, R. H. Templer, R. J. Mirkin, G. J. T. Tiddy, *Langmuir*, **1997**, *13*, 3706.
- [156] Ö. Dag, S. Alayoglu, C. Tura, Ö. Celik, *Chem. Mater.*, **2003**, *15*, 2711.
- [157] S. A. El-Safty, T. Hanaoka, *Chem. Mater.*, **2004**, A - Q.
- [158] Ö. Dag, O. Samarskaya, N. Coombs, G. A. Ozin, *J. Mater. Chem.*, **2003**, *13*, 328.
- [159] Ö. Dag, A. Verma, G. A. Ozin, C. T. Kresge, *J. Mater. Chem.*, **1999**, *9*, 1475.
- [160] J. R. Owen, 4th International Conference, ABA-BRNO 2003 (Advanced Batteries and Accumulators) 15-19 June 2003, 2 Strany, CZ.
- [161] N. Ulagappan, C. N. R. Rao, *Chem. Commun.*, **1996**, 2759.
- [162] G. S. Attard, P. N. Bartlett, N. R. B. Coleman, J. M. Elliot, J. R. Owen, *Langmuir*, **1998**, *14*, 7340.
- [163] P. N. Bartlett, J. Marwan, *Chem. Mater.*, **2003**, *15*, 2962.
- [164] P. N. Bartlett, B. Gollas, S. Guerin, J. Marwan, *Phys. Chem. Chem. Phys.*, **2002**, *4*, 3835.
- [165] G. M. Sheldrick, SHELXS-97, Program for the solution of crystal structures, Univ. Göttingen, **1997**.
- [166] G. M. Sheldrick, SHELXL-97, Program for the refinement of crystal structures, Univ. Göttingen, **1997**.
- [167] XP/PC, Molecular graphics program package for display and analysis of stereochemical data, Version 4.2 for MS-DOS, Siemens Analytical X-Ray Instruments, Inc., Madison, Wisconsin, USA, **1990**.
- [168] K. Brandenburg, G. Berberhoff, Visual Crystal Structure Information System Version 2.1, Bonn, **1998**.

Appendix

A1. Double Segment Electrode

A **Cu-Pt**-Double Segment Electrode (DSE) was used in this work to ascertain that there was no thin film formation on the copper electrode. This electrode was recently developed in our laboratory [69,70] and made of a copper segment metal as working electrode (WE), a platinum segment as indicator electrode (IE), a saturated calomel electrode (SCE) as reference electrode (RE) and a platinum gauze as counter electrode (CE). All electrodes are connected to a bipotentiostat which can operate remotely from a personal computer (PC). A schematic representation of the design of the DSE is shown in Fig. I [69,70].

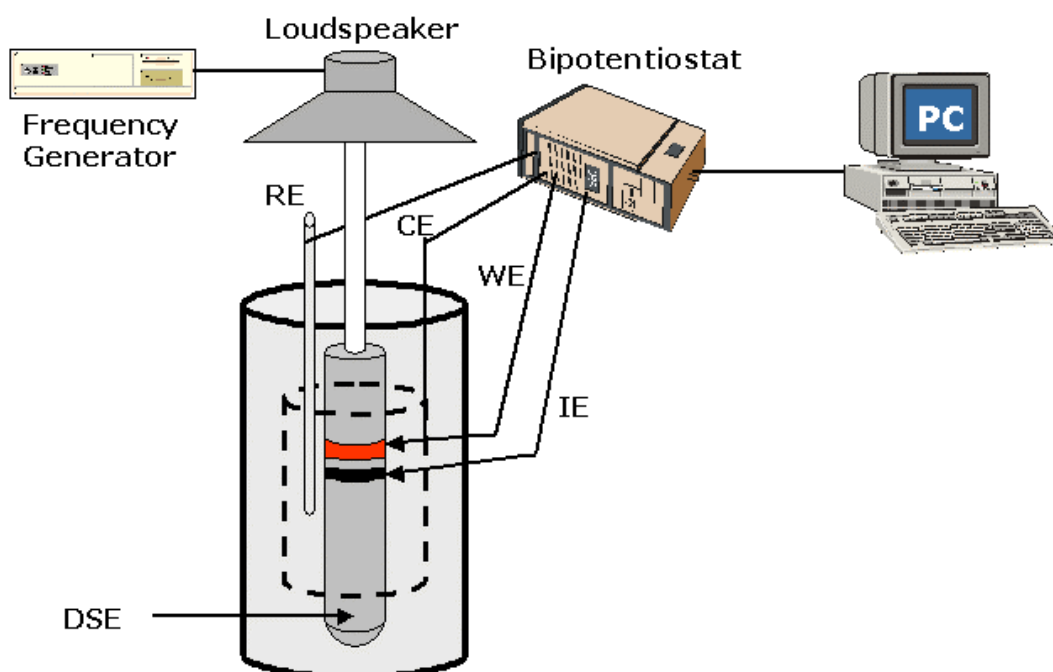


Fig. I Schematic representation of DSE

The working and the indicator electrodes are insulated from each other and having embedded material in the segments. The upper segment is the working electrode (WE) and the lower segment, the indicator electrode (IE). DSE represent a useful tool for corrosion studies or kinetic measurements.

In this work, DSE was used for qualitative measurements and its applicability was demonstrated by result of the anodic dissolution of copper in H_2SO_4 solutions. Schäfer [70] used a Cu-Cu-DSE made of copper working and indicator electrodes and found that the DSE curves are characterized by mass transport. This has been confirmed by Cu-Pt-DSE described above in 0.1 M H_2SO_4 (Fig. II).

The copper working electrode was polarized at +200 mV and the platinum indicator electrode at -400 mV. The bipotentiostat is switched on and 10 s after, the platinum segment is switched on (A) followed by the copper segment 25 s later (B) and an anodic current flows at the copper electrode. A cathodic current began to flow 25 s later at the platinum indicator electrode (C) and indicate that the copper ions generated at the working electrode diffuse into the solution. After two minutes of experiments, the working electrode is switch off (D) and no currents flow at both electrodes (copper ions are not more generated) as it is shown on Fig. II. This indicates a relationship between both currents.

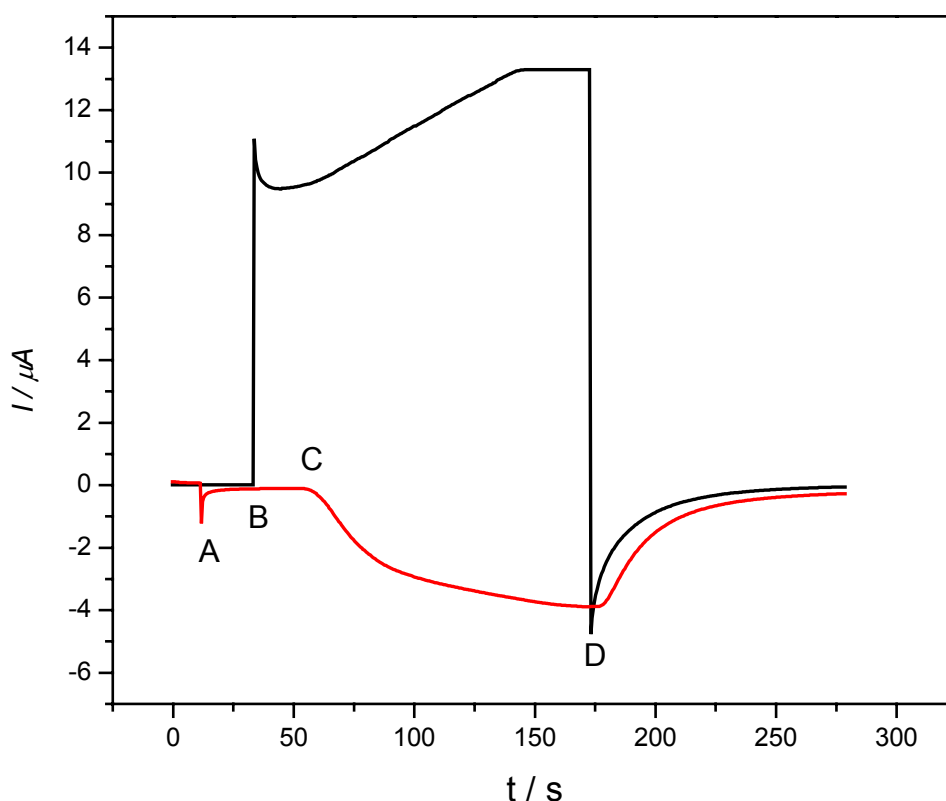


Fig. II Current–time curve at the DSE in 0.1 M H_2SO_4 when the anode is potentiostatically polarized.

A2. Crystal data and experimental details of X-ray structure

A2.1. Crystallographic data for $[\text{Cu}(\mu\text{-C}(\text{CN})_3)(\text{PPh}_3)_2]_2$ (1)

Empirical formula	$\text{C}_{80}\text{H}_{60}\text{Cu}_2\text{N}_6\text{P}_4$	Z	1
Formula weight	1356.30 [g·mol ⁻¹]	Calculated density [g/cm ³]	1.277
Temperature [K]	220(2)	μ (MoK α) [mm ⁻¹]	0.741
Wavelength [Å]	0.71073	F(000)	700
Crystal system	Triclinic	Crystal size [mm]	0.24 x 0.24 x 0.18
Space group	$P\bar{1}$	θ range for data collection [°]	1.5 to 26.0
Unit cell dimensions		Limiting indices h, k, l	-14/13, -15/15, -16/16
a [Å]	12.186(3)	Reflections collected/ unique	10625 / 6285 [R(int) = 0.0319]
b [Å]	12.877(3)	Obs. reflection [I>2 σ (I)]	4887
c [Å]	13.077(3)	Data / restraints / parameters	6285 / 0 / 410
α [°]	85.48(2)	R1/wR2/S(all data)	R1 = 0.0532, wR2 = 0.0996
β [°]	69.46(2)	R1/wR2/S[I>2 σ (I)]	R1 = 0.0345, wR2 = 0.0867
γ [°]	66.95(2)	$\Delta\rho$ (min./max.) [e.Å ⁻³]	-0.544 / 0.448
Volume [Å ³]	1764.1(6)		

A2.2. Crystal data for $\text{cis-}[\text{Cu}_2(\mu\text{-CN})(\text{PPh}_3)_2(\text{Phen})_2]_2[\text{C}(\text{CN})_3][\text{BF}_4]\cdot 2\text{CH}_3\text{CN}$ (2)

Empirical formula	$\text{C}_{130}\text{H}_{98}\text{Cu}_4\text{N}_{15}\text{P}_4\text{BF}_4$	Z	2
Formula weight	2335.13 [g·mol ⁻¹]	Calculated density [g/cm ³]	1.368
Temperature [K]	298	μ (MoK α) [mm ⁻¹]	0.862
Wavelength [Å]	0.71073	F(000)	2400
Crystal system	Monoclinic	Crystal size [mm]	0.07 x 0.35 x 0.57
Space group	P2/c	θ range for data collection [°]	1.5 to 26.0
Unit cell dimensions		Limiting indices h, k, l	-26/27, 0/11, -34/11
a [Å]	22.028(4)	Reflections collected/ unique	11392 / 11154, [R(int) = 0.2283]
b [Å]	9.302(2)	Obs. reflection [I>2 σ (I)]	5794
c [Å]	28.057(7)	Data / restraints / parameters	11154 / 0 / 716
β [°]	99.605(16)	R1/wR2/S(all data)	0.1954 / 0.1598 / 1.175
Volume [Å ³]	5668(2)	R1/wR2/S[I>2 σ (I)]	0.0870 / 0.1181 / 1.175
		$\Delta\rho$ (min./max.) [e.Å ⁻³]	-0.40 / 0.38

A2.3. Crystallographic data for [Cu₂(μ-CN)(PPh₃)₆][BF₄] (3)

Empirical formula	C ₁₀₉ H ₉₀ B Cu ₂ F ₄ N P ₆	Volume [Å ³]	9031.56(3)
Formula weight [g·mol ⁻¹]	1813.53	Z	4
Temperature [K]	293(2)	Calculated density [g/cm ³]	1.334
Wavelength [Å]	0.71069	μ (MoKα) [mm ⁻¹]	0.636
Crystal system	Monoclinic	F(000)	3760
Space group	C 1 2/c 1 (no. 15)	Limiting indices h, k, l	-35/35, -16/18, -36/36
Unit cell dimensions		Obs. reflection [I>2σ(I)]	5561
a [Å]	25.666(5)	Data / restraints / parameters	12487 / 0 / 735
b [Å]	13.481(3)	R1/wR2/S(all data)	0.1499/ 0.0917/ 0.926
c [Å]	26.107(5)	R1/wR2/S[I>2σ(I)]	0.0559/ 0.0775/ 0.926
β [°]	91.06(3)		

A2.4. Crystal data for trans-[Cu₂(μ-CN)(PPh₃)₂(bipy)₂][BF₄]·THF (4)

Empirical formula	C ₆₅ H ₆₂ BCu ₂ F ₄ N ₅ O ₂ P ₂	Volume [Å ³]	1489.2(6)
Formula weight	[g·mol ⁻¹]	Z	1
Temperature [K]	220(2)	Calculated density [g/cm ³]	1.404
Wavelength [Å]	0.71073	μ (MoKα) [mm ⁻¹]	0.836
Crystal system	Triclinic	F(000)	650
Space group	P $\bar{1}$	θ range for data collection [°]	2.35 to 26.03
Unit cell dimensions		Limiting indices h, k, l	-10 / 10, -13 / 13, -20 / 20
a [Å]	8.7896(19)	Reflections collected/ unique	11422 / 5400 [R(int)= 0.0483]
b [Å]	10.906(2)	Obs. reflection [I>2σ(I)]	5794
c [Å]	16.468(4)	Data / restraints / parameters	5400 / 0 / 472
α [°]	106.98(3)	R1/wR2/S(all data)	0.0797 / 0.1739 / 1.005
β [°]	94.45(3)	R1/wR2/S[I>2σ(I)]	0.0570 / 0.1557 / 1.005
γ [°]	96.69(3)	Δρ (min./max.) [e.Å ⁻³]	-0.59 / 0.867

A2.5. Crystallographic data for [Cu(CN)(bipy)(PPh₃)] (6)

Empirical formula	C ₂₉ H ₂₃ CuN ₃ P	Volume [Å ³]	1193(5)
Formula weight [g·mol ⁻¹]	508.01	Z	2
Temperature [K]	220(2)	Calculated density [g/cm ³]	1.413
Wavelength [Å]	0.71073	μ (MoKα) [mm ⁻¹]	0.862
Crystal system	Triclinic	F(000)	524
Space group	P $\bar{1}$	Crystal size [mm]	0.42 x 0.30 x 0.30
Unit cell dimensions		θ range for data collection [°]	2.46 to 25.93
a [Å]	9.062(2)	Limiting indices h, k, l	-11/11, -11/11, -19/19
b [Å]	9.194(2)	Reflections collected/ unique	9233 / 4254, [R(int) = 0.0405
c [Å]	15.705(4)	Data / restraints / parameters	4254 / 0 / 399
α [°]	89.93(3)	R1/wR2/S(all data)	0.0353/ 0.0840 / 1.083
β [°]	92.05(3)	R1/wR2/S[I>2σ(I)]	0.0304 / 0.0880 / 1.083
γ [°]	114.09(3)	Δρ (min./max.) [e.Å ⁻³]	-0.463 / 0.47

A2.6. Crystallographic data for [Cu(CN)(phen)(PPh₃)] (7)

Empirical formula	C ₃₁ H ₂₃ CuN ₃ P	Volume [Å ³]	1274.5(4)
Formula weight [g·mol ⁻¹]	532.03	Z	2
Temperature [K]	220(2)	Calculated density [g/cm ³]	1.386
Wavelength [Å]	0.71073	μ (MoKα) [mm ⁻¹]	0.945
Crystal system	Triclinic	F(000)	548
Space group	P $\bar{1}$	Crystal size [mm]	0.33 x 0.30 x 0.10
Unit cell dimensions		θ range for data collection [°]	2.44 to 25.90
a [Å]	9.193(18)	Limiting indices h, k, l	-10/10, -11/11, -20/19
b [Å]	9.155(18)	Reflections collected/ unique	9881 / 4570 [R(int) = 0.0425]
c [Å]	16.757(4)	Data / restraints / parameters	11154 / 0 / 716
α [°]	84.72(2)	R1/wR2/S(all data)	0.0491/ 0.1092/ 1.120
β [°]	86.45(2)	R1/wR2/S[I>2σ(I)]	0.0363/ 0.0883/ 1.120
γ [°]	65.20(2)	Δρ (min./max.) [e.Å ⁻³]	-0.91 / 0.61

A2.7. Crystallographic data for [Cu(BPVA)(Phen)(PPh₃)] (9)

Empirical formula	C ₄₆ H ₃₆ CuN ₄ P	Z	4
Formula weight [g·mol ⁻¹]	739.30	Calculated density [g/cm ³]	1.317
Temperature [K]	293(2)	μ (MoKα) [mm ⁻¹]	0.667
Wavelength [Å]	0.71073	F(000)	1536
Unit cell dimensions		θ range for data collection [°]	2.36 to 25.93
a [Å]	9.1633(17)	Limiting indices h, k, l	-11/11, -19/19, -31/31
b [Å]	15.925(3)	Reflections collected/ unique	25427 / 7192 [R(int) = 0.0599]
c [Å]	25.557(4)	Data / restraints / parameters	7192 / 0 / 613
α [°]	90	R1/wR2/S(all data)	0.0465, 0.0813 / 1.007
β [°]	90	R1/wR2/S[I>2σ(I)]	0.0349, 0.0765 / 1.007
γ [°]	90	Δρ (min./max.) [e.Å ⁻³]	-0.30 / 0.41
Volume [Å ³]	3729.5(11)		

A2.8. Crystallographic data for [Cu₃(CN)₂(phen)₃(PPh₃)₂][BF₄] (11)

Empirical formula	C ₇₄ H ₅₄ BCu ₃ F ₄ N ₈ P ₂	Volume [Å ³]	3195.7(14)
Formula weight	1394.62 [g·mol ⁻¹]	Z	2
Temperature [K]	220(2)	Calculated density [g/cm ³]	1.449
Wavelength [Å]	0.71073	μ (MoKα) [mm ⁻¹]	1.102
Crystal system	Triclinic	F(000)	1424
Space group	P $\bar{1}$	θ range for data collection [°]	2.15 to 26.09
Unit cell dimensions		Limiting indices h, k, l	-11/11, -22/21, -24/22
a [Å]	9.173(2)	Reflections collected/ unique	23206/11715[R(int)= 0.1433]
b [Å]	17.973(5)	Data / restraints / parameters	11715 / 0 / 824
c [Å]	20.031(5)	R1/wR2/S(all data)	0.2106/ 0.2244 / 0.881
α [°]	76.22(3)	R1/wR2/S[I>2σ(I)]	0.0791/0.1793/ 0.881
β [°]	85.36(3)	Δρ (min./max.) [e.Å ⁻³]	-0.68 / 0.99
γ [°]	87.36(3)		

A2.9. Crystal data of [Cu(CN)(phen)(PPh₃)₂·H₂O (12)

Empirical formula	C ₆₂ H ₄₆ Cu ₂ N ₆ OP ₂	Volume [Å ³]	2563.8(11)
Formula weight	1080.07 [g·mol ⁻¹]	Z	2
Temperature [K]	220(2)	Calculated density [g/cm ³]	1.399
Wavelength [Å]	0.71073	μ (MoKα) [mm ⁻¹]	0.942
Crystal system	Triclinic	F(000)	1112
Space group	P $\bar{1}$	Crystal size [mm]	0.24 x 0.12 x 0.03
Unit cell dimensions		θ range for data collection [°]	2.17 to 26.06
a [Å]	9.780(2)	Limiting indices h, k, l	-12/12, -16/19, -21/22
b [Å]	15.755(4)	Reflections collected/ unique	14279 / 9062 [R(int) = 0.0502]
c [Å]	18.579(4)	Data / restraints / parameters	9062 / 0 / 843
α [°]	110.82(3)	R1/wR2/S(all data)	0.0917 / 0.1723 / 1.019
β [°]	104.32(3)	R1/wR2/S[I>2σ(I)]	0.0535 / 0.1396 / 1.019
γ [°]	92.67(3)	Δρ (min./max.) [e.Å ⁻³]	-1.45/ 0.79

A2.10. Crystallographic data for [(CuCl)₂(μ-dppe)(η²-dppe)₂·CH₃CN (15)

Empirical formula	C ₈₂ H ₇₂ Cl ₂ Cu ₂ N ₂ P ₆	Volume [Å ³]	7450(3)
Formula weight	1469.22 [g·mol ⁻¹]	Z	4
Temperature [K]	220(2)	Calculated density [g/cm ³]	1.310
Wavelength [Å]	0.71073	μ (MoKα) [mm ⁻¹]	0.816
Crystal system	Monoclinic	F(000)	3040
Space group	I2/a	θ range for data collection [°]	2.02 to 25.96
Unit cell dimensions		Limiting indices h, k, l	-27/27, -13/13, -38/38
a [Å]	22.046(5)	Reflections collected/ unique	28325/7022 [R(int)=0.0546]
b [Å]	10.611(17)	Data / restraints / parameters	7022 / 0 / 568
c [Å]	31.988(7)	R1/wR2/S(all data)	0.0530 / 0.0838 / 0.988
α [°]	90	R1/wR2/S[I>2σ(I)]	0.0340 / 0.0762 / 0.988
β [°]	95.40(3)	Δρ (min./max.) [e.Å ⁻³]	-0.38/ 0.55
γ [°]	90		

A2.11. Crystallographic data for [(CuCl)₂(μ-dppe)(η²-dppe)₂]·(CH₃)₂SO (16)

Empirical formula	C ₈₂ H ₇₄ P ₆ Cu ₂ Cl ₂ S ₂ O ₂	Volume [Å ³]	1960.3(6)
Formula weight	1756.52 [g·mol ⁻¹]	Z	1
Temperature [K]	293(2)	Calculated density [g/cm ³]	1.488
Wavelength [Å]	0.71069	μ (MoKα) [mm ⁻¹]	0.842
Crystal system	Triclinic	F(000)	905
Space group	P $\bar{1}$ (No 2)	θ range for data collection [°]	2.02 to 25.96
Unit cell dimensions		Limiting indices h, k, l	-13/13, -15/15, -17/17
a [Å]	11.264(2)	Reflections collected/ unique	13926 / 7035
b [Å]	12.439(2)	Data / restraints / parameters	7035 / 0 / 577
c [Å]	14.372(3)	R1/wR2/S(all data)	0.1711 / 0.1353 / 0.949
α [°]	94.21(3)	R1/wR2/S[I>2σ(I)]	0.0691 / 0.1112 / 0.949
β [°]	100.48(3)		
γ [°]	96.03(3)		

Acknowledgements

I would like to express my deep gratitude to my supervisor Prof. Dr. W. Schäfer for the opportunity to work in his laboratory with the excellent research conditions. Also, I'm particularly thankful for his guidance and encouragements during the whole period of my PhD research and for believing in me and in my work.

Prof. Dr. G. Pelzl is grateful acknowledged for fruitful discussions and for polarized optical microscopy.

I would like to thank my colleagues Mrs. B. Martin and Dr. T. Schelenz for their support and cooperativeness, I'll never forget all these marvelous moments we spent together. And my former colleagues, Dr. M. Günther and Dr. V. Rjabova for creating a friendly and an international working atmosphere in the laboratory

The characterizations the copper(I) complexes prepared in this work could not be possible without the X-ray analyses. For this reason, Dr. C. Wagner is especially acknowledged for the X-ray analyses of compounds **1**, **4**, **6**, **7**, **9**, **11**, **12** and **15**. Dr. U. Baumeister is acknowledged for X-ray characterization and fruitful discussion on the compound **2** and Dr. B. Fokwa for the X-ray and EDX of **3** and **16**.

Dr. A. Hauser is acknowledged for AFM measurements and Dr. T. Müller for TG/DTA/DSC.

Dr. F. Majouomo is acknowledged for the EI-, FAB-, ESI-MS and IR. Dr. J.-P. Jemetio is acknowledged for EDX of compounds **5**, **13** and **14**. Dr. R. Fotsing is acknowledged for fruitful discussions.

I would like to express my deepest gratitude to my son and wife for all their love, care and attentions during this period. Finally my parents, brothers and sisters for all their sacrifices that made for me.

The **Land Sachsen-Anhalt** and the **Deutsche Forschungsgemeinschaft (DFG)** are gratefully acknowledged for the financial support.

Author's declaration

This thesis is an account of work carried out at the Martin-Luther-Universität Halle-Wittenberg under the supervision of Prof. Dr. Wieland Schäfer.

I declare that the work in this dissertation was carried out in accordance with the Regulations of the Martin-Luther-Universität Halle-Wittenberg. The work is original except where indicated by special references in the text and no part of the dissertation has not been presented to any other University for examination.

Eidesstattliche Erklärung

Ich erkläre hiermit, die vorliegende Dissertationsschrift selbständig und nur unter Verwendung der angegebenen Quellen und Hilfsmittel angefertigt zu haben.

Die Arbeit wurde bisher an keiner weiteren Hochschule oder Universität zur Promotion eingereicht.

Halle, 05. 08. 04.

CURRICULUM VITAE

FOTSING KAMTE, MARCELLIN MAGLOIRE

CIVIL STATUS Born in March 14, 1972 at Bafoussam, Cameroon
Nationality: Cameroonian.
Family status: Married with one Child.

EDUCATION

- **Dr. rer. nat. (Ph.D.)** in Electrochemistry, Martin-Luther-Universität Halle-Wittenberg, **2001 - 2004.**
- **First year doctorate Certificate (DEA)** in Inorganic Chemistry; Specialization in Analytical Chemistry – Electrochemistry, The University of Yaounde I, Cameroon, **1999 – 2000.**
- **M.Sc.** in Inorganic Chemistry Specialization in Analytical Chemistry, The University of Yaounde I, Cameroon, **1997 – 1999.**
- **B.Sc.** in Chemistry, The University of Yaounde I, Cameroon, **1992 – 1997.**

PROFESSIONAL EXPERIENCE

Martin-Luther-Universität Halle-Wittenberg, Germany

- Electrodeposition of mesoporous metal films from lyotropic liquid crystalline phases, **October 2003 to present** (current project).
- PhD Stipend, Graduate Study Program "Self-organization by Coordinative and non-covalent Interaction" at the Martin-Luther-Universität Halle-wittenberg, supported by Deutsche Forschungsgemeinschaft (DFG) and Land Sachsen-Anhalt, **October 2003 – August 2004.**
- PhD Stipend, Graduate Study Program "Synthesis and Reaction Behaviour of Organometallic Compounds and Metal Complexes" at the Martin-Luther-Universität Halle-wittenberg, supported by Deutsche Forschungsgemeinschaft (DFG) and Land Sachsen-Anhalt, **April 2001 – April 2003.**

The University of Yaounde I, Cameroon.

- Demonstrator / Instructor for physical chemistry practical and tutorial lessons, **1997 – 2000.**
- Master thesis on electrochemistry of clays: study of the electrochemical behavior of kaolinite clay groups using the carbon paste electrode, **1997 – 1999.**

AFFILIATION

- Member of the International Society of Electrochemistry (**ISE**)

FOTSING KAMTE, MARCELLIN MAGLOIRE

PUBLICATIONS

- **M. Fotsing Kamte**, Ch. Wagner and W. Schäfer, Direct Electrosynthesis of Cyano Copper(I) Complexes: X-ray Crystal Structure of (cyano-C)(2,2'-bipyridine-N,N')(triphenylphosphane)copper(I), *J. Coord. Chem.*, **2004**, 57, 55.
- **M. Fotsing Kamte**, U. Baumeister and W. Schäfer, Electrochemical Synthesis of Tricyanomethyl Copper Complexes, *Z. Anorg. Allg. Chem.* **2003**, 629, 1919-1924.

ORAL COMMUNICATIONS

- **M. Fotsing Kamte** and W. Schäfer, Electrochemical Reactions in Electrosynthesis of Organocopper(I) Compounds, Graduate School "Hydrogen Bridges and Hydrogen Bonds, Freie Universität Berlin", Berlin, June 30, 2004 (Invited speaker).
- **M. Fotsing Kamte** and W. Schäfer, Liquid Crystal as Templates for the Electrodeposition of Metals, Workshop of the Graduate Study Program "Self-organization by Coordinative and non-covalent Interaction", Schönburg, March 1 – 4, 2004.
- **M. Fotsing Kamte** and W. Schäfer, Direct Electrosynthesis of Organocopper Compounds, Department of Inorganic Chemistry, University of Yaounde I, August 05, 2003 (Invited talk).
- **M. Fotsing Kamte** and W. Schäfer, Electrosynthesis of Copper Nitrile Complexes, 11.Seminar des Arbeitskreises Elektrochemie in Sachsen (AKES), Ehrenkolloquium zum 65. Geburtstag von Professor W. J. Plieth, Dresden, December 5, 2002 (Invited talk).
- W. Schäfer, V. Rjabova, M. Günther, **M. Fotsing Kamte**, Electrosynthesis of Organocopper Compounds and Nitrile complexes, 53rd. ISE Meeting, Düsseldorf, DECHEMA e.V. Frankfurt 2002, p. 343.
- **M. Fotsing Kamte** and W. Schäfer, Synthesis of Organometallic Compounds at Macro- and Microscale, VIIth Regional Seminar of PhD Students on Organometallic and Coordination Chemistry, Bad Kösen, March 3–7, 2002, p 24.

POSTERS

- **M. Fotsing Kamte** and W. Schäfer, Direct Electrosynthesis of Copper(I) Complexes with Nitriles, 55th. ISE Meeting, Thessaloniki, Greece, 19–24 September 2004, S2FP14.
- **M. Fotsing Kamte** and W. Schäfer, Electrosynthesis of Copper(I) Nitrile Complexes, GDCh Annual Meeting, Munich, 6 – 11 October 2003.
- **M. Fotsing Kamte** and W. Schäfer, Direct Electrosynthesis of Organocopper Compounds, International Symposium on Modern Organocopper Chemistry, Dortmund, October 2002, P1.